AD-A258 027

(11)

THE OHIO STATE UNIVERSITY

Technical Report 1:

Pack Cementation Aluminide Coatings on Superalloys: Codeposition Of Cr and Reactive Elements (RE)

Technical Report 2:

Chromium and Reactive Element(RE)-Modified Aluminide Diffusion Coatings On Superalloys: Environmental Testing

Robert A. Rapp
Department of Materials Science and Engineering

DTIC
ELECTE
NOV 3 0 1992
S D
A

111 pgs
92-30243

Office of Naval Research
Arlington, Virginia 22217-5000

Grant No. N00014-90-J-1765
Technical Reports 1 & 2

This document has been approved for public release and sale; its distribution is unlimited.

November 1992

92 11 25 004

THE OHIO STATE UNIVERSITY

Technical Report 1:

Pack Cementation Aluminide Coatings on Superalloys: Codeposition Of Cr and Reactive Elements (RE)

Technical Report 2:

Chromium and Reactive Element(RE)-Modified Aluminide Diffusion Coatings On Superalloys: Environmental Testing

Robert A. Rapp
Department of Materials Science and Engineering

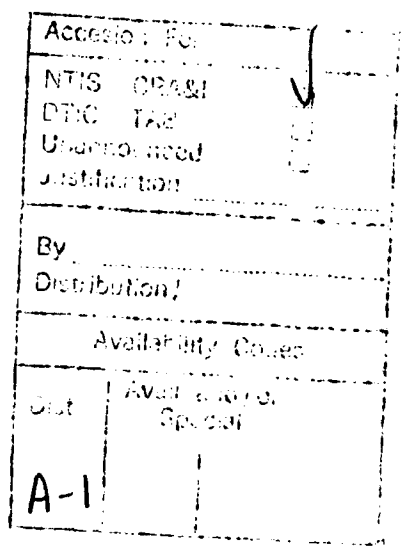

Office of Naval Research
Arlington, Virginia 22217-5000

Grant No. N00014-90-J-1765
Technical Reports 1 & 2
RF Project No. 768203/723314

November 1992

PACK CEMENTATION ALUMINIDE COATINGS ON SUPERALLOYS: Codeposition of Cr and Reactive Elements (RE)

Robert Bianco and Robert A. Rapp
Department of Materials Science and Engineering
The Ohio State University
Columbus, Ohio 43210

ABSTRACT

A single-step, chloride-activated pack cementation process has been developed for growing a Cr/RE(Y,Zr)-modified or a RE(Y,Zr,Hf)-doped aluminide diffusion coating on commercial Ni-base superalloys. The coatings consisted of an outward-grown, hypostoichiometric ß-NiAl layer with a substantial enrichment in Cr and a low reactive element content. The Cr was both dissolved in the ß-NiAl matrix and precipitated as α-Cr second-phase particles. Aluminide coatings grown outwards in a pack permitting powder contact with the substrate were embedded with Al_2O_3 and RE oxide pack particles. Physical separation of the substrates from the powder mixture eliminated powder entrapment, but reduced the growth rate and the amount of Cr enrichment in the coating. Isolation of the substrate from the pack introduced partial rate control by gaseous diffusion.

KEY WORDS: Diffusion Coating, Aluminizing/Chromizing, Reactive Element.

INTRODUCTION

Aluminide diffusion coatings are commonly applied by the pack cementation method to Ni-base superalloy turbine components to improve their oxidation resistance. However, aluminide coatings lack adequate resistance to hot corrosion (fused salt attack, e.g. by Na_2SO_4) and to thermal

stresses generated during gas turbine service. Therefore, some chemical modification in the composition of aluminide coatings is necessary to improve the overall environmental durability of the coated component. For example, McCarron et al.[1] determined that Cr additions in bulk ß-NiAl compounds (the principal phase in aluminide coatings) improved burner rig hot corrosion resistance considerably. Aluminide coatings modified with Cr[2,3] have been developed using the halide-activated pack cementation (HAPC) process in two sequential steps: a traditional aluminizing process followed by chromizing in a separate pack. It would be economically beneficial to codeposit Al and Cr in a single-step; however, this is not done commercially nor deemed feasible.[4,5]

HAPC is a high-temperature, closed-system chemical vapor deposition batch process in which the pack is comprised of three mixed powdered components: (a) a masteralloy powder of the element(s) to be deposited (e.g., Al, Cr, or Si), (b) a halide salt activator (e.g., NaCl, NaF, NH_4Cl), and (c) an inert filler powder (e.g., Al_2O_3). The parts to be coated are embedded in this powder mixture and heated in a vented retort. A controlled atmosphere, usually Ar or H_2/Ar, surrounds the pack as it is heated to an elevated temperature (e.g., 900-1150^{o}C), at which the masteralloy reacts with the halide salt activator to form volatile metal halide species of significant partial pressures according to the following reaction:[6]

$$Me(alloy) + AX_x(l,v) = MeX_x(v) + A(l,v) \qquad (1)$$

where, in this study, Me is Cr or Al; A is NH_4, Y, Zr, or Hf; and X is Cl. Several different vapor species may be formed for each element (e.g., Al, AlX, AlX_2, and AlX_3; Cr, CrX_2, CrX_3, and CrX_4). Partial pressure gradients, which support vapor transport for each vapor species to the substrate surface, result from the higher thermodynamic activity for the metallic component in the powdered masteralloy compared to its lower activity at the substrate surface. At the surface, deposition of the desired coating element(s) occurs via the dissociation or disproportionation of the halide molecules, or by a displacement reaction with the substrate.[6] Finally, the coating element(s) reacts and interdiffuses with the metallic substrate, producing some specific phase, composition, and microstructure at the surface.

In general, for resistance to oxidation and hot corrosion, a ternary alloy or coating, using the interaction of two oxidation-resistant elements, is more effective than a simple binary alloy or coating.[7] Therefore, one might suppose that a mixture of several pure elemental powders should produce codeposition. However, comparable negative pressure gradients for two or more elements (needed to support simultaneous codeposition) essentially never occur because of large differences in the standard Gibbs energies of formation for their respective halide species.[4,5] But, binary Cr-rich Cr-Al alloys exhibit highly negative deviations from ideal thermodynamic behavior, so that such masteralloys can be used to reduce the activity of the otherwise more reactive Al

component by several orders of magnitude.[8] Hence, by using such binary masteralloy powders, codeposition of Al and Cr into Ni- and Fe-base alloys has been achieved experimentally when an appropriately stable halide activator salt was also provided.[9-12] The Cr-Al masteralloy powder, with reduced thermodynamic activity for Al, generates lower vapor pressures for the otherwise favored halide species (i.e. AlX_x).[12,13] Computer-assisted equilibrium calculations can be used to determine the masteralloy composition for which the vapor pressures of the Al and Cr halide species are brought to comparable magnitudes, so that codeposition results via comparable fluxes for each component in a desired surface composition.

The protective oxide scales produced on high-temperature alloys and coatings are often exposed to stresses induced by thermal cycling[14] and by oxide formation and growth[15], which can induce loss of adherence and spalling of the scale. However, a small concentration (<1 wt.%) of a highly reactive element (e.g., Y, Zr, Hf, Th, Ce) can improve the adherence of chromia and alumina protective scales on Ni-, Co-, and Fe-base alloys and coatings.[15-18] This "reactive element effect" (REE) is well accepted and a number of interpretations have been suggested to explain the experimental observations: (a) improvement in the mechanical properties of the oxide scale[19], (b) localized doping of the oxide to reduce the concentration and/or mobility of dominant point defects[20,21], (c) segregation of RE ions or the formation of

RE-rich precipitates at or near oxide grain boundaries to block short-circuit diffusion paths and inhibit the growth of oxide grains[22-26], (d) formation of RE-rich internal oxide pegs mechanically anchoring external oxide scales to the metal substrates[15,17,18], (e) elimination of interfacial voids and convoluted scales improving scale epitaxy[16-18], (f) counteraction to the "sulfur effect"[27-29], and (g) the inhibition of the climb of misfit dislocations which otherwise annihilates the cation vacancies supporting cation diffusion. [30]

Barrett[31], Jedlinski and Mrowec[32,33], and Santoro et al.[34,35] have shown that small additions of Zr, Y, and to a lesser extent Si improve the adherence of alumina scales thermally grown on bulk ß-NiAl compounds. Therefore, to produce highly adherent alumina scales during oxidation, a coating process could be further altered to codeposit a small amount of a RE into the surface of the aluminide coating. Overlay coatings applied to Ni-base alloys by physical vapor deposition have always included a RE, but reactive elements are not generally deposited by other coating methods.

Jedlinski et al.[36] incorporated Y and Ce into the surface of NiAl coatings on Ni-base alloys by an ion implantation technique. Fuhui et al.[37] produced Y-modified aluminide coatings on IN 738 alloys by a standard aluminizing treatment followed by a fusion slurry technique to deposit Y. Only three investigations have used the pack cementation method with RE additions:

(a) Tu et al.[38] produced an Y-modified aluminide coating by a two-step process (aluminizing followed by yttrizing). The modified coatings consisted of an external aluminide layer with Y enrichment near the surface and along grain boundaries. Yttrium was deposited using a pack powder mixture of pure Y, NH_4Cl activator salt, and an Y_2O_3 filler which was heated at 1050°C for four hours.

(b) Rapp et al.[9] replaced a small amount (2 wt.%) of the pack alumina filler with yttria to codeposit Cr and Al on pure Fe and low-alloy steel substrates. Energy dispersive spectroscopy (EDS) analysis detected about 0.4 wt.% Y in the coating surface.

(c) LePrince et al.[39] used a high-activity process with a powder mixture of pure source elements to codeposit Al and Hf onto Ni-base fibers. The resulting coating consisted of a NiAl matrix with Ni_5Hf precipitates.

In all cases, the RE-doped, aluminide diffusion coatings exhibited improved oxide scale adherence during cyclic oxidation testing.

Two methods can be identified to provide doping of a third minor element (e.g., Zr or Y) into the surface of a Cr-modified aluminide diffusion coating produced by a single-step pack process.[12] A small amount of an oxide source of the desired element (e.g., ZrO_2 or Y_2O_3) can be added to the pack powder mixture, replacing some of the inert

filler.[9]. In this case, the dopant oxide must be converted in the high halogen activity of the pack to produce additional metal halide species according to Eq. (2):

$$xMO_y(s) + yMeX_x(v) = xMX_y(v) + yMeO_x(s) \quad (2)$$

where M is Zr or Y and Me is Al. Calculations of pack equilibria using the computer program ITSOL[40] and experiments using an atmospheric pressure sampling mass spectrometer[41] have substantiated these conversion reactions for ZrO_2 and Y_2O_3 additions to Al_2O_3. By a second method, the additional element could be introduced as the chloride activator source (e.g., $ZrCl_4$, YCl_3, or $HfCl_4$). For example, $ZrCl_4$ can react with the Cr-Al binary masteralloy to produce both $AlCl_x$ and $CrCl_x$ species as well as significant vapor pressures of the $ZrCl_x$ species according to Eq. (3):

$$\underline{Me}(s) + ZrCl_4(v) = MeCl_x(v) + ZrCl_{4-x}(v) \quad (3)$$

If the substrate does not contain the RE, the necessary driving force exists for some dissolution of the RE.

The objective of this investigation was to develop a single-step, halide-activated pack cementation process to codeposit Al, Cr, and a small concentration (<0.2 at.%) of a RE (e.g., Zr or Y) or else only Al and the RE (e.g., Zr, Hf, Y, or Si) into commercial Ni-base alloy substrates (IN 713LC, Mar-M247, René 80, René 80H, and René N4). The growth mechanisms and kinetics for the modified-aluminide coating are discussed. In the following paper, the resistance of these coatings to cyclic oxidation and hot corrosion is reported.

EXPERIMENTAL PROCEDURES

Both conventionally cast and directionally solidified columnar-grained and single-crystal Ni-base alloys were used for this investigation. Their nominal compositions (at.%) are given in Table 1. Each of these alloys is a multi-phase alloy (γ, γ', and carbides) at room temperature, with alloying elements to stabilize γ-Ni (e.g., Cr, Co, W, Mo) and γ'-Ni_3Al (e.g., Al, Ti, Nb) or to form carbides (e.g., W, Mo, Ti, Ta, Hf, Nb).

Alloy ingots were sectioned into 1 mm thick specimens approximately 1 cm x 1 cm using an electric discharge machine (EDM). These were ground through 400 grit SiC paper, measured, cleaned with soap and water, ultrasonically degreased in acetone and methanol, and then weighed. The specimens were placed in an alumina crucible with a powder mixture containing: a binary Cr-Al masteralloy powder (<100 mesh; Cerac, Inc.), a chloride activator salt (reagent grade), an inert alumina filler powder (80-200 mesh), and a RE oxide source when required. The RE source was either unstabilized monoclinic zirconia (Atlantic Equipment Engineers), silica gel (Fisher Scientific), or yttria (Johnson Matthey).

Two substrate/pack arrangements were used to produce the coatings. The first ("powder contacting") arrangement consisted of placing the substrate in intimate contact with the powder mixture in the retort. By the second ("above pack") arrangement shown in Fig. 1, the substrate was physically isolated from the powder mixture by a smaller, porous alumina enclosure (Selee Corp.) and plugged at both

ends by porous alumina paper (Zircar Products, Inc.). The pack powder mixtures were weighed and then mixed by tumbling in a ball mill for up to four hours. The alumina crucible was closed with an alumina lid using an alumina-base cement (Aremco Products, Inc.). The crucible was then placed in a horizontal, resistance-heated tube furnace, purged with prepurified Ar, heated ($4^{o}C$/min) to $1150\pm5^{o}C$, and held for 24 hours. After cooling in the furnace, the crucible was opened and the coated substrates were cleaned, degreased, and weighed.

To examine the coated cross-sections by optical microscopy, specimens were mounted in epoxy, sectioned with a low-speed diamond blade saw, and polished through 0.3 μm alumina. Phases and compositions were evaluated with the aid of x-ray diffraction (XRD) and electron probe microanalysis (EPMA). Secondary ion mass spectroscopy (SIMS) analysis was conducted on selected Y-doped coatings to quantify, the composition of the coating surface.

RESULTS AND DISCUSSION

A. Cr/RE(Zr,Y)-Modified Aluminide Coatings

"Powder Contacting" Arrangement: Computer-assisted (ITSOL) equilibrium calculations were used to determine potential pack chemistries (i.e. masteralloy composition and a chloride activator salt), which could generate dual vapor transport, by calculating the equilibrium vapor pressures of

all the chloride species evolved. These calculations have been presented elsewhere[40] and have eliminated needless trial and error experimentation during this development.

A representative cross-sectional micrograph of a coated René 80 alloy substrate is shown in Fig. 2a. The average surface compositions produced by several pack chemistries for René 80 alloys are presented in Table 2. Two limiting types of coatings were observed: the formation of an external carbide (e.g., $Cr_{23}C_6$) or else an external aluminide (e.g., ß-NiAl) coating. For masteralloy compositions with insufficient Al activities (i.e., Cr-5 wt.% Al) or with a RE oxide source (i.e., Cr-7.5 wt.% Al plus ZrO_2), an external $Cr_{23}C_6$ carbide layer was produced. This carbide layer was much thinner (50-60 μm) than the aluminide coatings and had a relatively large weight gain (40-55 mg/cm^2). Conversely, masteralloys with higher Al activities (i.e., Cr-7.5 wt.% Al without RE oxide source or Cr-10 wt.% Al plus a RE oxide source) resulted in an external ß-NiAl phase. The aluminide coatings were much thicker (85-150 μm), but had a smaller weight gain (20-35 mg/cm^2) resulting from the lower density of Al compared to Cr. The aluminide coatings consisted of two phases: an outward-grown, hypostoichiometric ß-NiAl matrix and a spheroidal or lamellar dispersion of α-Cr second-phase particles, which both precipitate near the original substrate surface and grow inward from the gas phase along grain

boundaries at the surface (Fig. 2a). A lamellar α-Cr microstructure was obtained from a relatively fast cooling rate (>1.75 ^{o}C/min) from the treatment temperature.

As verified with wavelength dispersive spectroscopy (WDS) and XRD analyses, some pack powder particles (e.g. Al_2O_3 and RE oxide) were embedded within the outer layer of substrates coated using the "powder contacting" arrangement. Because the coatings grow outward, the aluminide coating envelops or entraps particles during growth, degrading the integrity of the coating.

"Above Pack" Arrangement: Pack entrapment was eliminated by the "above pack" arrangement (Fig. 1). Figure 2b shows an example of an Al_2O_3-free, alloyed ß-NiAl coating with Y deposited from the gas phase. A series of experiments were performed to determine the optimum pack chemistry, including masteralloy composition and the content of the chloride activator and/or RE source. The results are summarized in Tables 3 and 4, and a representative cross-sectional micrograph of a coated René 80 alloy is shown in Fig. 2b. For masteralloys with low Al activities (e.g., Cr-5 wt.% Al), an external carbide layer was again produced. Masteralloys with higher Al activities (e.g., Cr-6 wt.% Al) resulted in an external, aluminide layer. These coatings again consisted of an outward-grown, hypostoichiometric ß-NiAl matrix with a spheroidal dispersion of α-Cr second-phase particles throughout the coating. A slow furnace cool (< 1^{o}C/min) produced the spheroidized α-Cr particles. According to the

Ni-Cr-Al phase diagram[42], Cr has a limited solubility in the ß-NiAl phase (~4 wt.% at 1150°C), which depends on temperature and the Ni/Al ratio. According to Tables 3 and 4, the Cr contents exceed this saturation, so a two-phase coating, α-Cr in the ß-NiAl matrix, is grown at temperature. Depending on the substrate composition, microanalysis of the coating also detected Cr, Co, Ti, Nb, and Mo (not listed in Tables 3 and 4) dissolved in the ß-NiAl coating phase resulting from outward diffusion during the coating process.

The average surface compositions listed in Tables 3 and 4 were measured by EPMA using a large beam diameter (between 10 and 30 μm). The measured bulk composition is dependent on the relative amounts of α-Cr second-phase particles in the ß-NiAl phase, typical of two-phase microstructures.

An interdiffusion zone between the outer, two-phase (ß-NiAl + α-Cr) coating and the Ni-base substrate was comprised of three phases: (a) blocky, refractory metal-rich carbides, (b) lamellar, refractory metal-rich sigma phase, and (c) a ß-NiAl matrix. For example, WDS analysis detected Cr(W,Mo)-rich carbides between the outer aluminide coating and the interdiffusion zone for René 80 alloy substrates; these marked the original substrate surface (Figs. 2a and 2b). Beneath the carbides, lamellar Cr(Mo,W,Co)-rich second-phases, probably sigma phase, were aligned perpendicular to the coating surface within the ß-NiAl matrix. Other alloy

substrates had somewhat different interdiffusion zone morphologies depending on their composition (i.e. contents of strong carbide formers).

The interdiffusion zone generally is formed by the depletion of Ni from the original substrate surface during the outward growth of the NiAl coating. In the interdiffusion zone, carbon reacts with the refractory elements in the Ni-depleted region at the base of the coating, where the carbon solubility is lower, and MC- and $M_{23}C_6$-type carbides are formed.[43] Once the free carbon is depleted, sigma phase rich in refractory metals then precipitates.

About a 33% reduction in the overall thickness (30-85 μm) of the outer aluminide coating layer resulted for the "above pack" method compared with coatings produced using the "powder contacting" arrangement. Further, the surface concentration in Cr (4-8 at.%) and the weight gain (10-20 mg/cm^2) values were also reduced significantly. Reductions of the Cr content cannot alone account for the reductions in weight gain values. Instead, the elimination of pack entrapment and the formation of a thinner aluminide coating were the main causes.

According to Levine and Caves[6], the growth of the NiAl coating produced from a pure Al source depends on the diffusion of volatile Al halides to the substrate surface. Experimentally, fluoride and chloride activators produced the thickest coatings because they generated the highest Al halide vapor pressures.[6] However, for the same pack chemistry

(equilibrium vapor composition), the current results indicate an important reduction in gas phase diffusion fluxes, resulting from use of the porous enclosure of Fig. 1. In this "above pack" arrangement, the powders and the substrate were separated by a porous alumina enclosure with a wall thickness of 10 mm. Obviously, the use of a thinner enclosure with optimized open porosity would increase the Cr content and coating kinetics approaching those observed for the "powder contacting" arrangement.

1. Effect of RE-Base Chloride Activator Content: The amount of RE-base chloride activator in the pack was varied for René 80 substrates (Table 3) to determine the optimum pack chemistry. When ß-NiAl was formed, the bulk contents of Y or Zr determined by EPMA were in the preferred range known to improve alumina scale adherence. The coating morphology remained the same, but the surface concentrations for the RE and Cr, and the overall coating thickness, varied. With an increase in the amount of the RE-base chloride activator, the fluxes of the $AlCl_x$, $CrCl_y$, and the $RECl_z$ species to the surface also increased. Higher fluxes for these species resulted in thicker aluminide coatings with higher Cr and RE enrichment, as previously demonstrated by Gupta et al.[44] for AlF_3-activated packs. These authors attributed the higher deposition rates to a transition in the deposition reaction from a recirculation to a condensation mechanism.

2. Effect of RE Oxide Content: Two distinct behaviors were observed (Table 3). According to pack equilibria

calculations (ITSOL) and mass spectrometer measurements[41], the vapor pressures of the $AlCl_x$ species decrease when the REO_y is converted to $RECl_y$ species. Thus, masteralloys with higher aluminum activities (i.e., Cr-7.5 wt.% Al or greater) are needed to produce an aluminide coating. Increasing the amount of RE oxide addition effectively increased the generation of the desired $RECl_x$ product. For example, increasing the Y_2O_3 content reduced the $AlCl_x$ vapor pressures while generating YCl_x with an increased vapor pressure. The vapor pressures of the $AlCl_x$ species are also reduced by an increase in the $CrCl_y$ vapor pressures. Therefore, higher fluxes and surface concentrations for Cr and Y should result. Because of the reduction in the $AlCl_x$ vapor pressures, a thinner aluminide coating is grown (e.g. from 56 to 32 μm for 2% to 4% Y_2O_3, respectively). The surface concentration of Y did not increase with increasing Y_2O_3 content, but the measured level of 0.03-0.07 at.% is about optimum to realize the REE.[44]

Zirconia additions to the pack, on the other hand, had the opposite effect. Chromium surface compositions actually decreased while the thickness of the aluminide coating increased (e.g. from 107, 115, and 120 μm for 2%, 4%, to 6% ZrO_2, respectively), without a significant increase in the aluminum surface concentration. The surface concentration of Zr generally increased with increasing ZrO_2 content, but stayed in the important range of 0.1-0.2 at.%.

3. Chromium Concentration: The further enrichment of Cr was attempted. Pack chemistries with a higher chromium activity for the Cr-Al binary masteralloy (e.g., Cr-6 wt.% Al and Cr-5 wt.% Al) were used to coat René 80 and IN 713LC alloy substrates with 4 wt.% of either $ZrCl_4$ or else YCl_3 activator at 1150°C for 24 hours. A summary of these results are presented in Table 4. The coating morphologies were similar to that shown in Fig. 2b. No significant chromium enrichment resulted from packs containing the Cr-6 wt.% Al masteralloy, although packs using Cr-5 wt.% Al did produce a significant chromium enrichment. In fact, $ZrCl_4$-activated packs formed an external $Cr_{23}C_6$ layer, while YCl_3-activated packs produced a hypostoichiometric ß-NiAl coating with up to 12 at.% Cr, mostly in the form of α-Cr second-phase particles. These coatings were difficult to reproduce and were sensitive to the overall size of the retort/pack dimensions. More development is necessary to increase the chromium concentration for an entrapment-free, NiAl coating.

4. Yttrium Content: The yttrium surface content was indeed quite low (0.02-0.05 at.%) and localized in the ß-NiAl coatings (Tables 3 and 4). Yttrium has a very limited solubility in the ß-NiAl compound (0.05 at.%)[45] and in NiCrAl alloys (0.08 at.%)[16], and therefore segregates to grain and interphase boundaries. WDS analysis could not detect any additional yttrium at the α-Cr/ß-NiAl interface. The EPMA-measured yttrium levels (0.02-0.50 at.%) were very low and close to the limits of the instrument. To supplement

EPMA analyses, SIMS analyses were conducted on two Cr/Y-modified aluminide coatings. The pack mixtures contained either 4 wt.% YCl_3 and 25 wt.% of Cr-6 wt.% Al or else 2 wt.% NH_4Cl, 2 wt.% Y_2O_3, and 25 wt.% of Cr-7.5 wt.% Al at 1150°C for 24 hours on René 80 alloys. SIMS uses a Ga^+ ion beam to ionize the surface atoms. The sputtered ions from the surface are then collimated and collected by the mass filter of a mass spectrometer for highly accurate discrimination. SIMS elemental maps for Ni, Al, Cr, and Y were determined for these two coatings, and a representative result is shown in Fig. 3. The surface consists of Cr-rich second-phase particles dispersed throughout the ß-NiAl grains as well as along grain boundaries. A Ni- and Y-rich phase, possibly Ni_3Y or Ni_5Y[16], was present adjacent to the grain boundaries, probably at the α-Cr/ß-NiAl interphase boundaries. Nevertheless, the Y-containing phase was not continuous. SIMS analysis could not measure the quantity of yttrium in the coating surface, but EPMA analysis, using an improved yttrium standard, identified between 0.02 and 0.08 at.% Y, which is the desired range to produce adherent Al_2O_3 scales upon oxidation exposure.

B. Oxidation-Resistant RE-Doped Aluminide Coatings

Chromium additions to ß-NiAl compounds and coatings have been found to improve their resistance to hot corrosion (fused salt) attack.[1] However, chromium additions above 3 at.% are not desired for optimum oxidation-resistance.[34] A RE (Zr,Hf,Y)-doped aluminide coating with low Cr was therefore

developed for IN 713LC and Mar-M247 alloys using the "above pack" arrangement. The results are listed in Table 5, and a representative cross-sectional micrograph is shown in Fig. 4.

These coatings consisted of an outward-grown, hypostoichiometric ß-NiAl matrix with a fine dispersion of α-Cr second-phase particles which precipitate near the original substrate surface resulting from the outward diffusion of chromium. The coating morphology and the surface compositions are consistent with aluminide coatings produced on Ni-15 at.% Cr alloys by a low activity (Ni-40 at.% Al) source using an AlF_3 activator at 1150°C[46], and by the commercial low-activity, aluminide coating, GE Codep C.

Both RE-base activators and RE oxide additions deposited significant RE amounts in the ß-NiAl coating layer. The more Al-rich Cr-10 wt.% Al masteralloy was used in all cases to limit Cr deposition. Although some preliminary coatings were produced using an Fe-10 wt.% Al masteralloy, to eliminate Fe contamination, the Cr-Al binary masteralloy was then used. However, a Ni-Al binary alloy powder with comparable Al activity should also suffice. These low Cr, RE-doped aluminide coatings were about 50-65 μm thick with about a 15-17 mg/cm^2 weight gain resulting from the coating process.

C. Chromium/Silicon-Modified Aluminide Coatings

Silicon additions have been found to improve the environmental durability resistance of both MCrAlY overlay[47] and aluminide coatings[48] as well as ß-NiAl compounds.[34,35] Although the role of Si has been widely debated, small Si

additions indeed reduce both the isothermal and cyclic oxidation rates of aluminide coatings. The effective Si additions are quite dilute (1-2 wt.%), so that a continuous SiO_2 scale should not form during exposure. According to Lee and Kröger[49], Si can dope Al_2O_3 scales, reducing dominant defect concentrations and ionic conductivity. A Si-modified, Cr-enriched aluminide diffusion coating on Mar-M247 Ni-base alloy substrates was attempted using a single-step, chloride-activated pack cementation process. Two coating treatments were tried: (a) a series of Cr-Al binary masteralloy compositions in combination with a constant silicon source (2 wt.% SiO_2) and (b) a combination of binary Cr-Al and Cr-Si binary masteralloys, both types of packs with the same activator (4 wt.% NH_4Cl).

SiO_2 Source: A summary of the coating results are listed in Table 6, and a representative cross-sectional micrograph is shown in Fig. 5a. Table 6 illustrates the difficulty in simultaneously depositing Al, Cr, and Si. Packs containing a Cr-10Al or Cr-15 wt.% Al masteralloy produced an outer $Cr_{23}C_6$ with minor amounts of Si. Beneath the outer carbide layer, Al_2O_3 internal oxide precipitates were detected by WDS x-ray maps for Al and oxygen. Figure 5a is a cross-sectional micrograph of a coating produced from a pack containing a Cr-25 wt.% Al masteralloy and NH_4Cl. This treatment produced an outward-grown, hypostoichiometric ß-NiAl coating with no second-phase α-Cr formation and very limited Cr or Si enrichment. Since the formation of an aluminide coating

required a higher Al activity (Al-rich masteralloy) than those previously used in the chrome-aluminizing treatments, relatively low Cr- and Si-halide vapor pressures resulted in low surface concentrations. To attempt an increase in Cr and Si enrichment, pack chemistries containing sequentially more SiO_2 were used. However, an outer Cr- and Si-rich carbide was formed with a large volume fraction of internal Al_2O_3 precipitates. The high SiO_2 content in the pack reduces the $AlCl_x$ vapor pressures below that necessary to form the aluminide phase. Instead, the volatile $CrCl_x$ and $SiCl_x$ species are sufficient to form an external carbide, and the increased SiO_2 content supports Al_2O_3 precipitation.

Masteralloy Combinations: Table 6 summarizes attempts to codeposit Cr and Si into NiAl by the use of two masteralloys. Packs containing Cr-10 wt.% Al or else Cr-15 wt.% Al plus Cr-10 wt.% Si produced an external, chromium- and silicon-rich carbide. Packs containing a Cr-20 wt.% Al plus Cr-Si masteralloy produced a hypostoichiometric, ß-NiAl coating, which was free of any α-Cr second-phase particles and lean in Cr and Si. To increase chromium and Si enrichment, successively higher Si containing Cr-Si masteralloy compositions and even pure Si were tried. Figure 5b is a cross-sectional micrograph of a Mar-M247 alloy coated in a pack containing 20 wt.% of Cr-20 wt.% Al, 5 wt.% of Cr-40 wt.% Si, and 4 wt.% NH_4Cl activator at 1150°C for 24 hours. This

pack produced an outward-grown, hyperstoichiometric ß-NiAl coating which lacked any α-Cr second-phase particles and was lean in Cr with a low Si content (0.22 at.%).

In the attempt to codeposit Al, Cr, and Si, the competition in the chlorination reactions between Al, Cr, and Si is very biased in favor of Al. Only a small range of pack chemistries produced the aluminide coating layer necessary for environmental durability, but these coatings lacked Cr and Si enrichment. Although the oxidation behavior of aluminide diffusion coatings may be substantially improved by Si[34,35], the realization of simultaneous Si deposition does not seem possible.

Carbon Effect: The real obstacle to depositing Al, Cr, and Si simultaneously is the relatively high carbon contents in commercial Ni-base alloys. In trying to codeposit Al and Cr into C-containing Fe- and Co-base alloys, carbon solute reacts with Cr arriving from the gas phase to form an outward-grown, blocking $Cr_{23}C_6$ layer.[9,50,51] Unless a pack with a relatively high Al activity masteralloy is used to form ß-NiAl and thereby reject carbon into the austenite substrate, external carbide coatings are formed. Most conventionally cast, Ni-base alloys have high carbon contents (Table 1), much of which is free at the 1150°C coating temperature. The sole solution is to reduce the carbon content to lower levels. For example, high-purity low-C alloys are used for directionally-solidified single crystals (Table 1), because carbides are not needed to stabilize the grain boundaries.

A simple experiment was performed to illustrate the "carbon effect" in coating Ni-base alloys. Two René 80 alloys (containing 0.8 at.% carbon) were coated in a 4 wt.% YCl_3 and 25 wt.% of Cr-7.5 wt.% Al masteralloy at 1150°C for 24 hours. After coating, a thin external carbide was identified by XRD analysis. This carbide was then mechanically removed by grinding with SiC paper. The carbide-free substrate was then recoated in an identical pack mixture and treatment to form an aluminide coating enriched with Cr and Y (10.7 at.% Cr and 0.05 at.% Y) with fewer carbides in the interdiffusion zone. This result illustrates the difficulty in coating alloys with high carbon activities, and also presents an impractical solution to the problem.

D. Kinetics and Formation Mechanisms for Cr/RE-Modified Aluminide Coatings

"Powder Contacting" Arrangement: The growth rate and compositions of the Cr/RE-modified aluminide coatings formed on René 80 at 1150°C were determined. The two pack chemistries containing 2 wt.% of either YCl_3 or else $ZrCl_4$ with 25 wt.% of Cr-7.5 wt.% Al masteralloy were studied. The dependence of the weight and outer coating thickness (measured by optical microscopy) on coating time at temperature is presented in Fig. 6. For the "powder contacting" method, weight-change measurements were tainted by pack entrapment, therefore thickness measurements may be more appropriate.

The kinetics of aluminide growth are governed by:

$$W = K_s t^n \qquad (4)$$

where W is the change in weight or layer thickness, K_s is the growth rate constant, and n is the exponent for the time dependence. The kinetic data calculated from Fig. 6 and listed in Table 7 indicate that coating growth was parabolic (n=1/2), and therefore diffusion controlled. In fact, the growth rates were comparable to those for aluminization of Ni-15 at.% Cr alloys with a Ni-40 at.% Al source and AlF_3 activator at 1100 and 1150°C.[46] Those parabolic kinetics had a growth rate constant of approximately 6 $mg/cm^2h^{\frac{1}{2}}$ at 1150°C and an apparent activation energy of 52 kcal/mol. This agreed very well with the activation energy for the interdiffusion of Ni and Al in a hypostoichiometric, ß-NiAl compound (Table 8).[52] In an earlier aluminization study, Levine and Caves[6] produced a hybrid aluminide diffusion coating from a pack containing a pure aluminum source and a NaCl activator at a temperature between 982° and 1149°C, which required no additional homogenization treatment. The growth of these aluminide coatings was parabolic and controlled by solid-state diffusion. The apparent activation energy of 88±12 kcal/mol was much higher than the interdiffusion values listed in Table 8. From that study, the higher activation energy resulted because of the formation and growth of a Ni_2Al_3 layer and its subsequent transformation to the ß-NiAl phase.

The growth rates for the YCl_3- and $ZrCl_4$-activated packs were slightly different. YCl_3-activated packs produced higher growth rates, by weight and thickness, compared to the $ZrCl_4$-activated packs (Table 7). Stable condensed activators,

such as YCl_3, may retain their (lower) equilibrium vapor pressures over the entire process time, thereby increasing the overall deposition rate or "throwing power".[53] Volatile activators, such as $ZrCl_4$, are vented from the semi-closed retort and do not retain their (higher) equilibrium vapor pressures calculated by ITSOL. Therefore, deposition and growth rates are higher than for condensed activators.[54]

The slow venting of volatile activators such as $ZrCl_4$ and $HfCl_4$ should decrease the overall rate of RE enrichment. For example, surface compositions of coatings formed in a $ZrCl_4$-activated pack versus time at temperature are shown in Fig. 7. Optimum Cr and Zr deposition (0.1-0.2 at.%) occurs within the first four hours of the coating process. Similar behavior for YCl_3-activated packs was observed, except yttrium levels were very low and generally independent of time.

Figure 8 presents a schematic illustration of the formation mechanism inferred for the Cr/RE-modified aluminide diffusion coating. Initially, the required pressure gradients exist for the volatile $RECl_x$ and $AlCl_x$ species because of the lower activities for the metallic components at the substrate (Fig. 8a). At later times (2-4 hours), the necessary partial pressure gradient for transport of the $CrCl_2(v)$ species develops because of the local depletion of aluminum in the adjacent pack, reducing the local Al activity and the vapor pressures of the $AlCl_x$ species, with a consequent decrease in Cr activity at the coating surface. Therefore, Cr is deposited and dissolved into the external surface of the

coating, saturating the ß-NiAl coating phase (Fig. 8b). Because of the limited solubility of Cr in the ß-NiAl phase[42], α-Cr second-phase particles are precipitated from the coating both during deposition and the furnace cool. The second-phase morphology is very dependent on the cooling rate following deposition. A lamellar morphology forms following a rapid furnace cool (>1.75 ^{o}C/min), whereas a spheroidal morphology forms upon a slower furnace cool (<1 ^{o}C/min). Also, α-Cr second-phase particles are formed adjacent to the original surface because outward Ni diffusion from the alloy increases the local Cr content during the coating process.[46]

"Above Pack" Arrangement: To eliminate the entrapment of pack powder, the "above pack" arrangement was used, but for given pack chemistries, thinner coatings with less Cr enrichment resulted. To explain this effect, a more detailed kinetic study was conducted. Both conventionally cast René 80 and Mar-M247 and directionally-solidified René 80H and René N4 alloys were coated in packs containing 2 wt.% NH_4Cl plus 2 wt.% Y_2O_3 and 25 wt.% of Cr-7.5 wt.% Al masteralloy at 1050^{o}, 1100^{o}, and 1150^{o}C. The average thicknesses and weight change measurements at 1150^{o}C for the coatings are presented in Fig. 9, and the corresponding kinetic values are listed in Table 9. Again isothermal coating growth is nominally parabolic, but the apparent activation energies calculated from weight and thickness changes were 27±3 and 24±5 kcal/mol, respectively. These values are well below those measured for low-activity processes using powder contacting arrangements,

where solid-state diffusion controls the coating growth (see Table 8). Therefore, another step in the coating process gains dominance. For local equilibrium both in the bulk of the pack and at the substrate surface, the gaseous metal chloride molecules must diffuse through the porous pack medium to the substrate surface. Obviously, vapor transport is inhibited by the isolation of the substrate in the porous enclosure of considerable thickness (10 mm). Vandenbulcke et al.[55] showed that coating growth rates during pack aluminizing could be reduced by increasing the diffusion distance or by reducing the total pressure of the process. Parzuchowski[53] determined the "throwing power" (i.e. the ability to coat internal passages) for a gaseous phase or out-of-contact aluminizing process for Ni-base alloys at 1093^{o}C. The "throwing power" increased as the Al-halide vapor pressure decreased. The activation energy for the rate of chloridation of Fe and Ni, where gaseous diffusion through a stagnant boundary layer is controlling, is around 10 to 17 kcal/mol.[56] The apparent activation energy for the present "above pack" process (20-30 kcal/mol) approaches these values, indicating that gaseous diffusion contributed to the control of the growth rate.

1. Substrate Effect: An effect of the substrate composition on the morphology of the interdiffusion zone carbides was observed. The interdiffusion zone for coated Mar-M247 alloys contained a dispersion of (Hf, Ta, W, Cr)-rich carbides in a ß-NiAl matrix (e.g., Fig. 5), but no continuous

chain of carbides as observed for the René alloy substrates. Such a continuous chain of blocky carbides should act as a diffusion barrier, inhibiting the outward diffusion of Ni from the substrate and reducing the growth rate of the coating. In fact, coatings produced on Mar-M247 alloy substrates possessed the fastest rates at all three temperatures (Table 9). Generally, aluminide coatings on single-crystal substrates possessed faster growth rates compared to the polycrystalline substrates (Table 9), indicating that solid-state diffusion for these low-C alloys was not blocked by carbides.

The outer ß-NiAl layer was alloyed with Co, Ti, and Cr and to a lesser extent W, Mo, Ta, Hf, Nb, and Zr from outward diffusion during coating growth. No major difference in alloying elements was observed between Mar-M247 and the René alloys to account for any second-element effect on the diffusivity of Ni and/or Al in the ß-NiAl coating.

CONCLUSIONS

1). Single-step, chloride-activated pack cementation processes for producing Cr/RE(Y,Zr)-modified and RE(Y,Zr,Hf)-doped aluminide diffusion coatings on commercial Ni-base superalloys have been developed. These coatings were produced from a pack mixture containing either an NH_4Cl activator salt plus a RE oxide source or else a RE-base chloride activator salt with a suitable Cr-Al binary masteralloy at 1150°C for 24 hours. Computer-assisted (ITSOL) equilibrium calculations were instrumental in determining these optimum pack chemistries.

2). The Cr/RE-modified aluminide coatings consisted of two phases: an outward-grown, hypostoichiometric ß-NiAl matrix and a dispersion of α-Cr second-phase particles which both precipitate near the original substrate surface and which grow inward from the gas phase along grain boundaries at the coating surface.

3). For the "above pack" process, both a substantial enrichment of Cr (6-8 at.% Cr) and an optimum concentration of the RE dissolved in the coating surface (0.02-0.08 at.% Y, 0.1-0.2 at.% Zr, or 0.15-0.2 at.% Hf). SIMS analysis detected yttrium as Y-rich precipitates (e.g., Ni_3Y or Ni_5Y) at the ß-NiAl/α-Cr interphase boundaries.

4). An attempt to dope such modified coatings with Si was not successful. Packs which resulted in ß-NiAl formation contained little Cr or Si enrichment.

5). Outward-grown aluminide (low-activity) coatings, produced from the "powder contacting" arrangement, were embedded with Al_2O_3 and RE oxide pack particles. Physical separation of substrates from the powder mixture in an "above pack" arrangement eliminated powder entrapment, but reduced coating growth rates and Cr enrichment of the surface. The apparent activation energy for this coating process between 1050-1150°C was 27 ± 3 and 24 ± 5 kcal/mol from weight and thickness changes, respectively; these values are about 50% below that for the solid-state interdiffusion of Ni and Al in the ß-NiAl

compound. Pack isolation inhibits vapor transport to support coating growth, so that the coating rate is limited more importantly by gaseous diffusion.

ACKNOWLEDGMENTS

The authors wish to thank D. Little for EPMA results, C. A. McDonald for WDS results, R. Hussey of the National Research Council, Ottawa, for SIMS analysis, W. B. Connor of GE Aircraft Engines for supplying directionally-solidified alloys, and A. J. Sedriks of ONR and T. A. Kircher of NADC for funding the projects N00014-87-K-0030 and N00014-90-J-1765.

REFERENCES

1. R.L. McCarron, N.R. Lindblad, and D. Chatterji, Corrosion, **32** (1976) 476.

2. P. Galmiche, Metals and Materials, **2** (1968) 241.

3. E. Godlewska and K. Godlewski, Oxid. Met., **22** (1984) 117.

4. J.E. Restall, U.S. Patent #4,687,684 (1987).

5. P.N. Walsh, in Proceeding of the Fourth International Conference on Chemical Vapor Deposition, G.F. Wakefield and J.M. Blocher (Eds.), The Electrochemical Society, Inc., Pennington, NJ (1973) 147.

6. S.R. Levine and R.M. Caves, This Journal, **121** (1974) 1051.

7. C. Wagner, Corr. Sci., **5** (1965) 751.

8. W. Johnson, K. Komarek, and E. Miller, Trans. AIME, **242** (1968) 1685.

9. R.A. Rapp, D. Wang, and T. Weisert, in Metallurgical Coatings, M. Khobaib and R. Krutenat (Eds.), TMS-AIME, Warrendale, PA (1987) 131.

10. D.M. Miller, S.C. Kung, S.D. Scarberry, and R.A. Rapp, Oxid. Met., **29** (1988) 239.

11. G.H. Marijnissen, in First International Conference on Surface Engineering, Volume III, Brighton, U.K. (1985) 81.

12. R. Bianco and R.A. Rapp, in High Temperature Chemistry V, W.B. Johnson and R.A. Rapp (Eds.), The Electrochemical Society Inc., Pennington, NJ (1990) 211.

13. S.C. Kung and R.A. Rapp, Oxid. Met., **32** (1989) 89.

14. D.L. Deadmore and C.E. Lowell, Ibid, **11** (1977) 91.

15. F.A. Golightly, F.H. Stott, and G.C. Wood, Ibid, **10** (1976) 163.

16. A. Kumar, M. Nasrallah, and D.L. Douglass, Ibid, **8** (1974) 227.

17. I.M. Allam, D.P. Whittle, and J. Stringer, Ibid, **12** (1978) 35.

18. J.K. Tien and F.S. Pettit, Metall. Trans., **3** (1972) 1587.

19. J.R. Nicholls and P. Hancock, in First International Conference on Active Elements, Petten, The Netherlands (1988) 1.

20. A. M. Huntz, Mater. Sci. Eng., **87** (1987) 251.

21. N. Patibandla, T.A. Ramanarayanan, and F. Cosandey, This Journal, **138** (1991) 2176.

22. K. Przybylski, A.J. Garratt-Reed, and G.J. Yurek, Ibid, **135** (1987) 509.

23. K. Przybylski and G.J. Yurek, Ibid, **135** (1987) 517.

24. E. Tsuzi, Metall. Trans., **11A** (1980) 1965.

25. T.A. Ramanarayanan, M. Raghavan, and R. Petkovic-Luton, This Journal, **131** (1984) 923.

26. T.A. Ramanarayanan, R. Ayer, R. Petkovic-Luton, and D.P. Leta, Oxid. Met., **29** (1988) 445.

27. J.G. Smeggil, N.S. Bornstein, and M.A. DeCrescente, Ibid, **30** (1988) 259.

28. J.L. Smialek, Metall. Trans., **18A** (1987) 164.

29. J.L. Smialek, Ibid, **22A** (1991) 739.

30. B. Pieraggi and R.A. Rapp, in Proceedings of the 3rd

International Symposium on High-Temperature Corrosion and Protection of Materials, Les Embiez, France (1992).

31. C.A. Barrett, Oxid. Met., **30** (1988) 361.

32. J. Jedlinski and S. Mrowec, Mater. Sci. Eng., **87** (1987) 281.

33. S. Mrowec and J. Jedlinski, in Oxidation of High-Temperature Intermetallics, T. Grobstein and J. Doychak (Eds.), TMS-AIME, Warrendale, PA (1988) 57.

34. G.J. Santoro, D.L. Deadmore, and C.E. Lowell, NASA TN D-6414, 1971.

35. C.E. Lowell and G.J. Santoro, NASA TN D-6838, 1972.

36. J. Jedlinski, K. Godlewski, and S. Mrowec, Mater. Sci. Eng., **A121** (1989) 539.

37. W. Fuhui, L. Hanyi, B. Linxiang, and W. Weitao, Ibid, **A121** (1989) 387.

38. D.C. Tu, C.C. Lin, S.J. Liao, and J.C. Chou, J. Vac. Sci. Techn., **A4** (1986) 2601.

39. G. LePrince, S. Alpérine, L. Vandenbulcke, and A. Walder, Mater. Sci. Eng., **A121** (1989) 419.

40. H. Flynn, A.E. Morris, and D. Carter, in Proceedings of the 25th CIM Conference of Metallurgists, TMS-CIM, Toronto, Canada (1986) 67.

41. R. Bianco, R.A. Rapp, and N.S. Jacobson, Oxid. Met., **38** (1992) 33.

42. S.M. Merchant and M.R. Notis, Mater. Sci. Eng., **66** (1984) 47.

43. P. Shen, D. Gan, and C.C. Lin, Ibid., **78** (1986) 171.

44. B.K. Gupta, A.K. Sarkel, and L.L. Seigle, Thin Solid Films **39** (1976) 313.

45. E.W.A. Young and J.H.W. deWit, Oxid. Met., **26** (1986) 351.

46. D.C. Tu and L.L. Seigle, Thin Solid Films, **95** (1982) 47.

47. H.W. Grünling and R. Bauer, Ibid, **95** (1982) 1.

48. L. Swadzba, B. Formanek, and A. Maciejny, Mater. Sci. Eng.

A121 (1989) 407.

49. C.H. Lee and F.A. Kröger, J. Amer. Cer. Soc., **68** (1985) 92.

50. V.A. Ravi, P.A. Choquet, and R.A. Rapp, in Oxidation of High-Temperature Intermetallics, T. Grobstein and J. Doychak (Eds.), TMS-AIME, Warrendale, PA (1988) 127.

51. D.M. Miller, Ph.D. Thesis, The Ohio State University, 1990.

52. S. Shankar and L.L. Seigle, Metall. Trans., **9A** (1978) 1468.

53. R.S. Parzuchowski, Thin Solid Films, **45** (1977) 349.

54. S.C. Kung and R.A. Rapp, This Journal, **135** (1988) 731.

55. L. Vandenbulcke, G. LePrince, and B. Nciri, Mater. Sci. Eng., **A121** (1989) 379.

56. P.L. Daniel and R.A. Rapp, in Advances in Corrosion Science and Technology, Vol. 5, M.G. Fontana and R.W. Staehle (Eds.), Plenum Press, New York (1975) 55.

57. L. Singheiser, G. Wahl, and W. Thiele, Thin Solid Films, **107** (1983) 443.

58. H.M.J. Mazille, Ibid, **65** (1980) 67.

FIGURE CAPTIONS

1. Schematic diagram of the "above pack" arrangment.

2. Cross-sectional optical micrograph of a René 80 alloy susbtrate coated at 1150°C for 24 hours in a (2:1) YCl_3/$CrCl_2$-activated pack containing 25 wt.% of Cr-7.5 wt.% Al masteralloy. (a) "Powder contacting" and (b) "above pack" arrangement.

3. SIMS maps for Ni, Al, Cr, and Y of a René 80 alloy substrate coated at 1150°C for 24 hours in 3 wt.% YCl_3-activated pack containing 25 wt.% of Cr-7.5 wt.% Al masteralloy. "Above pack" arrangement.

4. Cross-sectional optical micrograph for a René 80 alloy substrate coated at 1150°C for 24 hours in 2 wt.% NH_4Cl-activated pack containing 2 wt.% Y_2O_3 and 25 wt.% of Cr-10 wt.% Al masteralloy. "Above pack" arrangement.

5. Cross-sectional optical micrograph for a Mar-M247 alloy substrate coated at 1150°C for 24 hours in 4 wt.%

NH_4Cl-activated pack containing (a) 4 wt.% SiO_2 and 25 wt.% of Cr-25 wt.% Al masteralloy or (b) 20 wt.% of Cr-20 wt.% Al and 5 wt.% Cr-40 wt.% Si masteralloys. "Above pack" arrangement.

6. Kinetic results for a René 80 alloy substrate coated at 1150°C in a 2 wt.% YCl_3- or $ZrCl_4$-activated pack containing 25 wt.% of Cr-7.5 wt.% Al masteralloy: (a) weight and (b) coating thickness changes. "Powder contacting" arrangement.

7. Kinetic results for a René 80 alloy substrate coated at 1150°C in a 2 wt.% $ZrCl_4$-activated pack containing 25 wt.% of Cr-7.5 wt.% Al masteralloy: (a) composition changes and (b) magnification of (a). "Powder contacting" arrangement.

8. Schematic illustrations of the formation mechanism for the modified aluminide coating: (a) relatively short times and (b) longer times.

9. Kinetic results for Ni-base alloy substrates coated at 1150°C in a 2 wt.% NH_4Cl-activated pack containing 2 wt.% Y_2O_3 and 25 wt.% of Cr-7.5 wt.% Al masteralloy: (a) weight and (b) coating thickness changes. "Above pack" arrangement.

Table 1: Nominal compositions of nickel-base alloys (at.%).

Alloy	Ni	Cr	Co	Nb	Mo	W	Al	Ti	Ta	Other
IN 713LC	bal	13	-	1	2.5	-	12	.7	-	.2C,.06Zr .5B
Mar-M247	bal	9	10	-	.4	3.2	12	1.2	1	.8C,.06Zr .1B,.5Hf
René 80	bal	15	9	-	2.3	1.2	6	6	-	.8C,.08B, .02Zr
René 80H[a]	bal	15	9	-	2.3	1.2	6	6	-	.8C,.08B, .02Zr,.2Hf
René N4[b]	bal	11	7.5	.3	1	2	9	4	1.5	.3C,.02B .05Hf

a=columnar-grained, directionally solidified
b=single-crystal, " "

Table 2: Coatings on René 80 alloy substrates coated at 1150°C for 24 hours in a pack containing 25 wt.% of Cr-7.5 wt.% Al masteralloy. "Powder contacting" arrangement.

Pack Chemistry	Average Surface Composition Ni	Al	Cr	RE (at.%)	XRD Phase
NH_4Cl(2)	45.7	40.1	9.9	-	Al_2O_3,ß-NiAl
* " " /ZrO_2(2)	44.9	45.6	3.1	2.0	", ", ZrO_2
YCl_3(2)	43.5	35.9	10.7	.03	Al_2O_3,ß-NiAl
" (4)	42.4	35.8	12.1	.02	", "
$YCl_3/CrCl_2$(2)	45.3	38.2	13.8	.02	" , " ,α-Cr
$ZrCl_4$(2)	49.3	35.2	7.2	.18	" , "

Amounts in parentheses, wt.%.
*=Cr-10 wt.% Al masteralloy used.

Table 3: Coatings on René 80 alloy substrates coated at 1150°C for 24 hours in a pack containing 25 wt.% of Cr-7.5 wt.% Al masteralloy. "Above pack" arrangement.

Pack Chemistry	Average Surface Composition Ni	Al	Cr	RE (at.%)	XRD Phase
YCl_3(2)	48.5	40.2	4.3	.02Y	ß-NiAl
" (4)	48.8	35.9	6.2	.02Y	"
",Y_2O_3(2)	49.4	39.7	4.6	.01Y	"
", " (4)	50.4	37.3	5.8	.02Y	"
$ZrCl_4$(2)	49.8	40.1	5.0	.07Zr	"
" (4)	49.8	33.4	7.2	.24Zr	"
" (6)	50.1	34.1	7.8	.16Zr	"
NH_4Cl,ZrO_2(2)	47.5	36.8	7.5	.18Zr	"
" " (4)	52.9	35.1	5.3	.17Zr	"
" " (6)	50.9	37.3	4.8	.22Zr	"
" ,Y_2O_3(2)	49.9	40.6	4.3	.02Y	"
" " (4)	47.9	38.9	6.4	.03Y	"
YCl_3/$CrCl_2$(2:1)	49.7	35.8	7.5	.03Y	"
" " (1:1)	47.4	37.2	7.2	.02Y	"

Amounts in parentheses, wt.%.

Table 4: Coatings on nickel-base alloy substrates coated at 1150°C for 24 hours in a pack containing 4 wt.% activator and 25 wt.% masteralloy. "Above pack" arrangement.

Pack Chemistry	Average Surface Composition Ni	Al	Cr	RE (at.%)	XRD Phase
René 80:					
YCl_3,Cr5Al	47.4	35.1	10.5	.04Y	ß-NiAl
" ,Cr6Al	48.1	40.6	4.6	.03Y	"
$ZrCl_4$,Cr5Al	13.6	2.1	79.6	-	$Cr_{23}C_6$
" ,Cr6Al	47.2	41.9	4.5	.23Zr	ß-NiAl
IN 713LC:					
YCl_3,Cr5Al	50.1	32.8	12.3	.07Y	ß-NiAl,α-Cr
" ,Cr6Al	46.8	43.6	3.8	.05Y	ß-NiAl
$ZrCl_4$,Cr5Al	15.3	2.5	78.7	-	$Cr_{23}C_6$
" ,Cr6Al	51.6	44.1	4.1	.10Zr	ß-NiAl

Table 5: Coatings on IN 713LC and Mar-M247 alloy substrates coated at 1150°C for 24 hours in a pack containing 25 wt.% of Cr-10 wt.% Al masteralloy. "Above pack" arrangement.

Pack Chemistry	Average Surface Composition Ni	Al	Cr	RE (at.%)	XRD Phase
IN 713LC:					
NH_4Cl,Y_2O_3(2)	49.1	45.1	2.1	.06Y	ß-NiAl
" ,ZrO_2(2)	51.4	45.6	2.6	.21Zr	"
" ,no RE	50.3	44.8	2.6	-	"
YCl_3(4)	49.8	45.8	2.9	.08Y	"
$ZrCl_4$(4)	52.3	44.1	2.5	.17Zr	"
$HfCl_4$(4)	50.2	46.9	2.8	.15Hf	"
Mar-M247:					
NH_4Cl,Y_2O_3(2)	50.2	46.6	2.2	.05Y	"
" ,no RE	49.2	45.8	2.4	-	"
YCl_3(4)	48.9	46.3	2.5	.04Y	"

Amounts in parentheses, wt.%.

Table 6: Coatings on Mar-M247 alloy substrates coated at 1150°C for 24 hours in 4 wt.% NH_4Cl-activated pack containing 20 wt.% of Cr-Al masteralloy and a Si source. "Above pack" arrangement.

Pack Chemistry	Average Surface Composition Ni	Al	Cr	Si (at.%)	XRD Phase
SiO_2 source:					
Cr15Al,(2)	15.3	2.1	78.5	1.25	$Cr_{23}C_6$
Cr20Al,(2)	49.2	41.3	3.5	.08	ß-NiAl
" ,(4)	14.5	2.3	79.3	1.87	$Cr_{23}C_6$
Cr25Al,(2)	50.1	40.5	3.1	.02	ß-NiAl
Cr-Si masteralloy(5):					
Cr10Al,Cr10Si	6.1	0.1	90.4	.62	$Cr_{23}C_6$
Cr20Al,Cr20Si	46.7	45.9	2.4	.08	ß-NiAl
" ,Cr30Si	42.1	52.4	2.6	.13	"
" ,Cr40Si	40.1	54.7	1.9	.22	"
Cr10Al,Si	49.1	41.4	3.5	.08	"

Amounts in parentheses, wt.%.

Table 7: Kinetic results of René 80 alloy substrates coated at 1150°C in a "powder contacting" arrangement with a pack containing 2 wt.% activator and 25 wt.% of Cr-7.5 wt.% Al masteralloy.

Average Growth Kinetics

Activator	Ks"($\mu m/h^{\frac{1}{2}}$)	Ks'($mg/cm^2h^{\frac{1}{2}}$)	n"(th.)	n'(wt.)
YCl_3	23.68	5.94	.52	.56
$ZrCl_4$	22.40	5.30	.51	.47
AlF_3,1150°C*	-	6.02	-	.51
" ,1100°C*	-	3.10	-	.55

*=Ni-40 at.% Al masteralloy[46]

Table 8: Aluminizing/chromizing and interdiffusion studies for the Ni-Al system.

Investigation	Activation Energy (kcal/mol)	Reference
Interdiffusion Data:		
Ni-38 at.% Al	55±2	[52]
Ni-45 at.% Al	59±6	"
Ni-51 at.% Al	43±8	"
Pack Aluminizing:		
NaCl, pure Al	88±12	[6]
AlF_3, Ni-40at.%Al	51±5	[46]
*This Study	27±3 (by weight)	
* " "	25±5 (by thickness)	
CVD Aluminizing:		
$AlCl_3$ source	41±5	[57]
CVD Chromizing:		
NH_4Cl/Cr source	50+4	[58]

*="Above pack" arrangement.

Table 9: Kinetic results for nickel-base alloy substrates coated in an "above pack" arrangement with a 2 wt.% NH_4Cl-activated pack containing 2 wt.% Y_2O_3 and 25 wt.% of Cr-7.5 wt.% Al masteralloy.

Average Growth Kinetics

Alloy	Ks"($\mu m/h^{\frac{1}{2}}$)	Ks'($mg/cm^2 h^{\frac{1}{2}}$)	n"(th.)	n'(wt.)
1150°C:				
Mar-M247	16.21	2.71	.41	.42
René 80	17.09	2.46	.43	.42
René 80H	16.22	2.44	.42	.39
René N4	16.36	2.36	.40	.37
1100°C:				
Mar-M247	12.02	1.71	.47	.42
René 80	11.61	1.46	.37	.30
René 80H	12.13	1.52	.57	.40
René N4	9.85	1.57	.39	.43
1050°C:				
Mar-M247	9.34	1.31	.68	.58
René 80	6.21	1.13	.55	.58
René 80H	7.14	0.96	.53	.56
René N4	7.07	1.09	.60	.62

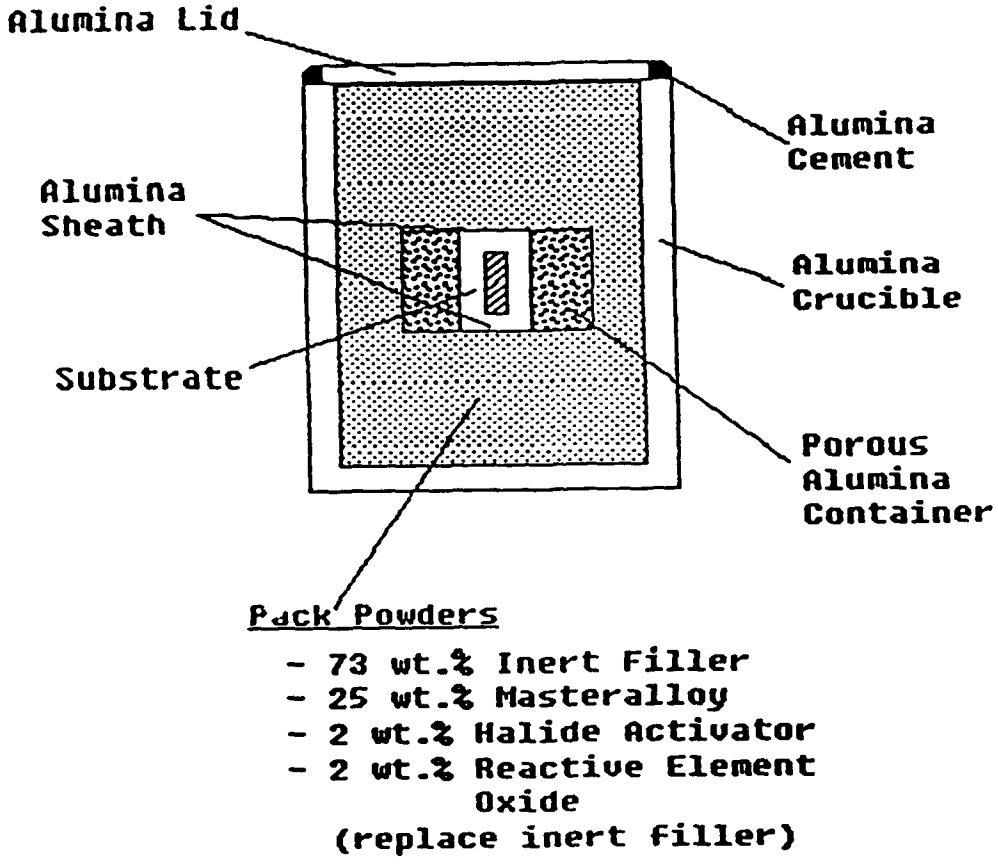

Figure 1: Schematic diagram of the "above pack" arrangement.

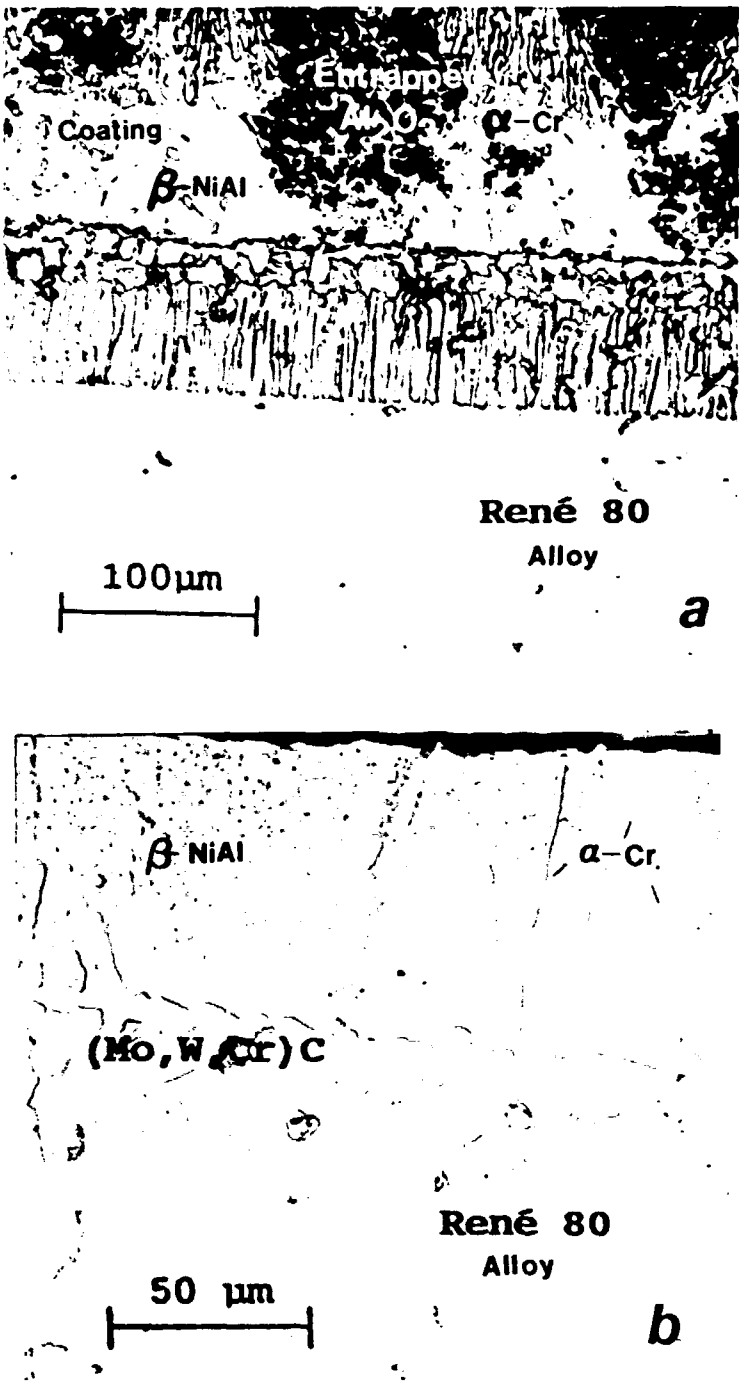

Figure 2: Cross-sectional optical micrograph for a René 80 alloy substrate coated at 1150°C for 24 hours in a (2:1) $YCl_3/CrCl_2$-activated pack containing 25 wt.% of Cr-7.5 wt.% Al masteralloy. (a) "Powder contacting" and (b) "above pack" arrangement.

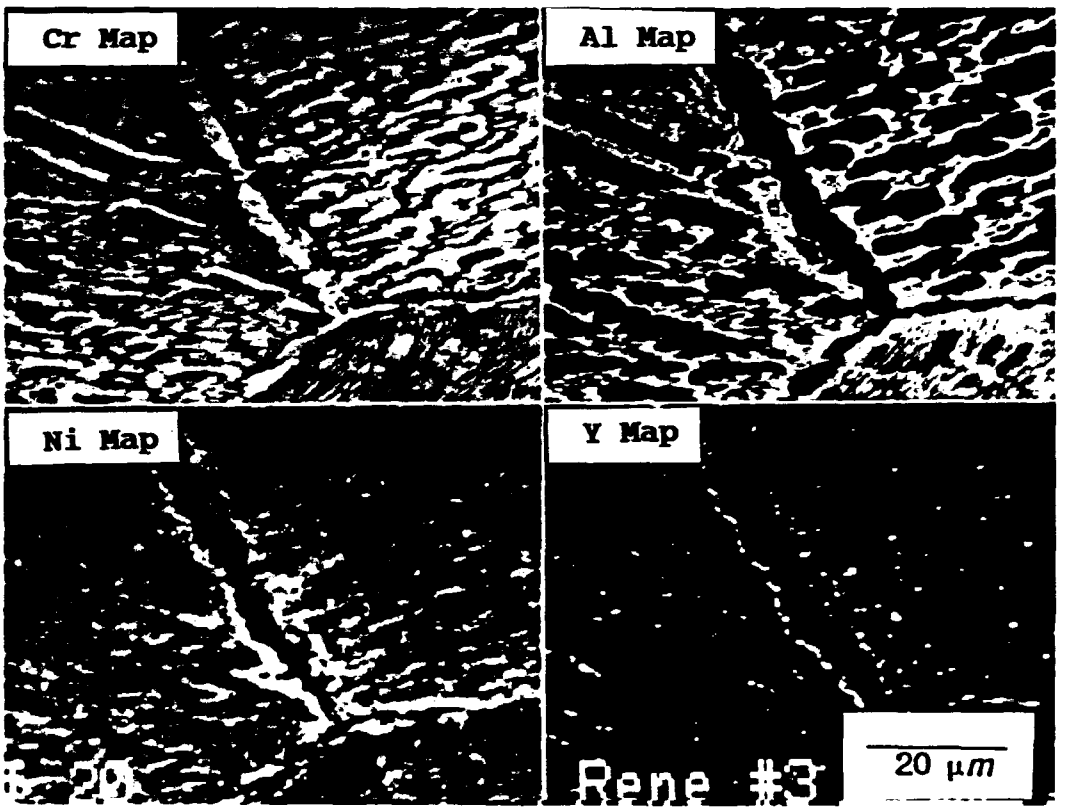

Figure 3: SIMS maps for Ni, Al, Cr, and Y of a René 80 alloy substrate coated at 1150°C for 24 hours in a 3 wt.% YCl_3-activated pack containing 25 wt.% of Cr-7.5 wt.% Al masteralloy. "Above pack" arrangement.

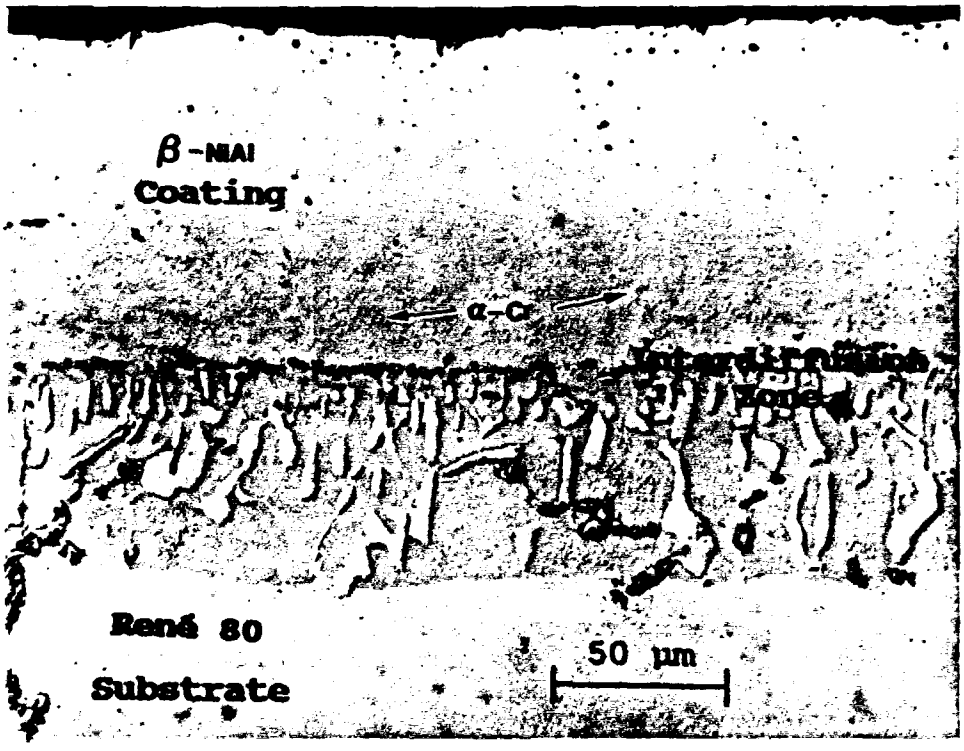

Figure 4: Cross-sectional optical micrograph of a René 80 alloy substrate coated at 1150°C for 24 hours in a 2 wt.% NH_4Cl-activated pack containing 2 wt.% Y_2O_3 and 25 wt.% of Cr-10 wt.% Al masteralloy. "Above pack" arrangement.

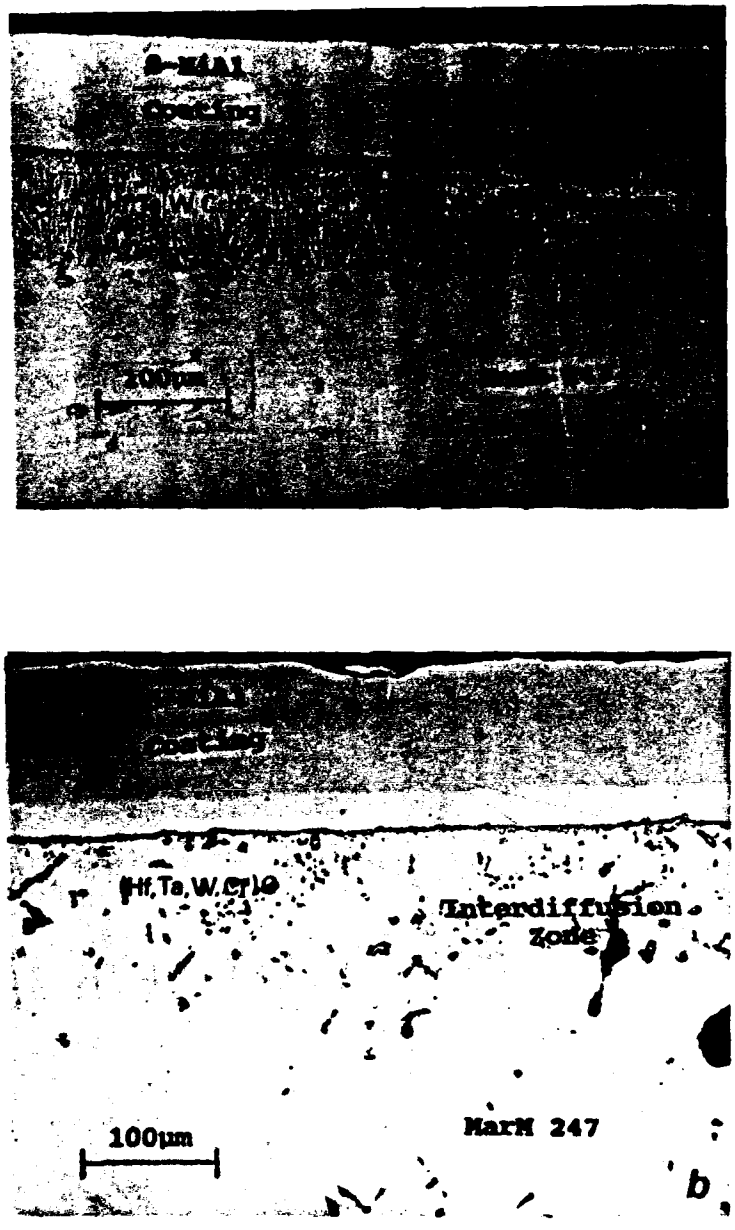

Figure 5: Cross-sectional optical micrograph of a Mar-M247 alloy substrate coated at 1150°C for 24 hours in 4 wt.% NH_4Cl-activated pack containing (a) 4 wt.% SiO_2 and 25 wt.% of Cr-25 wt.% Al masteralloy or (b) 20 wt.% of Cr-20 wt.% Al and 5 wt.% Cr-40wt.% Si masteralloys. "Above pack" arrangement.

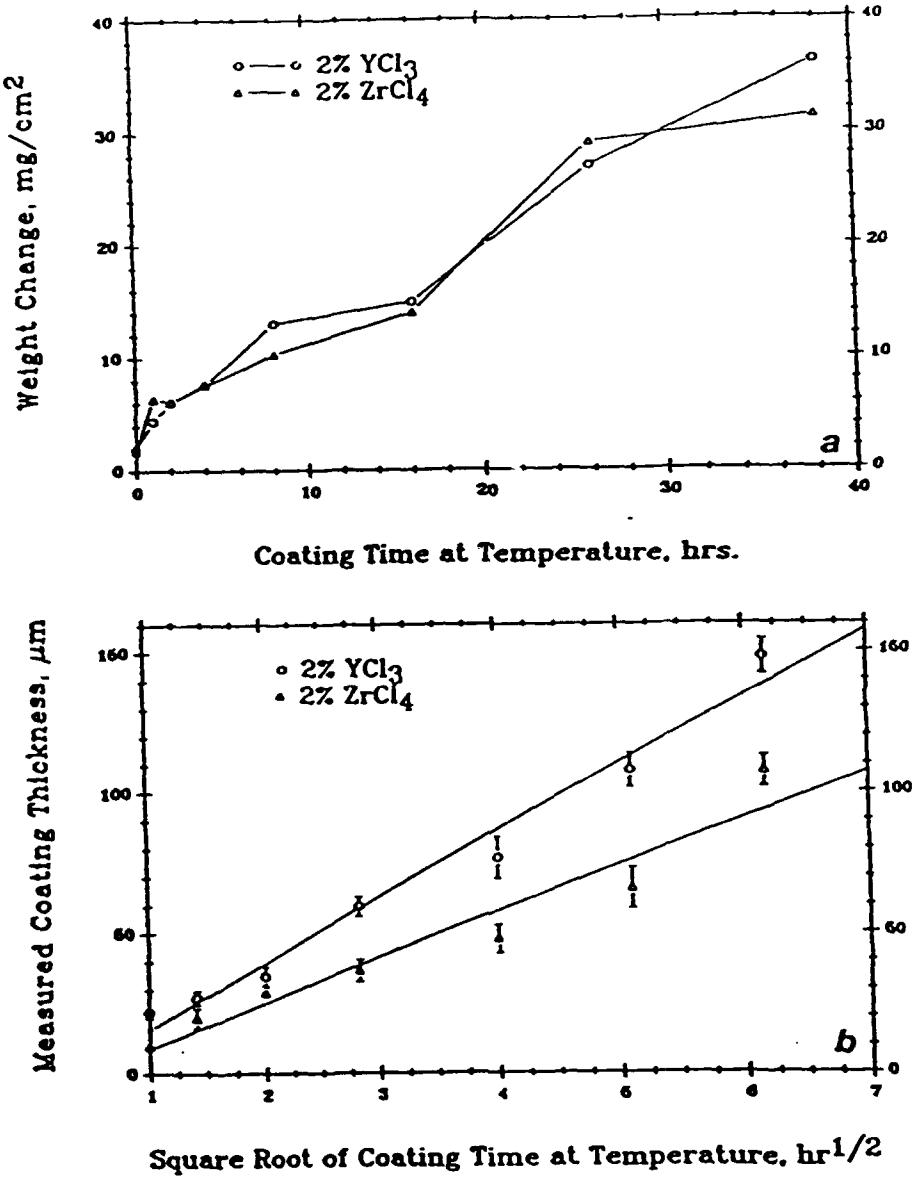

Figure 6: Kinetic results for a René 80 alloy substrate coated at 1150°C in a 2 wt.% YCl_3- or $ZrCl_4$-activated pack containing 25 wt.% of Cr-7.5 wt.% Al masteralloy: (a) weight and (b) coating thickness changes. "Powder contacting" arrangement.

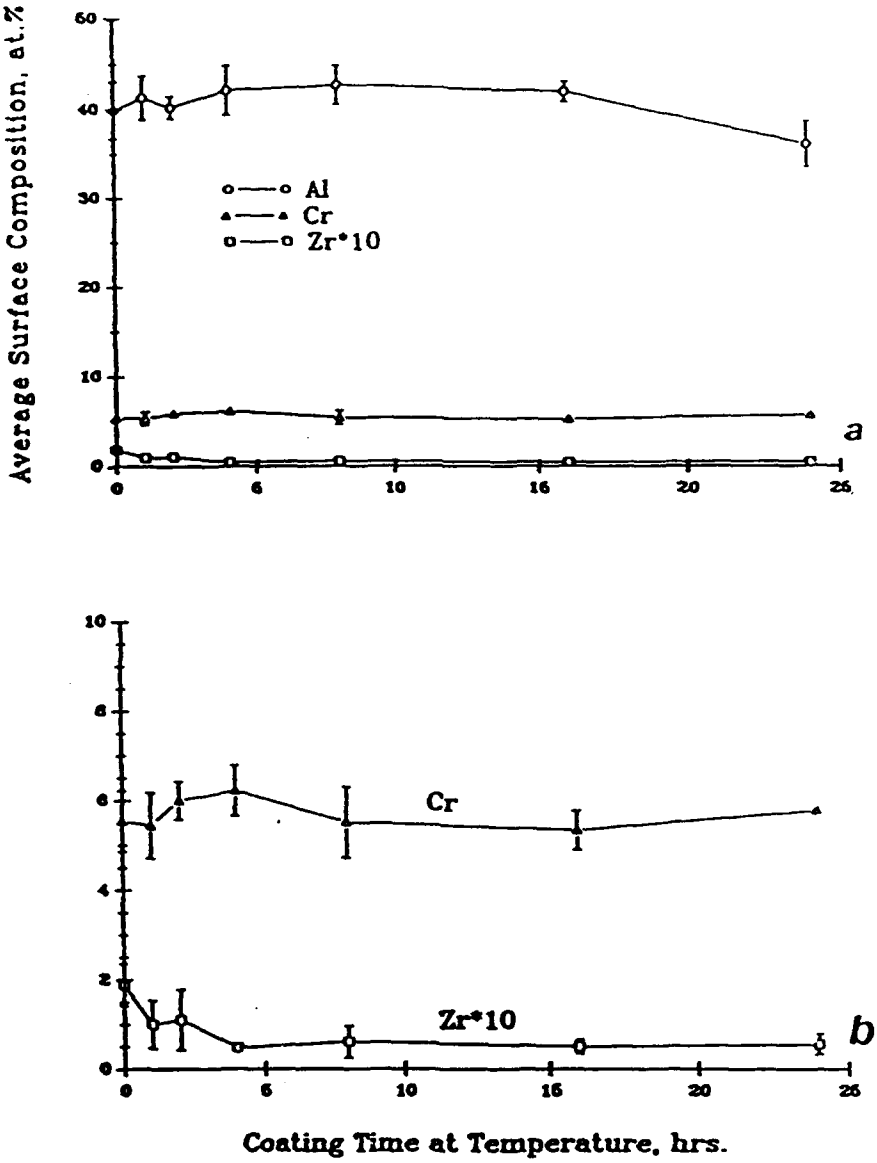

Figure 7: Kinetic results for a René 80 alloy substrate coated at 1150°C in a 2 wt.% $ZrCl_4$ -activated pack containing 25 wt.% of Cr-7.5 wt.% Al masteralloy: (a) composition changes and (b) magnification of (a). "Powder contacting" arrangement.

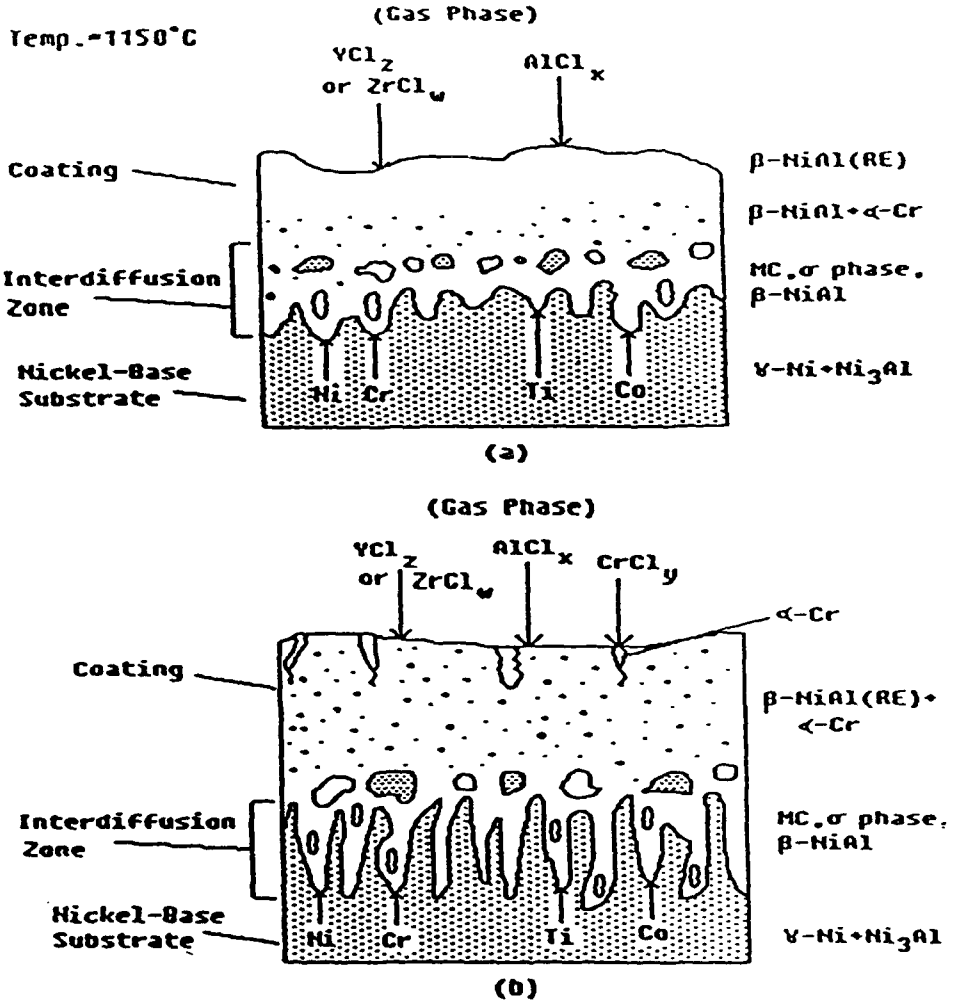

Figure 8: Schematic illustrations of the formation mechanism for the modified aluminide coating process: (a) relatively short times and (b) longer times.

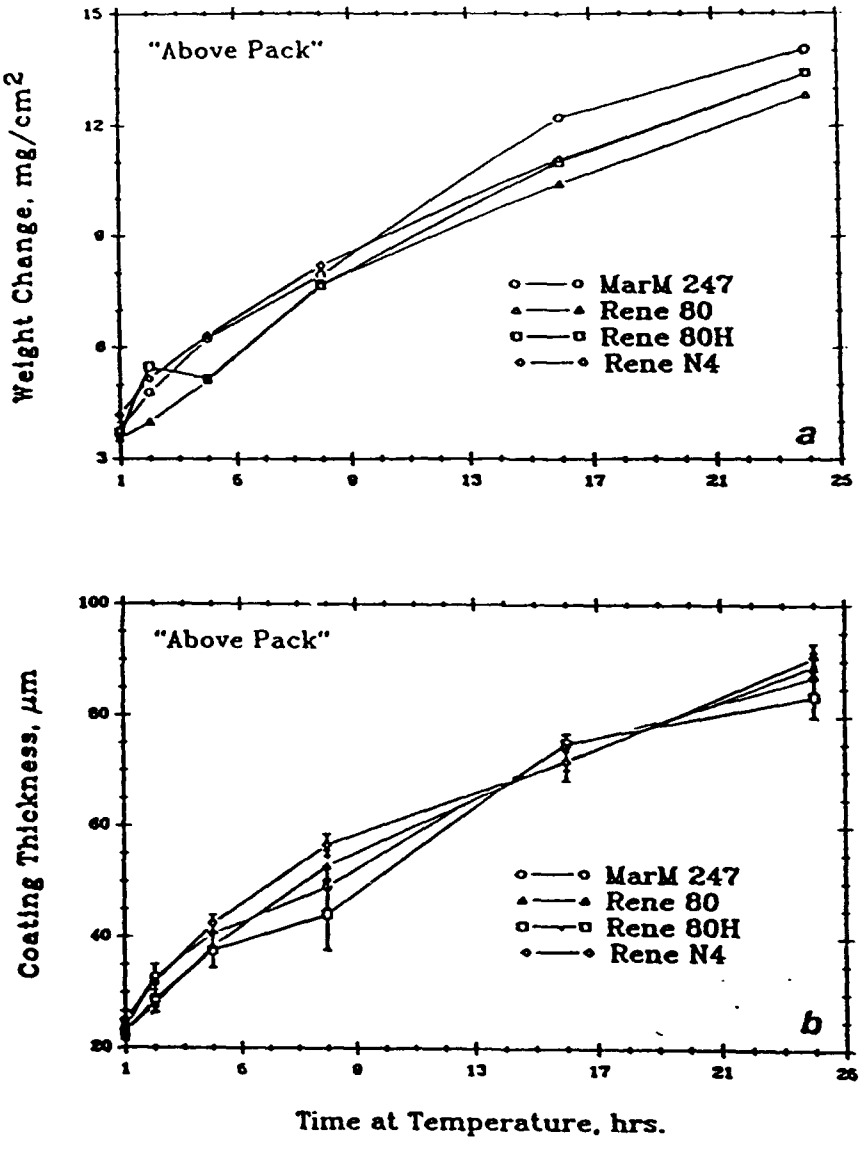

Figure 9: Kinetic results for Ni-base alloy substrates coated at 1150°C in a 2 wt.% NH_4Cl-activated pack containing 2 wt.% Y_2O_3 and 25 wt.% of Cr-7.5 wt.% Al masteralloy: (a) weight and (b) coating thickness changes. "Above pack" arrangement.

CHROMIUM AND REACTIVE ELEMENT(RE)-MODIFIED ALUMINIDE DIFFUSION COATINGS ON SUPERALLOYS: Environmental Testing

Robert Bianco and Robert A. Rapp
Department of Materials Science and Engineering
The Ohio State University
Columbus, Ohio 43210

James L. Smialek
National Aeronautics and Space Administration
Lewis Research Center
Cleveland, Ohio 44135

ABSTRACT

The isothermal oxidation of RE-doped aluminide coatings on IN 713LC alloy substrates at 1100°C in air formed a continuous, slow-growing α-Al_2O_3 scale after 44 hours of exposure. RE-free aluminide coatings were characterized by a cracked oxide scale which exposed an underlying voided coating surface.

The cyclic oxidation behavior of Cr/RE-modified aluminide diffusion coatings on René 80 and IN 713LC alloy substrates, and of RE-doped aluminide coatings on IN 713LC alloy substrates, at 1100°C in static air was determined. Coatings deposited by the "above pack" (AP) arrangement, as opposed to the "powder contacting" (PC) arrangement, showed improved resistance to cyclic oxidation attack. RE-doped and Cr/RE-modified aluminide coatings exhibited considerably more adherent protective Al_2O_3 scales compared to undoped aluminide coatings.

The hot corrosion behavior of Cr/RE-modified aluminide coatings on René 80 and Mar-M247 alloy substrates at 900°C in

a 0.1% SO_2/O_2 gas mixture was also determined. The Cr/RE-modified aluminide coatings provided better resistance to hot corrosion attack (i.e., thin film studies) than commercial low-activity aluminide coating. Coating lifetimes were strongly dependent on the chromium surface composition, since a mixed $(Al,Cr)_2O_3$ scale better resists attack by the molten salt.

KEY WORDS: Aluminide Diffusion Coatings, Oxidation, Oxide Scale Adherence, and Hot Corrosion.

INTRODUCTION

In service, diffusion aluminide coatings are exposed to aggressive environments and applied stresses at high temperatures and are known to suffer both mechanical and chemical degradation. The intermetallic compound of aluminide coatings can be the weak link in the fatigue resistance and fracture toughness of the coating/component couple.[1] Also, low-activity coatings, which form by outward diffusional growth, have a tendency to embed pack powder particles into their external layer.[2] These indigenous inclusions can reduce the fatigue resistance of the coating/component even further.

Aluminide diffusion coatings for use in gas turbines suffer from three forms of chemical degradation: (a) interdiffusion, (b) oxidation, and (c) fused salt (hot corrosion) attack. Interdiffusion and hot corrosion indirectly affect the surface or coating composition, thereby reducing the oxidation resistance of the coated component.

Interdiffusion: Smialek and Lowell[3] studied the effect of interdiffusion on the degradation of aluminide diffusion coatings on IN 100 and Mar-M200 commercial Ni-base alloys which were vacuum annealed for 300 hours at 1100°C. The coatings thickened and the Al concentration at the surface decreased, changes attributed to interdiffusion of the coating components with the substrate. In addition, carbides within the interdiffusion zone began to dissociate while others coarsened with time, thereby reducing the integrity of the interdiffusion zone. In fact, stable carbides aligned parallel to the surface may block interdiffusion degradation. For example, Mar-M200 alloys (which contain 12% W, 1% Nb, and 0.15% C) formed a blocky chain of carbides and did not suffer any significant interdiffusion degradation, whereas IN 100 alloys (which contain only 3% Mo, 5% Ti, and 0.18% C) formed more sporadic carbides and did suffer more severe interdiffusion degradation. Such prediffused coatings on IN 100 alloys suffered severe reductions in coating lifetimes upon cyclic oxidation in static air at 1100°C.[3] For these hyperstoichiometric (Al-rich) ß-NiAl compounds[4], depletion of Al both resulting from the growth of Al_2O_3 scales and interdiffusion with the substrate leads to an eventual failure (i.e. the inability to form a protective Al_2O_3 scale). Low-activity coatings, consisting of a hypostoichiometric (Ni-rich) ß-NiAl, where Ni is the dominant diffusing element, may not be so susceptible to interdiffusion degradation.[4]

Oxidation: The oxidation behavior of Ni-Al alloys has been widely investigated.[5-11] Pettit[5] studied the oxidation behavior of a series of Ni-Al alloys (Ni-3 to 25 wt.% Al) between 900 and 1300°C in 0.1 atm oxygen. Alloys with greater than 17 wt.% Al (or 32 at.%) exhibited the best oxidation behavior, i.e. parabolic kinetics limited by the growth of an external Al_2O_3 scale. Hindam and Smeltzer[6] studied the oxidation behavior of ß-NiAl (Ni-32 wt.% or 50 at.% Al) between 1000 and 1300°C in pure O_2. Slow parabolic kinetics resulted from the growth of a ridged, external α-Al_2O_3 scale after 30 minutes exposure. Oxide spalling or loss of adherence upon furnace cooling was attributed to the formation of interfacial voids during oxide growth.

The mechanism of Al_2O_3 growth on ß-NiAl is still widely debated. Hindam and Smeltzer[6] used inert platinum markers to determine that Al_2O_3 growth on undoped ß-NiAl is controlled by inward oxygen diffusion. However, the ridged scale morphology is often ascribed to outward Al diffusion via short-circuit paths, such as grain boundaries. Prescott et al. [7] confirmed that oxide grain boundaries are short-circuit paths for Al diffusion during alumina growth on ß-NiAl. Young and de Wit[8] used a two-stage, $^{16}O_2$ and then $^{18}O_2$, oxidation treatment with secondary ion mass spectroscopy (SIMS) analysis to determine the Al_2O_3 growth mechanism on ß-NiAl compounds. Outward Al_2O_3 growth involving cation diffusion occurred at 1000°C on undoped and slightly Y-doped NiAl compounds. NiAl compounds doped with 0.5 wt.% Y or more

exhibited Al_2O_3 growth controlled by inward anion diffusion.

In the transient oxidation of ß-NiAl, $NiAl_2O_4$ spinel, γ-Al_2O_3, and θ-Al_2O_3 were detected by transmission electron microscopy (TEM).[9,10] With increasing time, transformation of the metastable Al_2O_3 phases (whiskers) into α-Al_2O_3 (ridges) occurred at the scale/gas interface and proceeded inward. Metastable Al_2O_3 phases have much faster oxidation rates compared to the more protective α-Al_2O_3 phase, however the addition of a reactive element (e.g., Zr, Hf, Y), or significant Cr, facilitates the formation of the slower-growing, more protective α-Al_2O_3 scale.[11,12]

The oxidation behavior of coatings with an external ß-NiAl layer has also been investigated.[13-15] Both low- and high-activity coatings exhibit excellent oxidation resistance. However, after about 100 hours of exposure at 1200°C, the oxidation resistance drops considerably. Degradation of aluminide coatings occurs because of the selective depletion or consumption of Al from the coating, by the repetitive formation and spalling of protective Al_2O_3 scales and/or interdiffusion. Eventually, the reduced Al surface concentration is insufficient to support the formation of a protective Al_2O_3 scale, and less protective, nonadherent $NiAl_2O_4$ and NiO scales form.

The degradation of aluminide coatings can be reduced if the adherence of protective Al_2O_3 scales is improved, e.g. reducing Al interdiffusion losses or reducing the oxidation rate. In particular, small additions of reactive elements

(e.g., Y, Zr, Hf) considerably improve the adherence of thermally grown Al_2O_3 scales on bulk ß-NiAl compounds.[16-20] Recently, Bianco and Rapp[2] developed a RE-doped aluminide diffusion coating via the pack cementation process, which is expected to provide the same beneficial result.

Fused Salt Attack (Hot Corrosion): Hot corrosion is an important mode of material degradation in marine and industrial gas turbines, and it may occur in aircraft engines. Hot corrosion is the accelerated attack of a metallic component resulting from the presence of a condensed fused salt film (e.g., Na_2SO_4, $NaVO_3$, NaCl) in an oxidizing environment. The sulfation of NaCl vapor, introduced as an impurity either in the fuel or the ingested air, reacts with the oxides of sulfur from the combustion products of the fuel to form Na_2SO_4.[21] When the vapor pressure of Na_2SO_4 exceeds its dew point for given service conditions, condensation of a fused salt on the cooler turbine components may lead to passive or locally active attack of the surface.[21-29]

For resistance to hot corrosion, an alloy or coating must form a slow-growing and dense protective oxide scale with limited solubility in Na_2SO_4. Determinations of the solubilities of several oxides in pure Na_2SO_4 have shown that Cr_2O_3 and Al_2O_3 are acidic oxides because their solubility minima occur at very high acidity.[30] Hence, these oxides promise better resistance to acidic salts than more basic

oxides such as Fe_2O_3, NiO, or CoO. In fact, SiO_2 has no ionic acidic solute and is therefore hardly attacked by an acidic melt.[31]

Aluminide diffusion coatings produce a steady-state α-Al_2O_3 scale which does not provide adequate hot corrosion resistance. McCarron et al.[32] determined experimentally that Cr additions (~8 at.%) in bulk ß-NiAl improved burner rig hot corrosion performance considerably. An aluminide diffusion coating modified with Cr also exhibited excellent resistance to hot corrosion attack, so modification of the surface composition by Cr enrichment is required to produce a more protective scale.[33]

The purpose of this investigation was to determine the high-temperature performance of RE-doped and Cr/RE-modified aluminide diffusion coatings (described in the preceding paper) on commercial Ni-base alloy substrates (e.g., IN 713LC and René 80). The isothermal and cyclic oxidation behavior at 1100°C in air of these coatings was determined, and the hot corrosion (thin film) resistance of Cr/RE-modified aluminide coatings at 900°C in 0.1% SO_2/O_2 was also determined. The mechanisms of coating degradation are discussed.

EXPERIMENTAL PROCEDURES

The experimental procedures and surface composition results for the RE-doped and Cr/RE-modified aluminide diffusion coatings have been presented previously.[2,34] Samples coated by both the "powder contacting" and the "above pack" arrangements were evaluated.

Oxidation: The high-temperature oxidation behavior of the coatings was determined by both isothermal and cyclic oxidation tests. Isothermal oxidation rates at 1100°C in air (0.21 atm O_2) at a flow rate of 0.1 l/min (STP) were measured using a Cahn TG-171 automated thermogravimetric analyzer (TGA) equipped with the Cahn DACS plus software. Specimens were placed in an alumina crucible which was suspended from the microbalance by a sapphire wire. Parabolic rate constants were calculated from the weight change data.

Cyclic oxidation at 1100°C in static air was performed at the NASA Lewis Research Center. Two specimens each were placed in six, FeCrAl crucibles suspended by a platinum wire and separated with an alumina spacer. Specimens were pneumatically lowered and retracted from the hot zone after a one-hour exposure followed by a twenty-minute cool to ambient temperature. Specimens were removed periodically to be weighed and inspected. Screening tests for up to 200 one-hour cycles were conducted. Resistant coatings were further evaluated for up to 500 one-hour cycles. X-ray diffraction (XRD) analysis was used to identify the oxide and coating phases present. In addition, a Hitachi S-510 scanning electron microscope (SEM) was used to observe the oxide morphology, and electron microprobe analysis (EPMA) was used to characterize the compositions of the oxidized coating surfaces. Other specimens were mounted in epoxy, sectioned,

and metallographically polished through 0.3 μm alumina. These cross-sections were then analyzed by EPMA to determine compositional and morphological changes in the coating.

Hot Corrosion Studies: The hot corrosion behavior of the coatings was determined using isothermal thin film tests. Thin films of Na_2SO_4 were applied by heating coupons to about 200°C on a hot plate and applying an aqueous solution from an airbrush to generate a salt coating of 5 ± 1.5 mg Na_2SO_4/cm^2. Coated specimens were placed in an alumina boat which was inserted into a horizontal tube furnace at 900°C and exposed to a Pt-catalyzed 0.1% SO_2/O_2 mixture at a flow rate of 0.1 l (STP)/min. Specimens were removed periodically to be weighed, inspected, and recoated with salt. XRD analysis was used to determine the crystalline corrosion products. Cross-sections were prepared by sputtering a layer of Au/Pd and then electroplating a thick layer (10-25 μm) of Cu over the sample. These cross-sections were then examined by EPMA so that compositions and x-ray maps of S, O, Na, and other coating elements could be obtained.

RESULTS AND DISCUSSION

A. Isothermal Oxidation Behavior

The isothermal oxidation behavior of RE-doped aluminide diffusion coatings on IN 713LC produced from a cementation pack containing 20 wt.% of Cr-10 wt.% Al masteralloy with various chloride activator salts and/or RE sources at 1150°C for 24 hours, using an "above pack" arrangement, was determined at 1100°C in air at a flow rate of 0.1 l/min (STP).

The oxidation kinetics are presented in Fig. 1, and XRD analyses and parabolic rate constants calculated from Fig. 1 are listed and compared to literature values in Table 1.

True parabolic rate constants, k_p, for isothermal oxidation were calculated by linear regression of the weight gain versus square-root of time data, as suggested by Pieraggi.[34] The data fit produced R^2 values over 0.90. In all cases, a slow-growing Al_2O_3 scale was produced on the RE-doped aluminide coatings. The rate constants for both the undoped and the RE-doped, aluminide coatings agreed well with those for undoped ß-NiAl[5], for Y-implanted ß-NiAl coatings on Ni-base alloys in pure oxygen[16], and for bulk ß-NiAl containing other RE additions at 1100°C[11] (Table 1).

The kinetic results were characterized by a short transient oxidation (~5 hours) resulting from the rapid formation of $NiAl_2O_4$ spinel and $(Cr,Al)_2O_3$ scales. Eventually, the spinel was isolated by a steady-state, slow-growing Al_2O_3 scale. The rate of steady-state oxide growth was comparable for each of the RE-doped aluminide coatings. The Cr carbide coating produced from a pack containing 2 wt.% NH_4Cl activator plus 2 wt.% ZrO_2 oxidized with a parabolic rate constant that was an order of magnitude higher (Table 1).

Representative scanning electron micrographs of the surface oxides are shown in Fig. 2. A ridged Al_2O_3 scale, as typically found on oxidized ß-NiAl[6], was observed on all aluminide coatings. The carbide coatings formed by the NH_4Cl

plus ZrO_2 pack produced a very compact, thick scale comprised of a thin, outer $NiAl_2O_4$ spinel layer with an inner Al_2O_3 layer containing a large dispersion of ZrO_2 particles. For undoped coatings, cracked or spalled scales were evident near grain boundaries of the coating, exposing the voided interface (Figs. 2a and b). Cracking and/or spalling of the oxide was also evident from the oxidation kinetics, because at the end of the transient oxidation stage, a small drop in weight was recorded. For RE-doped coatings, a much smaller fluctuation was measured. As shown in Figs. 2c and d, scale cracking originated near the coating grain boundaries for an Y-doped aluminide coating. However, a tenacious Al_2O_3 scale with a trace of Y was detected by EPMA analysis beneath the outer, cracked scale. Other RE-doped aluminide coatings produced uncracked surface oxides. For example, a Hf-doped aluminide coating formed a ridged and relatively flawless, external Al_2O_3 scale (Fig. 2e). XRD analysis identified weak signals for $YAlO_3$, ZrO_2, and HfO_2 phases on the Y-, Zr-, and Hf-doped aluminide coatings, respectively (Table 1).

Generally, the RE-doped aluminide coatings produced a continuous, slow-growing Al_2O_3 scale. However, weight fluctuations from scale spallation made calculations of true parabolic rate constants difficult, so comparison of rate constants for RE-doped and undoped aluminide coatings could not be drawn. Nevertheless, the RE-doped aluminide coatings exhibited overall superior isothermal oxidation behavior for the IN 713LC alloy.

B. Cyclic Oxidation Behavior

Powder Contacting Arrangement: Cyclic oxidation tests at 1100°C in static air of the Cr/RE-modified aluminide coatings on René 80 alloy substrates, produced by the powder contacting arrangement, were conducted at the NASA Lewis Research Center and some have been presented in a previous publication.[35] The diffusion coatings were produced from cementation packs containing 25 wt.% of Cr-7.5 wt.% Al masteralloy and 2 wt.% of an NH_4Cl or RE-base activator and/or RE oxide sources heated at 1150°C for 24 hours. The original surface compositions for these coatings are tabulated in the preceding paper.[2] The weight change measurements versus cycle time are presented in Fig. 3, and XRD analysis of the surface phases and any spalled oxide collected are listed in Table 2, from the strongest to the weakest peak. The cyclic oxidation kinetics were compared to the bulk uncoated alloy[36] and to a commercial, low-activity aluminide diffusion coating, GE Codep C, for the same alloy substrate.

The Cr/RE-modified (e.g., $ZrCl_4$- and YCl_3-activated packs) and the Cr-modified (e.g., NH_4Cl-activated) aluminide coatings improved the adherence and lifetimes of Al_2O_3 scales on the coated substrates considerably. Overall, the cyclic oxidation behavior was dependent on the structure of the coating itself (aluminide or else carbide) and the presence of the RE in the coating. For example, a 2 wt.% $AlCl_3$-activated pack containing 2 wt.% ZrO_2 produced a $Cr_{23}C_6$ carbide coating which failed to protect the substrate (Fig. 3a). The

remaining pack chemistries produced aluminide coatings which provided exceptional protection. However coatings produced from packs containing ZrO_2 additions failed to improve coating lifetimes or scale adherence, which can be attributed to the excessive amounts of Zr in the aluminide coatings, mainly as ZrO_2 entrapment.[2] For Fig. 3 and Table 2, outward-grown aluminide coatings also possessed various amounts of entrapped Al_2O_3 filler powder, depending on the physical state of the activator used. Liquid activator salts, such as YCl_3, cause wetting of the pack powders and aggregation of the particles. On the other hand, volatile activator salts, such as $ZrCl_4$, do not wet pack powders, so that a more random dispersion and larger amount of entrapment is produced.

Entrapped oxide particles can severely degrade the aluminide coating and cause the premature failure of the protective Al_2O_3 scales, even on coatings containing sufficient RE content (Fig. 3). Entrapped particles can also initiate fatigue cracks at the surface, thereby reducing the overall mechanical durability (e.g., thermal fatigue resistance) of the coated component.

XRD analysis of oxidized coatings indicated that successful coatings produced an α-Al_2O_3 scale with minor peaks of $NiAl_2O_4$ and TiO_2 phases, with no spall was collected after 200 cycles. Unprotective coatings (e.g., carbide or ZrO_2 entrapped coatings) failed to form an adherent Al_2O_3 scale; instead external Cr_2O_3, NiO, TiO_2, and spinel phases formed and spalled during thermal cycling.

For successful coatings after oxidation at 1100°C for 200 one-hour cycles, a thin and adherent Al_2O_3 scale was present on the surface, beneath which Al_2O_3 entrapment was evident. After oxidation, the coating consisted of a single-phase, ß-NiAl compound without any α-Cr second-phase particles. Due to interdiffusion between the Ni-base substrate and the coating, a second chain of W-, Cr-, and Mo-rich carbides began to form beneath the original one. For nonprotective coatings, the consumption of Al led to a nonprotective and nonadherent Al_2O_3 scale. No external ß-NiAl coating was present; instead, a two-phase ($\gamma+\gamma'$) surface layer with little or no interdiffusion zone was observed, typical of an uncoated substrate. Although several coatings formed protective Al_2O_3 scales, an improvement over GE Codep C was not realized. In general, the "powder contacting" arrangement is not acceptable.

"Above Pack" Arrangement: Cyclic oxidation tests were done at 1100°C in static air for entrapment-free, Cr/RE-modified and RE-doped aluminide coatings on René 80 and IN 713LC and on IN 713LC alloy substrates. The weight change measurements versus cycle time are presented in Figs. 4-6, and XRD analyses of the surface phases are listed in Tables 3 and 4. The oxidation behavior of both Cr/Cr/RE-modified and RE-doped aluminide diffusion coatings are summarized in Table 5.

1. RE-Doped Aluminide Coatings: Figures 7 and 8 illustrate representative cross-sectional and surface

microstructures, respectively, of RE-doped aluminide coatings cyclically oxidized for 500 cycles. The cyclic oxidation behavior followed three general types of attack: (1) a planar Al depletion front (e.g., Fig. 7c), (2) a planar Al depletion front with associated internal oxidation (e.g., Fig. 7b), or (3) localized Al depletion fronts along the surface and/or grain boundaries (e.g., Fig. 7a). In Fig. 7a, localized Al depletion led to the formation of the lower aluminide phase, γ'-Ni_3Al, and localized spalling to bare metal as indicated in Figs. 8a and b. The localized spalling may explain the weight fluctuations in the kinetic results of Fig. 4. According to SIMS analysis[2], Y deposition was sufficient but localized in the surface of the aluminide coating layer. Generally, the Y-doped aluminide coatings improved the adherence of α-Al_2O_3 scales (Fig. 4). In Fig. 7a, an additional interdiffusion zone containing (Nb,Mo,Cr,Ti)-rich carbides is observed beneath the original zone. However, this further interdiffusion between the substrate and the coating during oxidation did not seem to affect the overall cyclic oxidation behavior.

Coatings produced from RE-base chloride activator salts (Figs. 7b, c, and d) were characterized by a 15-25 μm thick Al depletion zone (i.e., γ'-Ni_3Al layer), deterioration of the interdiffusion zone, and the formation of nonprotective $NiAl_2O_4$ and TiO_2 scales (Table 3). Undoped (RE-free) aluminide coatings were characterized by excessive depletion of Al (> 40 μm), transformation into the lower aluminide phase

(i.e., γ'-Ni_3Al) and even the Ni solid solution (i.e., γ-Ni), and interdiffusion with the substrate (e.g., Figs. 4 and 7d).

Figure 7b illustrates another unique type of attack. Because of excessive levels of zirconium (0.2-0.3 at.%) in the aluminide coating, internal oxides rich in Al and Zr were detected by EPMA analysis within the Al depletion zone (γ'-Ni_3Al layer) of the coating. Zirconia (ZrO_2) particles were also evident within the Al_2O_3 scale of the oxidized surface (indicated by arrows in Fig. 8e) and were detected by the XRD analysis (Table 3). Although an Al depletion zone was apparent for all the coatings produced with RE-base chloride activators, the coating produced from a pack containing 2 wt.% NH_4Cl activator plus 2 wt.% ZrO_2 (Fig. 7b) formed Zr- and Al-rich oxide pegs which seemed to anchor and improve the adherence of the Al_2O_3 scale (Fig. 4). This behavior is typical for Zr-doped, Ni_3Al compounds.[37] On the other hand, although RE contents deposited from RE-base chloride activators were not excessive, no internal oxide pegs were observed after 500 cycles. In fact, those coatings offered only limited improvement (up to 300 cycles) in scale adherence compared to the coatings produced with a RE-oxide source (Fig. 4). Scanning electron micrographs of the oxidized surfaces revealed rough and textured areas where nonprotective $NiAl_2O_4$ and Al_2O_3 scales had spalled, exposing the Al depleted, Ni_3Al surface layer (Fig. 8c and d).

Overall, RE-doped aluminide coatings offered considerable improvements in the adherence of Al_2O_3 scales compared to

RE-free aluminide coatings and uncoated substrates (Fig. 4). The cyclic oxidation behavior of the RE-doped aluminide coatings was dependent on the physical state of the RE source. For example, the RE oxide sources were present in the pack throughout the coating process and deposited more effective RE levels (e.g., NH_4Cl-activated packs with ZrO_2 or Y_2O_3 sources), whereas RE-base chloride activators were extremely volatile[2] and failed to deposit sufficient RE levels to improve scale adherence for the entire 500 cycles.

2. Cr/RE-Modified Aluminide Coatings: The cyclic oxidation behavior of the Cr/RE-modified aluminide coatings was slightly different from the RE-doped aluminide coatings. First, the Cr (5.5-8.0 at.%) plus RE (.02-.30 at.%) additions led to improved scale adherence for coatings produced from only certain pack chemistries, compared to the RE-doped aluminide coatings (Figs. 5 and 6). Second, the interdiffusion zones coarsened and broadened more noticeably during the oxidation exposures. However, the degraded interdiffusion zones did not limit the effectiveness of the Cr/RE-modified aluminide coatings.

The weight change measurements of Figs. 5 and 6, and the XRD analyses in Table 4 have identified several pack chemistries which improved the adherence of Al_2O_3 scales independent of the coating thickness. Overall, the best coatings were produced from packs containing either 4 wt.% $ZrCl_4$, 4 wt.% YCl_3, or 2 wt.% NH_4Cl plus 2 wt.% Y_2O_3, but the first two chloride activators did not produce optimum cyclic

oxidation behavior for the RE-doped aluminide coatings. Although both Cr/RE-modified and RE-doped aluminide coatings generated Al depletion zones, the Cr/RE-modified coatings were more protective. Possibly, the hypostoichiometric (40 at.% Al compared to 45 at.% Al) ß-NiAl phase in the Cr/RE-modified aluminide coatings contained larger solubilities for Zr and Y, which provided improvement in the scale adherence. Alternatively, as for the NiCrAl alloy system[38], the Cr additions (~5.5 to 8.0 at.% Cr) to the ß-NiAl phase may have enhanced the Al diffusivity, allowing for more rapid formation of the protective Al_2O_3 scale. This would explain the thicker Al depletion zones (Ni_3Al layers) in the Cr/RE-modified coatings compared to the RE-doped coatings (compare Figs. 7a and 9, 10, or 11) and, possibly, the relatively adherent Al_2O_3 scales grown on the Ni_3Al surface layers. In addition, the Cr enrichment may have increased the Al diffusivity in the γ'-Ni_3Al (~4 to 5 at.% Cr) and the γ-Ni (~15 to 20 at.% Cr) phases, to enable the growth of a more protective Al_2O_3 scale (Figs. 10 and 11).

The ß-NiAl phase is an ordered intermetallic compound with the B2 (CsCl) crystal structure. The NiAl phase exists over a wide range of stoichiometry, from 30 to 58 at.% Al, and exhibits intrinsic disorder by antistructure defects, i.e. by mutual substitution. For hypostoichiometric (Ni-rich) compounds, Al atoms are simply replaced by Ni atoms; whereas, for the hyperstoichiometric (Al-rich) compound, Ni atoms are replaced by Al atoms from 50 to 50.5 at.% Al, but Ni vacancies

compensate for further increases in Al composition.[39,40] In Cr/RE-modified aluminide coatings, Cr atoms substitute for Al atoms in the hypostoichiometric lattice. Since the CrAl compound possesses a larger disorder and vacancy concentration, Cr additions into the NiAl compound may inject vacancies into this lattice.[40] These excess vacancies could increase the Al, Cr, and Ni diffusivities, thereby increasing the rate of Al depletion and promoting interdiffusion degradation, i.e. a coarsened microstructure. The interdiffusion degradation of high-activity aluminide diffusion coatings on single-crystal, Ni-base superalloys was recently reported.[41] The transformation from a B2-type NiAl phase to a $L1_2$ $Ni_3(Al,Ti)$ phase during exposure at temperatures of 850 and 950°C in vacuum, nucleated at grain and interphase boundaries within the interdiffusion zone. These boundaries can possess excess vacancies, thereby promoting rapid Al boundary diffusion and interdiffusion degradation.

RE-free and RE-lean coatings, or ones produced from a pack containing 2 wt.% NH_4Cl plus 2 wt.% ZrO_2 showed consistently poor cyclic oxidation behavior. Coatings produced from this pack failed to produce an aluminide coating layer; instead, an external chromium carbide layer ($Cr_{23}C_6$) were formed with very poor cyclic oxidation resistance. Similarly, carbide coatings were also produced from two other packs: 2 wt.% $ZrCl_4$ and NH_4Cl for René 80 substrates. To produce an aluminide coating, a masteralloy containing a higher Al activity (i.e.,

Cr-10 wt.% Al) would be required, but then, the aluminide coating had only about 2 at.% Cr.

XRD and EPMA surface analyses detected the γ'-Ni_3Al phase on almost all coatings after 500 cycles. In addition, α-Al_2O_3 and $NiAl_2O_4$ spinel oxide phases were evident. Less protective surface phases such as γ-Ni and TiO_2 were also detected especially on René 80 alloy substrates (Table 4).

Representative cross-sectional, backscattering electron micrographs and composition profiles (EPMA) of oxidized coatings are presented in Figs. 9-11. A 5-15 μm thick, Al depleted layer (Ni_3Al) was characteristic of all protective coatings, except the one shown in Fig. 9. This one exception was an IN 713LC alloy substrate treated in a pack containing 4 wt.% $ZrCl_4$. This coating contained an external ß-NiAl layer with an inner, three-phase region comprised of ß+γ'+γ. EDS analyses detected Zr-rich internal oxides near the surface for this and other Zr-doped aluminide coatings (Figs. 9 and 10). Such internal oxides are characteristic of ß-NiAl compounds with additions of 0.2 at.% Zr, which produced very adherent Al_2O_3 scales at 1100°C.[18] In addition, a coarsened interdiffusion zone was observed, consisting of large refractory-rich carbides ($M_{23}C_6$-type) and sigma phase (for René 80 alloy substrates only).

3. Coating Thickness: To determine any effect of coating thickness, coatings were produced from packs containing 15 wt.% of Cr-7.5 wt.% Al masteralloy powder and various activators and/or RE sources at 1150°C for 4 and 24 hours.

These heat treatment times produced coatings averaging 20-25 μm and 80-85 μm thick, respectively. Thicker coatings produced only limited improvements in coating lifetimes. Thinner coatings produced by the 4-hour treatment formed adherent scales up to 200 to 300 cycles (Fig. 3). A 20 μm thick, Ni_3Al layer at the coating surface and a similarly coarsened interdiffusion zone were again observed for coatings oxidized for 500 one-hour cycles. At that time, the Al depletion zone (Ni_3Al layer) consumed almost the entire coating thickness; therefore, thicker coatings of the same composition did offer longer protection (compare Figs. 5 and 6). The thick coating increases the Al reservoir and permits more Al loss before the transformation to ß-NiAl into the less protective, $\gamma' Ni_3Al$ phase.[42] For both coating thicknesses, the most protective coatings, i.e. those, which optimized oxide scale adherence, were produced from the same pack chemistries.

4. Substrate Composition: Cyclic oxidation was generally affected most by the coating composition at the surface. Aluminide coatings contain various alloying elements from the substrate which diffuse outward during the coating process. IN 713LC and René 80 alloy substrates have two major composition differences. IN 713LC contains no Co and only 0.7 at.% Ti, so only little transfer of Ti occurs to the coating. Aluminide coatings on René 80 alloy substrates, however, contain about 4-5 at.% Co and about 1 at.% Ti. Although small additions (1-3 at.%) of Ti are reported to improve the cyclic

oxidation behavior of ß-NiAl[43], excessive Ti and Co levels promote the formation of less protective oxides such as TiO_2 and NiO.[44] Uncoated IN 713LC provides better protection than uncoated René 80 during cyclic oxidation, and, in fact, coated IN 713LC provided the best overall cyclic oxidation resistance.

5. Degradation Mechanism: Figure 12 is a schematic illustration of the degradation mechanism for the Cr/RE-modified and RE-doped aluminide diffusion coatings. Transient oxides, including $Ni(Al,Cr)_2O_4$ spinel and α-$(Al,Cr)_2O_3$ oxides[45], form during the initial exposure and eliminate internal oxidation by reducing the oxygen activity at the coating/scale interface. Chromium additions decrease the time of transient oxidation of ß-NiAl within the 850-1050^{o}C range by nucleating the isomorphous mixed oxide, $(Cr,Al)_2O_3$.[12] With increasing time, the transient oxides thicken until a continuous, steady-state α-Al_2O_3 scale forms at the coating/scale interface, interrupting the supply of Ni to the transient spinel oxide. Chromium is then depleted from the surface oxides by either evaporation or else by spallation of the transient oxides. In addition, interdiffusion zone carbides and sigma phase (for René 80 alloy substrates) coarsen at the expense of smaller particles, Cr and refractory element solutes in the adjacent substrate and coating. EPMA analysis determined that further exposure transforms the MC-type carbides into $M_{23}C_6$-type carbides.[14] As time passes, a second interdiffusion zone containing Cr-

and refractory-rich carbides (probably $M_{23}C_6$ and MC-type carbides) begins to form beneath the original zone, because of the depletion of Ni and other alloying elements from the substrate. Aluminum is continuously depleted from the surface and along grain boundaries (Fig. 11) of the coating upon the formation and growth of the external, Al_2O_3 protective scale. This Al depletion is increased substantially if the external Al_2O_3 scale spalls for every oxidation cycle[38]. Aluminum depletion results in the transformation of the ß-NiAl coating layer into the γ'-Ni_3Al phase, whereupon, the formation of less protective oxide scales such as $NiAl_2O_4$ and NiO cause the end of the coating protection.[42] However, microprobe analyses detected about 0.05 at.% Y and Zr in the Ni_3Al layer which, according to Taniguchi and Shibata[37] and Kuenzly and Douglass[46], may be sufficient to produce adherent Al_2O_3 scales during further oxidation exposure. This explains why slow kinetics and good adherence were observed for extended times after the Ni_3Al had formed (Figs. 6, 9, and 11).

In contrast to the Cr/RE-modified coatings, the degradation of the RE-doped aluminide coatings is controlled solely by the depletion of Al at the surface, because only limited coarsening of the interdiffusion zone was observed prior to the formation of Ni_3Al following 500 cycles. Once the surface of the coating transforms to γ'-Ni_3Al (35-36 at.% Al at 1100°C[47]), and possibly γ-Ni, a protective and adherent Al_2O_3 scale cannot be sustained in cyclic oxidation, probably because of slower Al diffusion in the low-Cr Ni_3Al

phase.[4] Instead, a less protective $NiAl_2O_4$ spinel and NiO scale form. According to Figs. 4 and 7, the presence of Ni_3Al, however, may not lead to immediate failure if an adherent Al_2O_3 scale is anchored to the coating by oxide pegs.

C. Hot Corrosion (Fused Salt Attack) Behavior

To evaluate the resistance to high-temperature (Type I) hot corrosion attack (HTHCA), the Cr/RE-modified aluminide diffusion coatings were subjected to isothermal thin film tests. XRD results of the corrosion products are listed in Tables 6 and 7 for alloys coated in the "above pack" and in the powder contacting arrangement, respectively. In addition, the hot corrosion performance of Cr/RE-modified aluminide diffusion coatings is presented in Table 8. Chromium/RE-modified aluminide coatings were also compared to the commercial low-activity coating, GE Codep C, for the same alloy substrate. The GE Codep C process is basically an aluminizing treatment which forms an outward-grown, hypostoichiometric ß-NiAl coating with only limited Cr enrichment (~2.2 at.%) from the alloy.

<u>"Above Pack" Arrangement:</u> René 80 and Mar-M247 substrates were coated in packs containing various chloride activator and RE sources with a suitable masteralloy composition in the "above pack" (AP) arrangement, and only René 80 substrates were coated in a "powder contacting" arrangement. The salted coatings (5.0 ± 1.5 mg Na_2SO_4/cm^2) were placed in a flowing Pt-catalyzed 0.1% SO_2/O_2 gas mixture (actually, 841 ppm SO_2/O_2) at 900^oC. Exposed samples were periodically quenched

to room temperature (e.g., following 24, 72, 144, 240, 360, and 504 hours) to facilitate scale spallation. The coupons were weighed, resalted, and replaced into the furnace for up to 672 total hours. The weight changes for each alloy and pack/substrate arrangement during the corrosion process are presented in Figs. 13-15. Severely corroded coupons were prematurely removed from the test, as indicated by a stoppage of the kinetic measurements.

As shown in Table 8, coatings from the AP arrangement failed to provide any substantial resistance to hot corrosion attack, except for one specific substrate and pack chemistry (Mar-M247 substrate coated with 2 wt.% NH_4Cl and 25 wt.% of Cr-6 wt.% Al masteralloy). XRD results and cross-sectional analysis of selected microstructures revealed that the original ß-NiAl coating layer was generally absent and that a number of unprotective external oxides and internal sulfides were present (Table 6).

The hot corrosion kinetics were characterized by an initial incubation period where a relatively protective oxide was present (Figs. 13 and 14). With time, the product scale was further attacked by the molten salt and the oxidant, exposing the coated substrate and leading to rapid weight gains. While the hot corrosion mechanism is not obvious here, continuing scale dissolution/precipitation reactions can eventually destroy the protective product scale.[29] Alloy sulfidation can result in a large increase in the basicity of the salt film and the formation of less protective basic

oxides formed (Table 6), which should support synergistic basic dissolution/precipitation of Cr_2O_3 and Al_2O_3, as reported by Hwang and Rapp.[48] Overall coating failure is seen in Figs. 13 and 14. The general failure of these AP coatings resulted because inadequate Cr was enriched in the coating.

"Powder Contacting" Arrangement: For the PC arrangement, several pack chemistries provided adequate resistance to hot corrosion attack, except for the $ZrCl_4$-activated pack. Chromium-enriched aluminide coatings (Y-doped and undoped) were protective up to at least 360 hours. This reconfirmed that Cr and not RE is the most important alloying addition to an aluminide coating or ß-NiAl compound in order to improve the resistance to hot corrosion attack.[32] The coatings produced from $YCl_3/CrCl_2$-activated packs survived 672 hours with limited attack. In fact, these coatings still had detectable remnants of the original aluminide coating and formed more protective Al_2O_3 and $NiAl_2O_4$ oxide phases (Table 7), enriched with Cr (~5-7 at.%), according to EPMA analysis. The Y-doped and undoped, Cr-enriched aluminide coatings were characterized by initial linear kinetics, after which transient, protective scales formed and grew with slow parabolic steady-state kinetics (Fig. 15). Substrates coated with $ZrCl_4$-activated packs were severely corroded within the first 24 hours of exposure, forming a thick, porous scale consisting of NiO and $NiAl_2O_4$ (Table 7). This behavior was attributed to the lower Cr concentrations.

Cross-sectional electron micrographs and the corresponding elemental x-ray maps of the coating/corrosion product couple were made, as are presented in Figs. 16-18. Little attack of the ß-NiAl coating was observed after 144 hours of exposure for René 80 substrates coated in a pack containing 2 wt.% of either YCl_3 or else $ZrCl_4$ and 25 wt.% of Cr-7.5 wt.% Al masteralloy, using a PC arrangement. XRD analyses detected a thin, external Al_2O_3 scale which protected the coating from the molten salt (Fig. 16). Microprobe analyses did not detect any significant reduction in the Cr surface composition for either coating after 144 hours of exposure, but EPMA analysis did detect a measurable amount of Cr (~5-7 at.%) in the surface oxide.

Significant attack was observed after 672 hours of exposure. The surfaces of both coatings were severely pitted by the oxidation/corrosion process (Figs. 17a and 18a). For $YCl_3/CrCl_2$-activated coatings, a thin layer of Ni_3Al at the surface resulted from the gradual depletion of Al which occurred during the oxidation/dissolution/precipitation reactions of the corrosion process. Beneath the thin, Ni_3Al layer, the original ß-NiAl coating layer was still evident. A thick Al_2O_3 scale was also detected by WDS and XRD analyses. The interdiffusion zone consisted of coarsened carbides rich in Cr, Mo, and W, probably $M_{23}C_6$-type carbides, and lacked any sigma phase.

For $ZrCl_4$-activated coatings, the surface was completely transformed into a two-phase region containing γ'-Ni_3Al and γ-

Ni with a dispersion of chromium-rich internal sulfides (indicated by arrows in Fig. 18a). A thick, nonprotective NiO and $NiAl_2O_4$ scale was present, and a carbide-free interdiffusion zone rich in Cr, Co, W, and Mo, probably sigma phase precipitates. For the $ZrCl_4$- and the $YCl_3/CrCl_2$-activated coatings, EPMA also indicated a significantly low Cr surface composition, 0.96 and 2.13 at.%. These Cr reductions mainly resulted from the formation of internal sulfides or an external chromium-rich product scale, although no internal sulfides were detected in the $YCl_3/CrCl_2$-activated coatings.

Degradation Mechanism: Generally, "cleaner" coatings containing lower Cr produced in the AP arrangement provided less protection from fused salt attack than the pack embedded PC coatings. The AP samples suffered similar attack to that of the commercial coatings produced with the GE Codep C process with no additional Cr enrichment (Fig. 15). Clearly, the overall effectiveness of aluminide coatings in Type I hot corrosion is governed by the Cr surface composition (Table 8). The as-deposited AP coatings consisted of two regions: an inner region comprised of ß-NiAl and α-Cr, and an outer region comprised of a single-phase, ß-NiAl layer with limited Cr enrichment (e.g., 4-5 at.%) from the gas phase. PC coatings also consisted of the external ß-NiAl + α-Cr region but with considerably more Cr enrichment (e.g., 8-13 at.% Cr). At steady-state, both AP and PC Cr/RE-modified aluminide coatings produced an external Al_2O_3 scale (not a Cr_2O_3 scale) during hot corrosion attack. However, EPMA analysis detected

a significant amount of Cr within the Al_2O_3 scale for the PC coatings. Therefore, the enhanced resistance to hot corrosion attack must be attributed to this Cr modification of the Al_2O_3 scale.

Santoro et al.[39] have determined the oxidation behavior of Ni-(50-x)Al-xCr alloys in air at 1100°C where x=0,1,3, or 10 at.% additions of Cr. After 100 hours of isothermal oxidation, XRD analysis detected Al_2O_3 and $NiCr_2O_4$ spinel phases. After cyclic oxidation in static air at 1100°C for 100 one-hour cycles, no Cr-rich oxide was formed; instead, Al_2O_3 and $NiAl_2O_4$ spinel phases were detected. Therefore, as proposed earlier, a transient mixed oxide such as α-$(Al,Cr)_2O_3$ and $Ni(Al,Cr)_2O_4$ may form early upon exposure, as indicated by EPMA analysis of corroded coatings. These transient scales may provide enhanced resistance to acidic dissolution/precipitation reactions because the CrO_4^{2-} basic solute, as contrasted to the AlO_2^- basic solute, would tend to reprecipitate inward rather than outward, according to the P_{O2}-dependence for CrO_4^{2-} solubility.[49] At locally reducing sites such as cracks and grain boundaries, the CrO_4^{-2} solute saturates the melt and can precipitate out as Cr_2O_3, thereby preventing or inhibiting salt/coating contact and sulfidation (Fig. 19). This mechanism is very similar to the action of chromate inhibitors in aqueous corrosion.

Thus, Cr-enriched aluminide coatings provide better resistance to fused salt attack compared to traditional

aluminide coatings. However, as exposure continues, both Cr and Al are depleted from the coating surface, either to reform or else to grow these mixed, protective oxides. Eventually, a low-Cr spinel or Al_2O_3 scale is produced, as for the traditional low-Cr aluminide coating. According to the current investigation, a protective mixed oxide scale can no longer form once the Cr surface composition falls below about 4 at.% (Figs. 13-15). The molten salt locally attacks this oxide scale more rapidly than the mixed oxide scale, penetrating to the underlying coating surface. The salt then "cathodically overpolarizes" the coating, forming metal sulfides (e.g., CrS), beneath the external surface of the coating, further depleting Cr (Fig. 17). Less protective oxide scales are continuously attacked by the molten salt, exposing the underlying surface to the salt phase, depleting the surface of Al, and transforming the coating surface to γ'-Ni_3Al and γ-Ni (see Fig. 12). Finally, the coating can no longer provide protection to the substrate and fails, as characterized by rapid corrosion kinetics (Figs. 13 and 14).

Since the higher-Cr AP coatings show better hot corrosion resistance, but worse cyclic oxidation resistance than the cleaner low-Cr AP coatings, further revision of the AP geometry and chemistry is needed to develop Cr/RE-modified AP aluminide coatings with a higher Cr content.

CONCLUSIONS

1). In isothermal oxidation at 1100°C in air, RE-doped aluminide coatings on IN 713LC substrates formed a continuous, slow-growing α-Al_2O_3 scale after 44 hours of exposure. The RE-doped aluminide coatings were protected by either an outer, ridged Al_2O_3 scale with an inner, compact Al_2O_3 scale rich in the RE, or else by a continuous, compact scale without any noticeable cracks or flaws. Conversely, RE-free aluminide coatings exhibited large fluctuations in the weight measurements, indicating that periodic cracking and spalling of the oxide scale. Surface micrographs revealed a cracked oxide scale which exposed an underlying voided interface. The parabolic oxidation rate constants, k_p, for the RE-doped aluminide coatings were generally lower than that for RE-free aluminide coatings. The oxidation rates for the coatings agreed well with those for undoped and RE-doped ß-NiAl compounds.

2). The cyclic oxidation behavior of Cr/RE-modified aluminide coatings on René 80 and IN 713LC alloys and of RE-doped aluminide coatings on IN 713LC alloys at 1100°C in static air was determined. Pack powder entrapment from the PC process detracted significantly from the overall cyclic oxidation performance. Coatings produced from the "powder contacting" (PC) arrangement suffered severe degradation from thermal fatigue. For coatings by the AP arrangement, pack powder entrapment was eliminated and pack chemistries were identified which provided resistance to cyclic oxidation, producing adherent Al_2O_3 scales for 500 one-hour cycles. Certain

RE-doped and Cr/RE-modified aluminide coatings improved the adherence of protective Al_2O_3 scales considerably over undoped aluminide coatings. Chromium additions in conjunction with RE dopant improved the resistance to cyclic oxidation attack by, presumably, increasing the diffusivity of Al in both the ß-NiAl and γ'-Ni_3Al phases.

3). The Type I hot corrosion behavior of Cr/RE-modified aluminide coatings on René 80 and Mar-M247 alloy substrates at 900°C in a catalyzed 0.1% SO_2/O_2 gas mixture was determined. The Cr/RE-modified aluminide coatings produced from the PC arrangement provided significantly better resistance to hot corrosion attack (e.g., thin film studies) than commercial low-activity aluminide coatings (e.g., GE Codep C) and Cr/RE-modified aluminide coatings (of lower Cr content) produced by the AP arrangement. Coating lifetimes were strongly dependent on the Cr surface composition needed to form a mixed $(Al,Cr)_2O_3$ oxide which resists attack by the molten salt. Although AP arrangement eliminates powder entrapment, the increased diffusion distance reduced the Cr flux and the resulting Cr surface composition. Thus, the resistance to fused salt for AP aluminides attack was substantially decreased. Further development of the AP arrangement is required to enrich more Cr in the coating.

ACKNOWLEDGMENTS

The authors wish to thank D. Little for EPMA results; C. A. McDonald for electron microscopy results; J. A. Nesbitt,

C. A. Barrett, M. A. Gedwill, and D. L. Humphreys of NASA LeRC for cyclic oxidation results; R. Garlick of NASA LeRC for preliminary XRD results; and A. J. Sedriks of ONR and T. A. Kircher of NADC for funding the projects N00014-87-K-0030 and N00014-90-J-1765.

REFERENCES

1. J.W. Holmes and F.A. McClintock, Metall. Trans., **21A** (1990) 1209.

2. R. Bianco and R.A. Rapp, preceeding paper submitted to This Journal.

3. J.L. Smialek and C.E. Lowell, This Journal, **121** (1974) 800.

4. S. Shankar and L.L. Seigle, Metall. Trans., **9A** (1978) 1468.

5. F.S. Pettit, Trans. AIME, **239** (1967) 1296.

6. H.M. Hindam and W.W. Smeltzer, This Journal, **127** (1980) 1630.

7. R. Prescott, T.E. Mitchell, M.J. Graham, and J. Doychak, to be published in Proceedings of the 24th International SAMPE Technical Conference, Toronto, October 1992.

8. E.W.A. Young and J.H.W. de Wit, Oxid. Met., **26** (1986) 351.

9. J. Doychak, J.L. Smialek, and T.E. Mitchell, Metall. Trans., **20A** (1989) 499.

10. J. Doychak and M. Rühle, Oxid. Met., **31** (1989) 431.

11. G.C. Rybicki and J.L. Smialek, Ibid., **31** (1989) 275.

12. H.J. Grabke, M. Brumm, and M. Steinhorst, Mater. Sci. Techn., **8** (1992) 339.

13. G.W. Goward, D.H. Boone, and C.S. Giggins, Trans. ASM, **60** (1967) 228.

14. T.K. Redden, Trans. AIME, **242** (1968) 1695.

15. H.C. Bhedwar, R.W. Heckel, and D.E. Laughlin, Metall. Trans., **11A** (1980) 1303.

16. J. Jedlinski and S. Mrowec, Mater. Sci. Eng., **87** (1987) 281.

17. S. Mrowec and J. Jedlinski, in Oxidation of High-Temperature Intermetallics, T. Grobstein and J. Doychak (Eds.), TMS, Warrendale, PA (1988) p. 57.

18. C.A. Barrett, Oxid. Met., **30** (1988) 361.

19. J. Doychak, J.L. Smialek, and C.A. Barrett, in Oxidation of High-Temperature Intermetallics, T. Grobstein and J. Doychak (Eds.), TMS, Warrendale, PA (1988) p. 41.

20. Private communication with J. Doychak, NASA Lewis Research Center, April (1992).

21. M.A. DeCrescente and N.S. Bornstein, Corrosion, **24** (1968) 127.

22. J.L. Luthra and O.H. LeBlanc, Jr., Mater. Sci. Eng., **87** (1987) 329.

23. J.A. Goebel, F.S. Pettit, and G.W. Goward, Metall. Trans., **4** (1973) 261.

24. N.S. Bornstein and M.A. DeCrescente, Corrosion, **26** (1970) 209.

25. D.M. Johnson, D.P. Whittle, and J. Stringer, Corr. Sci., **15** (1975) 721.

26. G.C. Fryburg, F.J. Kohl, and C.A. Stearns, This Journal, **131** (1984) 2985.

27. J. Stringer, Mater.Sci. Techn., **3** (1987) 482.

28. F.S. Pettit and C.S. Giggins, in Superalloys II, C.T. Sims, N.S. Stoloff, and W.C. Hagel (Eds.), John Wiley & Sons, New York (1987) p. 327.

29. R.A. Rapp and K.S. Goto, in Molten Salts, J. Braunstein and J.R. Selman (Eds.), The Electrochemical Society, Inc., Pennington, NJ (1981) p. 159.

30. R.A. Rapp, Corrosion, **42** (1986) 568.

31. N.S. Jacobson, Oxid. Met., **31** (1989) 91.

32. R.L. McCarron, N.R. Lindblad, and D. Chatterji, Corrosion, **32** (1976) 476.

33. E. Godlewska and K. Godlewski, Oxid. Met., **22** (1984) 117.

34. B. Pieraggi, Ibid., **27** (1987) 177.

35. R. Bianco and R.A. Rapp, in High Temperature Materials Chemistry V, W.B. Johnson and R.A. Rapp, (Eds.), The Electrochemical Society, Inc., Pennington, NJ (1990) p. 211.

36. C.A. Barrett, R.G. Garlick, and C.A. Lowell, NASA TM-83665, (1989).

37. S. Taniguchi and T. Shibata, Oxid. Met., **25** (1986) 201.

38. G.R. Wallwork and A.Z. Hed, Ibid., **3** (1971) 229.

39. A. Steiner and K.L. Komarek, Trans. AIME, **230** (1964) 786.

40. M. Ettenberg, K.L. Komarek, and E. Miller, Ibid., **242** (1968) 1801.

41. W.F. Gale and J.E. King, Metall. Trans., **23A** (1992) 2657.

42. J.A. Nesbitt, E.J. Vinarcik, C.A. Barrett, and J. Doychak, Mater. Sci. Eng., **A153** (1992) 561.

43. G.J. Santoro, D.L. Deadmore, and C.A. Lowell, NASA TN D-6414, (1971).

44. R. Pichoir, in High Temperature Alloys for Gas Turbines, D. Coutsouradis, P. Felix, H. Fischmeister, L. Habraken, Y. Lindblom, and M.O. Speidel (Eds.), Applied Science Publishers, Ltd., London (1978) p. 191.

45. M. Brumm, Ph.D. Thesis, Universität Dortmund, 1991.

46. J.D. Kuenzly and D.L. Douglass, Oxid. Met., **8** (1974) 139.

47. M.F. Singleton, J.L. Murray, and P. Nash, in Binary Alloy Phase Diagrams, T.B. Massalski (Ed.), ASM, Metals Park, OH (1986) p. 141.

48. Y.S. Hwang and R.A. Rapp, This Journal, **137** (1990) 1276.

49. N. Otsuka and R.A. Rapp, Ibid., **137** (1990) 53.

FIGURE CAPTIONS

1. Oxidation kinetics for IN 713LC alloys coated at 1150°C for 24 hours in a pack containing various activator salts/RE sources with 20 wt.% of Cr-10 wt.% Al masteralloy and isothermally oxidized at 1100°C in air at a flow rate of 0.1 l/min (STP). "Above pack" arrangement.

2. Surface scanning electron micrograph of an IN 713LC alloy coated at 1150°C for 24 hours in a pack containing (a,b) 2 wt.% NH_4Cl, (c,d) 2 wt.% NH_4Cl plus 2 wt.% Y_2O_3, and (e) 4 wt.% $HfCl_4$ with 20 wt.% of Cr-10 wt.% Al masteralloy and isothermally oxidized at 1100°C for 44 hours in air at a flow rate of 0.1 l/min (STP). "Above pack" arrangement.

3. Oxidation kinetics for a René 80 alloy coated at 1150°C for 24 hours with a suitable Cr-Al binary masteralloy and cyclically oxidized at 1100°C in static air for up to 200, one-hour cycles: (a) ZrO_2 source and (b) RE-base activators. "Powder contacting" arrangement.

4. Oxidation kinetics for an IN 713LC alloy coated at 1150°C for 24 hours in a pack containing 20 wt.% of Cr-10 wt.% Al masteralloy with various activator salts/RE sources and cyclically oxidized at 1100°C in static air for up to 500 one-hour cycles. "Above pack" arrangement.

5. Oxidation kinetics for (a) René 80 and (b) IN 713LC alloys coated at 1150°C for 4 hours in a pack containing various activator salts/RE sources with 15 wt.% of Cr-7.5 wt.% Al masteralloy and cyclically oxidized at 1100°C in static air for up to 500 one-hour cycles. "Above pack" arrangement.

6. Oxidation kinetics for (a) René 80 and (b) IN 713LC alloys coated at 1150°C for 24 hours in a pack containing various activator salts/RE sources with 15 wt.% of Cr-7.5 wt.% Al masteralloy and cyclically oxidized at 1100°C in static air for up to 500 one-hour cycles. "Above pack" arrangement.

7. Cross-sectional optical micrograph of an IN 713LC alloy coated at 1150°C for 24 hours in a pack containing (a) 2 wt.% NH_4Cl plus 2 wt.% Y_2O_3, (b) 2 wt.% NH_4Cl plus 2 wt.% ZrO_2, (c) 4 wt.% $HfCl_4$, and (d) 2 wt.% NH_4Cl with 20 wt.% of Cr-10 wt.% Al masteralloy and cyclically oxidized at 1100°C in static air for 500 one-hour cycles. "Above pack" arrangement.

8. Surface scanning electron micrograph of an IN 713LC alloy coated at 1150°C for 24 hours in a pack containing (a,b) 2 wt.% NH_4Cl plus 2 wt.% Y_2O_3, (c,d) 4 wt.% $HfCl_4$, and (e) 2 wt.% NH_4Cl plus 2 wt.% ZrO_2 with 20 wt.% of Cr-10 wt.% Al masteralloy and isothermally oxidized at 1100°C in air for 44 hours. "Above pack" arrangement.

9. Cross-sectional backscattering electron micrograph and composition profile of an IN 713LC alloy coated at 1150°C for 24 hours in a 4 wt.% $ZrCl_4$-activated pack containing 15 wt.% of Cr-7.5 wt.% Al masteralloy and cyclically oxidized for 500 one-hour cycles at 1100°C in static air. "Above pack" arrangement.

10. Cross-sectional backscattering electron micrograph and composition profile of a René 80 alloy coated at 1150°C for 24 hours in a 4 wt.% $ZrCl_4$-activated pack containing 15 wt.% of Cr-7.5 wt.% Al masteralloy and cyclically oxidized for 500 one-hour cycles at 1100°C in static air. "Above pack" arrangement.

11. Cross-sectional backscattering electron micrograph and composition profile of a René 80 alloy coated at 1150°C for 24 hours in a 2 wt.% NH_4Cl-activated pack containing 2 wt.% Y_2O_3 and 15 wt.% of Cr-7.5 wt.% Al masteralloy and cyclically oxidized for 500 one-hour cycles at 1100°C in static air. "Above pack" arrangement.

12. Schematic illustration of the degradation mechanism of the modified aluminide diffusion coatings.

13. Hot corrosion kinetics and average surface compositions for Mar-M247 alloys coated at 1150°C for 24 hours in a pack containing various activator salts/RE sources with 25 wt.% of Cr-6 wt.% Al masteralloy and isothermally corroded at 900°C in a Pt-catalyzed, 0.1 % SO_2/O_2 gas mixture with 5.0 mg/cm^2 Na_2SO_4. "Above pack" arrangement.

14. Hot corrosion kinetics and average surface compositions for René 80 alloys coated at 1150°C for 24 hours in a pack containing various activator salts/RE sources with 25 wt.% of Cr-6 wt.% Al masteralloy and isothermally corroded at 900°C in a Pt-catalyzed, 0.1% SO_2/O_2 gas mixture with 5.0 mg/cm^2 Na_2SO_4. "Above pack" arrangement.

15. Hot corrosion kinetics for René 80 alloys coated at 1150°C for 24 hours in a pack containing various activator salts/RE sources with 25 wt.% of Cr-7.5 wt.% Al masteralloy and isothermally corroded at 900°C in a Pt-catalyzed, 0.1 % SO_2/O_2 gas mixture with 5.0 mg/cm^2 Na_2SO_4. "Powder contacting" arrangement.

16. (a,c) Cross-sectional backscattering electron micrograph and (b,d) corresponding oxygen x-ray map for a René 80 alloy coated at 1150°C for 24 hours in a 2 wt.% (a) YCl_3 or (c) $ZrCl_4$-activated pack containing 25 wt.% of Cr-7.5 wt.% Al masteralloy and isothermally corroded at 900°C for 144 hours in a Pt-catalyzed, 0.1% SO_2/O_2 gas mixture with 5.0 mg/cm^2 Na_2SO_4. "Powder contacting" arrangement.

17. Cross-sectional backscattering electron micrograph and corresponding x-ray maps of Ni, Al, Cr, O, Co, W, and Mo for a René 80 substrate coated at 1150°C for 24 hours in a 2 wt.% (2:1) $YCl_3/CrCl_2$-activated pack containing 25 wt.% of Cr-7.5 wt.% Al masteralloy and isothermally corroded at 900°C for 672 hours in a Pt-catalyzed, 0.1% SO_2/O_2 gas mixture with 5.0 mg/cm^2 Na_2SO_4. "Powder contacting" arrangement.

18. Cross-sectional backscattering electron micrograph and corresponding x-ray maps of Ni, Al, Cr, O, S, Co, and W for a René 80 substrate coated at 1150°C for 24 hours in a 2 wt.% $ZrCl_4$-activated pack containing 25 wt.% of Cr-7.5 wt.% Al masteralloy and isothermally corroded at 900°C in a Pt-catalyzed, 0.1% SO_2/O_2 gas mixture with 5.0 mg/cm^2 Na_2SO_4. "Powder contacting" arrangement.

19. Schematic representation of possible beneficial effect of chromium on hot corrosion of Ni-Cr alloy.

Table 1: Oxidation kinetics and XRD results of IN 713LC alloy substrates coated at 1150°C for 24 hours in a pack containing various activator salts/RE sources with 20 wt.% of Cr-10 wt.% Al masteralloy and isothermally oxidized at 1100°C for 44 hours in air at a flow rate of 0.1 l/min (STP), and comparison with literature values. "Above pack" arrangement.

Pack Chemistry	Parabolic Rate Constant ($gm/cm^2h^{\frac{1}{2}}$)	XRD Phases and Oxides
2% NH_4Cl	4.501×10^{-5}	1,2,3
2% " ,2% ZrO_2	6.201×10^{-5}	1,2,3,4
2% " ,2% Y_2O_3	2.586×10^{-5}	1,2,6,3
4% $ZrCl_4$	4.401×10^{-5}	1,2,4
4% YCl_3	1.751×10^{-5}	1,2,6
4% $HfCl_4$	3.942×10^{-5}	1,2,5,3

Key: 1=ß-NiAl, 2=Al_2O_3, 3=$NiAl_2O_4$, 4=ZrO_2, 5=HfO_2, and 6=$YAlO_3$

Alloys (at.%)	k_p ($gm/cm^2h^{\frac{1}{2}}$)	Atmosphere
Ni-42Al[5]	4.5×10^{-5}	0.1 atm O_2
Ni-47Al-.05Zr[11]	3.8×10^{-5}	0.2 " "
Ni-52Al+2×10^{16} Y^+/cm^2 impltd	9.2×10^{-4}	1.0 " "

Table 2: XRD results of René 80 alloy substrates coated at 1150°C for 24 hours in a pack containing various activator salts/RE sources with 25 wt.% of Cr-7.5 wt.% Al masteralloy and cyclically oxidized at 1100°C in static air for 200 one-hour cycles. "Powder contacting" arrangement.

Pack Chemistry	Oxide Phase(s)	Spall
NH_4Cl, ZrO_2	$NiAl_2O_4, TiO_2, ZrO_2, Al_2O_3$	$NiAl_2O_4$, NiO
YCl_3, ZrO_2	$Al_2O_3, NiAl_2O_4, TiO_2$	$NiAl_2O_4, TiO_2$ Al_2O_3
NH_4Cl	$Al_2O_3, TiO_2, NiAl_2O_4$	none
YCl_3	$Al_2O_3, NiAl_2O_4$	"
$ZrCl_4$	" , "	"
GE Codep C	" , "	"

XRD results are all listed from strongest to weakest peaks.

Table 3: XRD results of IN 713LC alloy substrates coated at 1150°C for 24 hours in a pack containing various activator salts/RE sources with 20 wt.%, Cr-10 wt.% Al masteralloy and cyclically oxidized at 1100°C in static air for 500 one-hour cycles. "Above pack" arrangement.

Pack Chemistry	Oxides Phase(s)
NH_4Cl	1,5,2,4
" $, Y_2O_3$	1,2,5,4
" $, ZrO_2$	1,5,2,6
YCl_3	5,1,2,4
$ZrCl_4$	5,1,2,4,6
$HfCl_4$	5,1,2,4

Key: 1=Al_2O_3, 2=$NiAl_2O_4$, 3=NiO, 4=TiO_2, 5=Ni_3Al, 6=ZrO_2

Table 4: XRD results for René 80 and IN 713LC alloy substrates coated at 1150°C for 4 and 24 hours in a pack containing various activator salts/RE sources with 15 wt.% of Cr-7.5 wt.% Al masteralloy and cyclically oxidized at 1100°C in static air for up to 500 one-hour cycles. "Above pack" arrangement.

	René 80		IN 713LC	
Pack Chemistry	4 h.	24 h.	4 h.	24 h.
2% $ZrCl_4$	n/a	1,2,3	1,3	1,2,3
4% "	3,2,4,1	1,2,3	1,2,3	2,3,5
4% YCl_3	n/a	1,2,4	1,2,3	1,2,3
2% NH_4Cl	1,4,3	1,4,2,3,6	1,2,3	1,2,3
2% " ,2% Y_2O_3	1,2,4	1,2,3	1,2,3	1,2,5
2% " ,2% ZrO_2	1,3,4	1,4,3,2,6	1,4,3	1,4,3,2

Key: 1=Ni_3Al, 2=Al_2O_3, 3=$NiAl_2O_4$, 4=Ni, 5=ß-NiAl, and 6=TiO_2.
n/a=not analyzed

Table 5: Cyclic oxidation results conducted at 1100°C in static air.

Alloy	Activator/RE Source (wt.%)	Masteralloy (wt.%)	Mode of Failure or Other Comments
Rene 80[a]	$AlCl_3$/(2) ZrO_2	(25) Cr-7.5 Al, 24 hrs	Formed carbide coating
"	NH_4Cl/(2) ZrO_2	"	Formed duplex carbide/aluminide coating
"	YCl_3/(2) ZrO_2	"	Aluminide coating with ZrO_2 entrapment
"	NH_4Cl	"	Protective up to 200 cycles
"	$ZrCl_4$	"	"
"	YCl_3	"	"
IN 713LC[b]	NH_4Cl	(20) Cr-10 Al, 24 hrs	Severe Al depletion and aluminide transformation
"	(4) $ZrCl_4$	"	Al depletion and aluminide transformation
"	(4) $HfCl_4$	"	"
"	(4) YCl_3	"	"
"	NH_4Cl/(2) ZrO_2	"	Al Depletion, aluminide transformation, oxide pegs
"	NH_4Cl/(2) Y_2O_3	"	Localized Al depletion and aluminide transformation
IN 713LC[b]	NH_4Cl	(15) Cr-7.5 Al, 4 hrs	Al depletion and aluminide transformation
"	NH_4Cl/(2) Y_2O_3	"	"
"	(4) YCl_3	"	"
"	$ZrCl_4$	"	", Zr-rich oxide pegs
"	(4) $ZrCl_4$	"	", "
"	NH_4Cl/(2) ZrO_2	"	Formed carbide coating
"	NH_4Cl	(15) Cr-7.5 Al, 24 hrs	Al depletion, aluminide transformation, and porous scale formation
"	NH_4Cl/(2) Y_2O_3	"	Al depletion and aluminide transformation
"	(4) YCl_3	"	"
"	$ZrCl_4$	"	RE-lean coating, severe Al depletion, unprotective
"	(4) $ZrCl_4$	"	Slight Al depletion and interdiffusion with substrate
"	NH_4Cl/(2) ZrO_2	"	Formed carbide coating
Rene 80[b]	NH_4Cl	(15) Cr-7.5 Al, 4 hr	Al depletion and aluminide transformation
"	NH_4Cl/(2) Y_2O_3	"	", but more severe

"	(4) YCl_3	"	Formed carbide coating
"	$ZrCl_4$	"	Sharp edges and corners cracked
"	(4) $ZrCl_4$	"	Formed carbide coating
"	NH_4Cl/(2) ZrO_2	"	"
"	NH_4Cl	(15) Cr-7.5 Al, 24 hrs	Severe Al depletion and aluminide transformation
"	NH_4Cl/(2) Y_2O_3	"	Al depletion and localized transformation
"	(4) YCl_3	"	Sharp edges and corners cracked
"	$ZrCl_4$	"	RE-lean coating, severe Al depletion and Zr-rich oxide pegs
"	(4) $ZrCl_4$	"	Some Al depletion and transformation, Zr-rich oxide pegs
"	NH_4Cl/(2) ZrO_2	"	Formed carbide coating
"a	NH_4Cl	(3)AlC/TiC, 4 hrs.	Al depletion and aluminide transformation, 200 cycles

* 2 wt.% of activators was used unless otherwise noted.
a="powder contacting" arrangement
b="above pack" arrangement

Table 6: XRD results of René 80 and Mar-M247 alloy substrates coated at 1150°C for 24 hours in a pack containing various activator salts/RE sources with 25% of Cr-6 wt.% Al masteralloy and isothermally corroded at 900°C for 672 hours in a Pt-catalyzed, 0.1% SO_2/O_2 gas mixture with 5.0 mg/cm^2 Na_2SO_4. "Above pack" arrangement.

Pack Chemistry	XRD Phases
René 80:	
2% NH_4Cl	1,7,2,5,3,4
2% " ,2% Y_2O_3	1,2,7,3,4,5
4% $ZrCl_4$	1,2,4,3,7,5
4% YCl_3	1,7,5,4,3
Mar-M247:	
2% NH_4Cl	2,6,1,3,5
2% " ,2% Y_2O_3	1,2,3
4% $ZrCl_4$	1,3,2,5
4% YCl_3,Cr6Al	2,6,1,3,5
4% " ,Cr5Al	1,7,5,3

Key: 1=NiO, 2=$NiAl_2O_4$, 3=Ni_3Al, 4=Ni, 5=CrS, 6=Al_2O_3, and 7=Co_3O_4.

Table 7: XRD results of René 80 alloy substrates coated at 1150°C for 24 hours in a pack containing various activator salts/RE sources with 25 wt.% of Cr-7.5 wt.% Al masteralloy and isothermally corroded at 900°C for 144 and 672 hours in a Ptcatalyzed 0.1% SO_2/O_2 gas mixture with 5.0 mg/cm^2 Na_2SO_4. "Powder contacting" arrangement.

	XRD Results	
Pack Chemistry	144 h.	672 h.
2% NH_4Cl	1,5	a
2% YCl_3	1,5	a
2% (2:1) $YCl_3/CrCl_2$	1,5	1,2,5,6,4
2% $ZrCl_4$	1,5	3,2,4,6
GE Codep C	3,6,7	n/t

Key: 1=Al_2O_3, 2=$NiAl_2O_4$, 3=NiO, 4=CrS, 5=ß-NiAl, 6=Ni_3Al, and 7=Ni.
a=destroyed
n/t=not tested

Table 8: Thin film, hot corrosion results conducted at 900°C in a Pt-catalyzed 0.1% SO_2/O_2 gas mixture with 5 ± 1.5 mg/cm^2 Na_2SO_4.

Alloy	Activator/RE Source	Masteralloy	Cr Surface Composition (at.%)	Weight Change (mg/cm^2)	Coating Lifetime (hrs)
Rene 80[a]	NH_4Cl	Cr-7.5 wt.% Al	11.45	5.12	504
"	$ZrCl_4$	"	8.21	22.12	240
"	YCl_3	"	10.65	7.51	360
"	$YCl_3/CrCl_2$	"	13.78	5.97	672
"[b]	NH_4Cl	AlC/TiC	2.35	20.61	120
Rene 80[c]	NH_4Cl/Y_2O_3	Cr-7.5 wt.% Al	4.19	53.22	240
"	NH_4Cl	Cr-6 wt.% Al	4.92	44.29	72
"	YCl_3	"	4.39	91.03	72
"	$ZrCl_4$	"	3.36	81.06	144
Mar-M247[c]	NH_4Cl/Y_2O_3	Cr-7.5 wt.% Al	4.87	15.65	504
"	NH_4Cl	Cr-6 wt.% Al	5.61	12.16	672
"	YCl_3	"	5.54	38.31	144
"	$ZrCl_4$	"	3.28	74.87	72
"	YCl_3	Cr-5 wt.% Al	12.33	9.92	360

a="powder contacting" arrangement
b=GE Codep C
c="above pack" arrangement

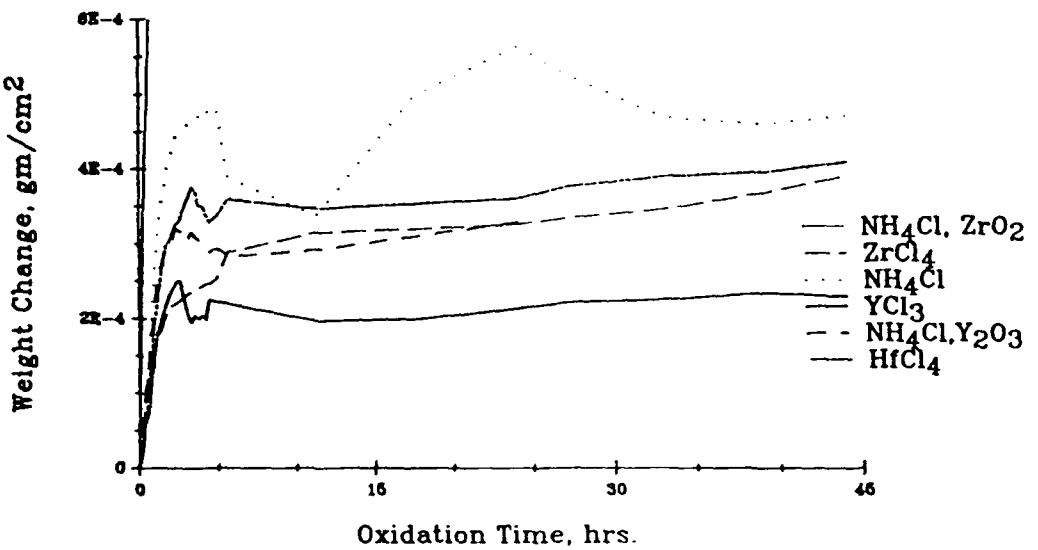

Figure 1: Oxidation kinetics for IN 713LC alloys coated at 1150°C for 24 hours in a pack containing various activator salts/RE sources with 20 wt.% of Cr-10 wt.% Al masteralloy and isothermally oxidized at 1100°C in air at a flow rate of 0.1 l/min (STP). "Above pack" arrangement.

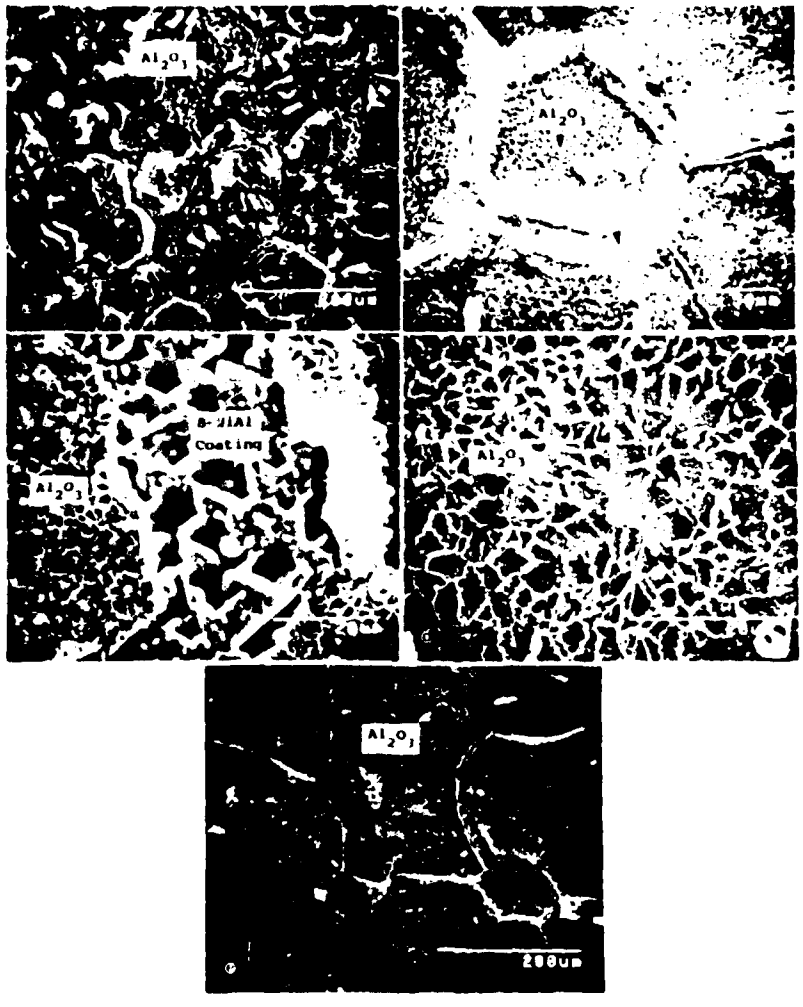

Figure 2: Surface scanning electron micrographs of IN 713 LC alloys coated at 1150°C for 24 hours in a pack containing (a,b) 2 wt.% NH_4Cl, (c,d,) 2 wt.% NH_4Cl plus 2 wt.% Y_2O_3, and (e) 4 wt.% $HfCl_4$ with 20 wt.% of Cr-10 wt.% Al masteralloy and isothermally oxidized at 1100°C for 44 hours in air at a flow rate of 0.1 l/min (STP). "Above pack" arrangement.

AD-A258 027 PACK CEMENTATION ALUMINIDE COATINGS ON SUPERALLOYS: CODEPOSITION OF CR AN.. (U) OHIO STATE UNIV COLUMBUS DEPT OF MATERIALS SCIENCE AND ENGI.. R A RAPP NOV 92 2/2

UNCLASSIFIED TR-1 XB-ONR N00014-90-J-1765 NL

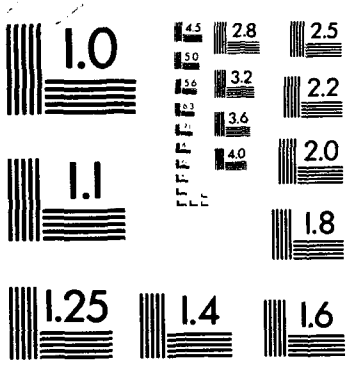
1.0
1.1
1.25
1.4
1.6
1.8
2.0
2.2
2.5
2.8
3.2
3.6
4.0
4.5
5.0
5.6
6.3

a).

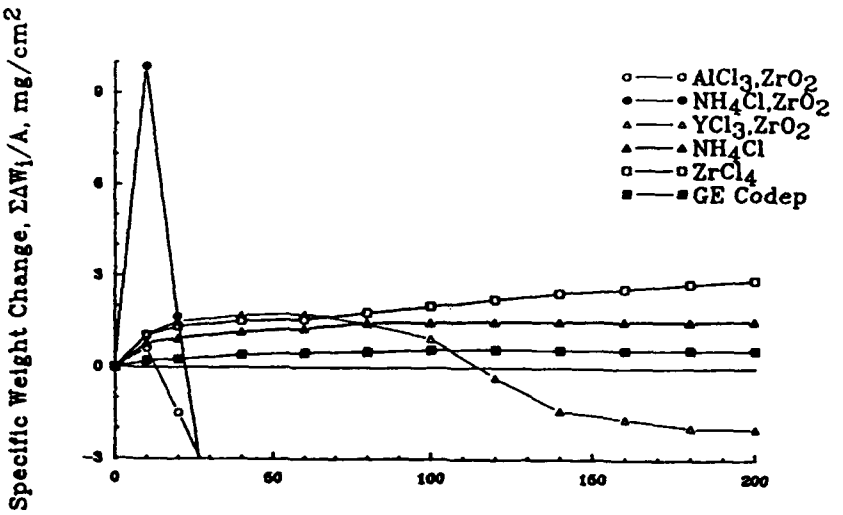

b).

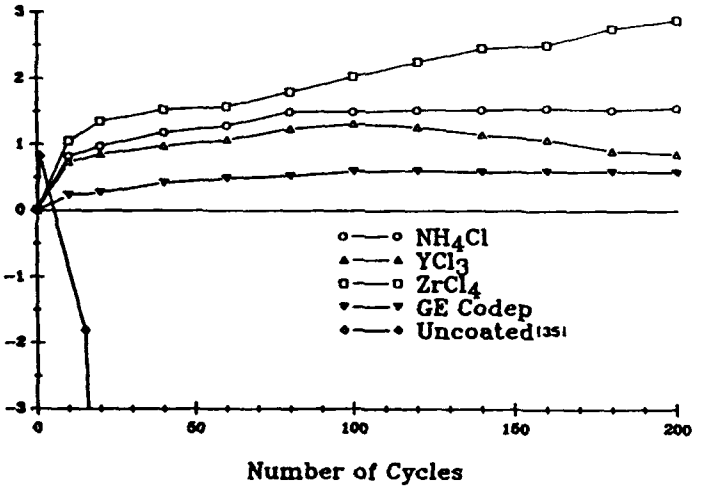

Figure 3: Oxidation kinetics for a René 80 alloy coated at 1150°C for 24 hours with 25 wt.% of a suitable Cr-Al binary masteralloy and cyclically oxidized at 1100°C in static air for up to 200, one-hour cycles: (a) ZrO_2 source and (b) RE-base activator salts. "Powder contacting"[2] arrangement.

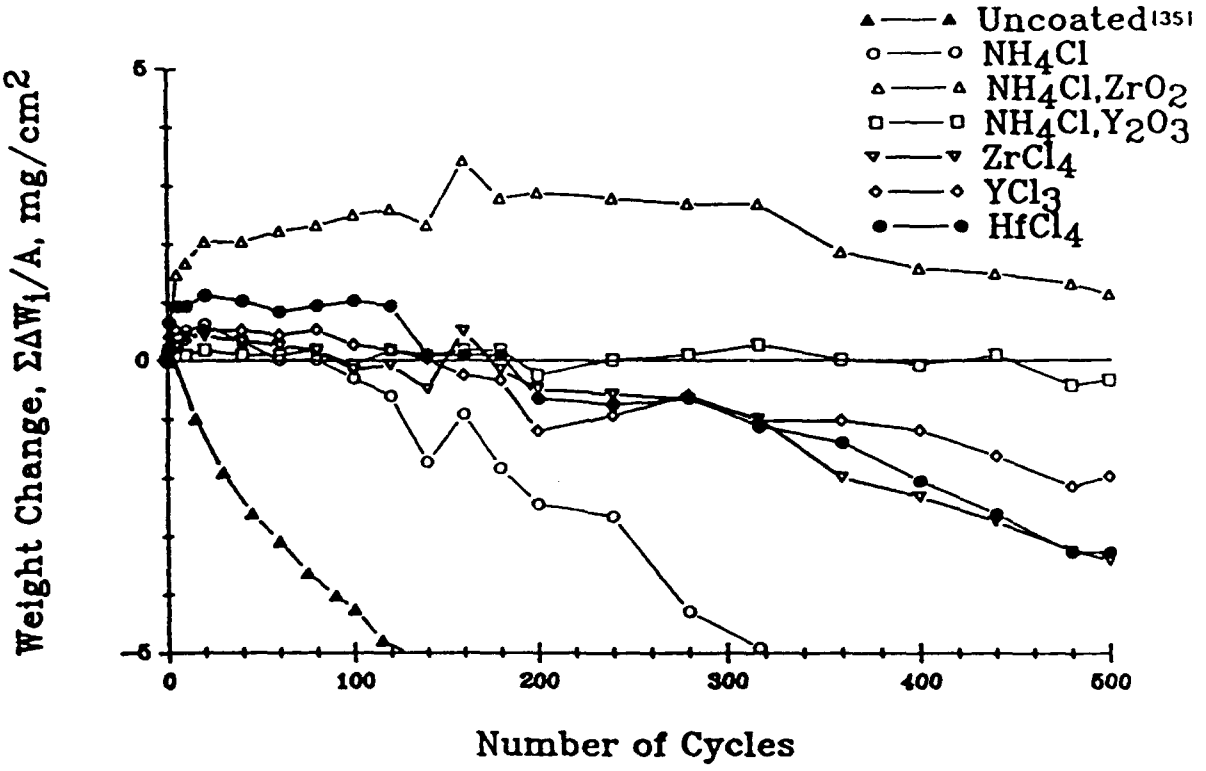

Figure 4: Oxidation kinetics for an IN 713LC alloy coated at 1150°C for 24 hours in a pack containing 20 wt.% of Cr-10 wt.% Al masteralloy with various activator salts/RE sources and cyclically oxidized at 1150°C in static air for up to 500 one-hour cycles. "Above pack" arrangement.

a).

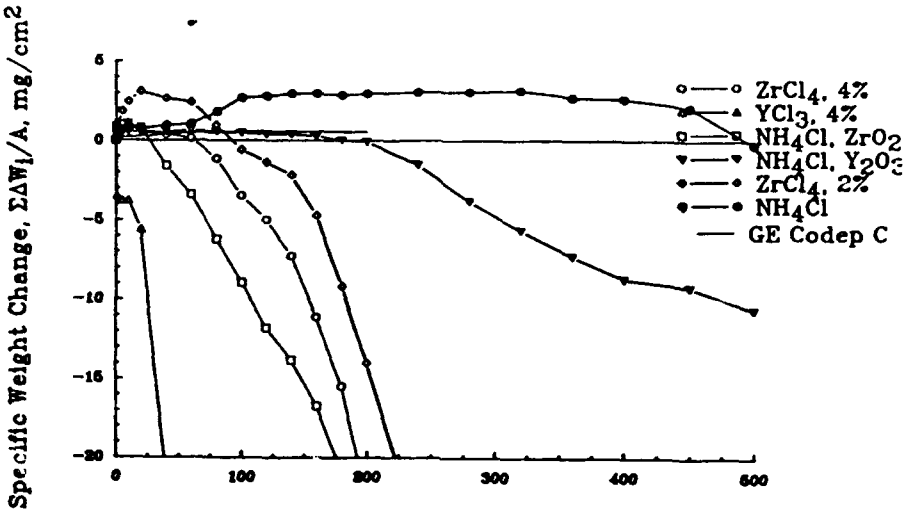

b).

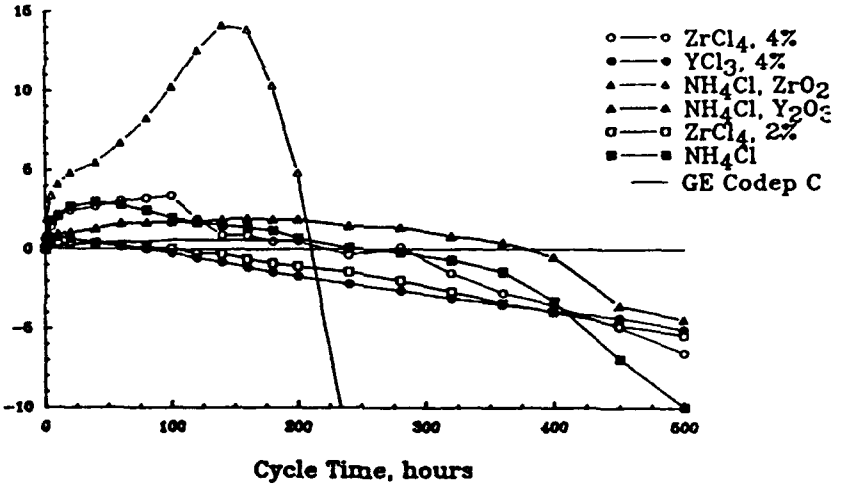

Figure 5: Oxidation kinetics for (a) René 80 and (b) IN 713LC alloys coated at 1150°C for 4 hours in a pack containing various activator salts/RE sources with 15 wt.% of Cr-7.5 wt.% Al masteralloy and cyclically oxidized at 1100°C in static air for up to 500 one-hour cycles. "Above pack" arrangement.

a).

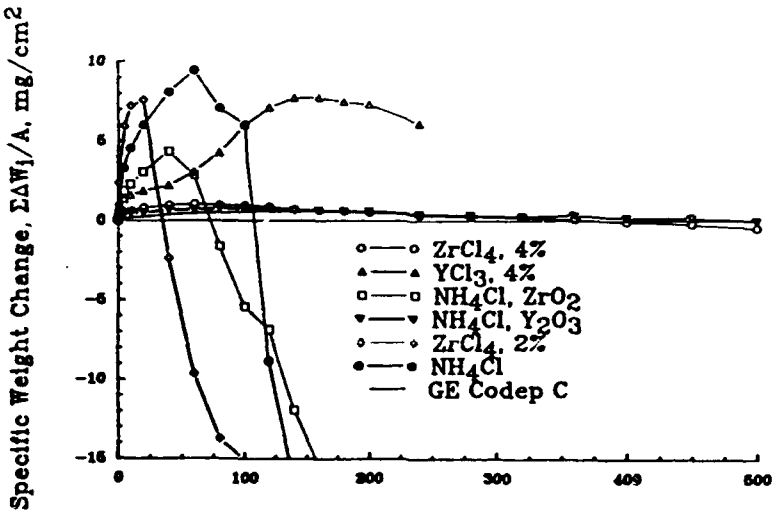

b).

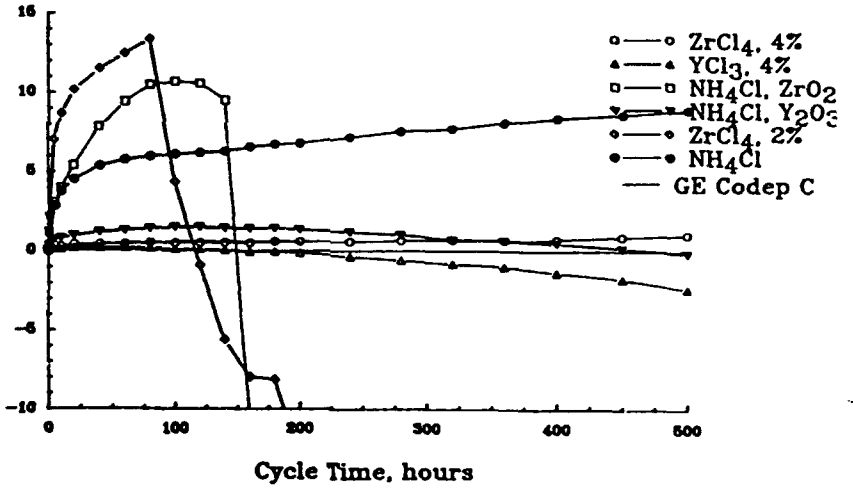

Figure 6: Oxidation kinetics for (a) René 80 and (b) IN 713LC alloys coated at 1150°C for 24 hours in a pack containing various activator salts/RE sources with 15 wt.% of Cr-7.5 wt.% Al masteralloy and cyclically oxidized at 1100°C in static air for up to 500 one-hour cycles. "Above pack" arrangement.

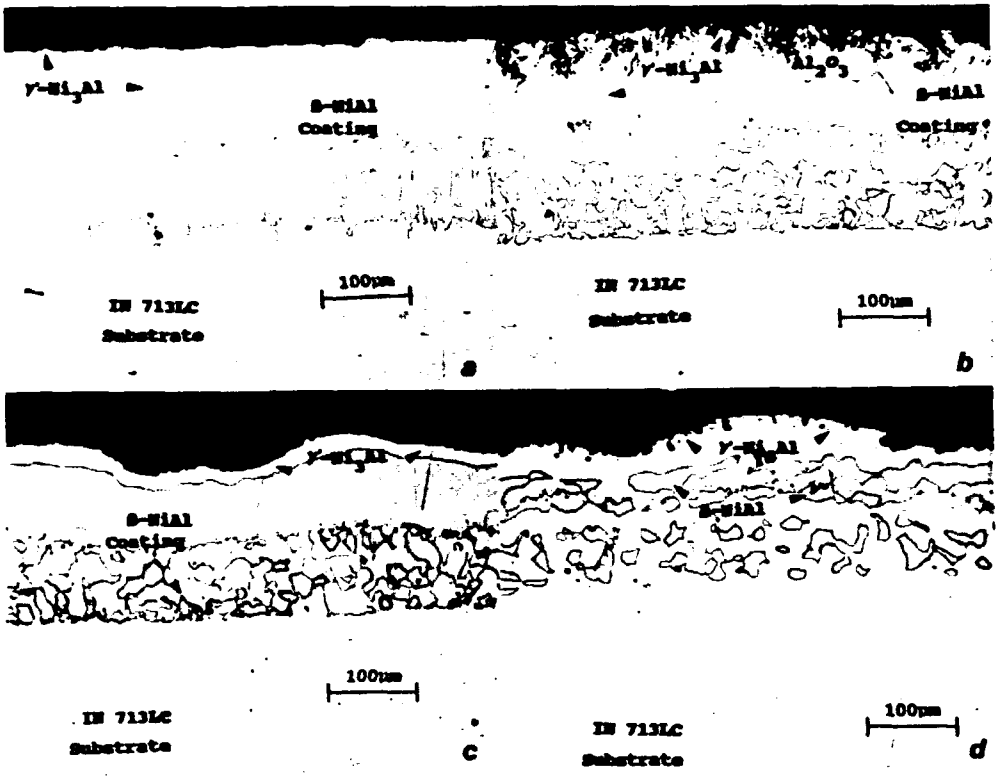

Figure 7: Cross-sectional optical micrographs of an IN 713LC alloy coated at 1150°C for 24 hours in a pack containing (a) 2 wt.% NH_4Cl plus 2 wt.% Y_2O_3, (b) 2 wt.% NH_4Cl plus 2 wt.% ZrO_2, (c) 4 wt.% $HfCl_4$, and (d) 2 wt.% NH_4Cl with 20 wt.% of Cr-10 wt.% Al masteralloy and cyclically oxidized at 1100°C in static air for 500 one-hour cycles. "Above pack" arrangement.

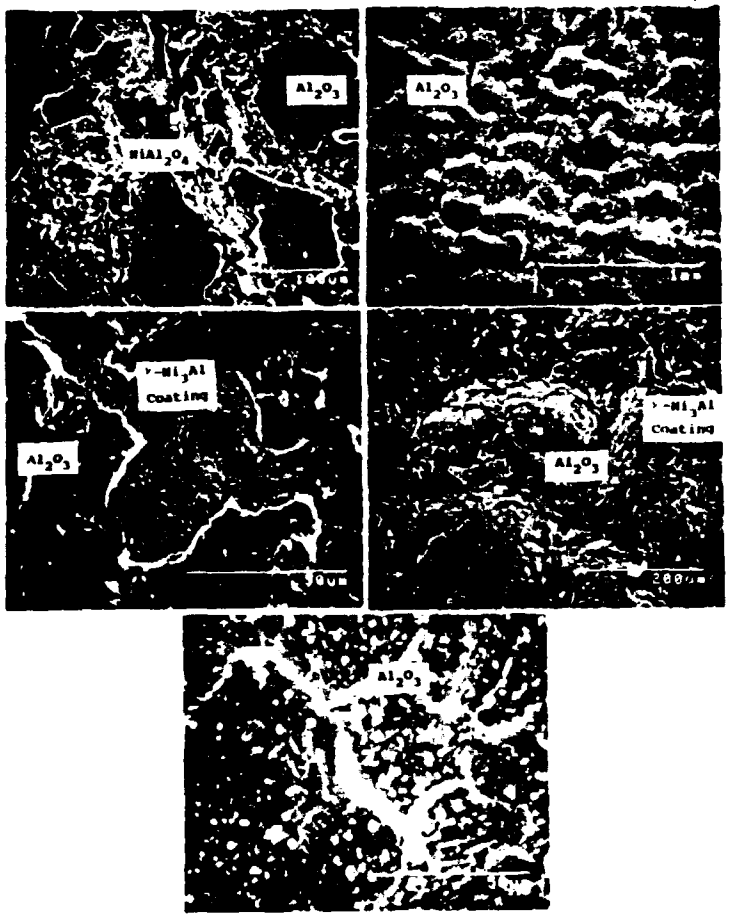

Figure 8: Surface scanning electron micrographs of an IN 713LC alloy coated at 1150°C for 24 hours in a pack containing (a,b) 2 wt.% NH_4Cl plus 2 wt.% Y_2O_3, (c,d) 4 wt.% $HfCl_4$, and (e) 2 wt.% NH_4Cl plus 2 wt.% ZrO_2 with 20 wt.% of Cr-10 wt.% Al masteralloy and cyclically oxidized at 1100°C in static air for up to 500, one-hour cycles. "Above pack" arrangement.

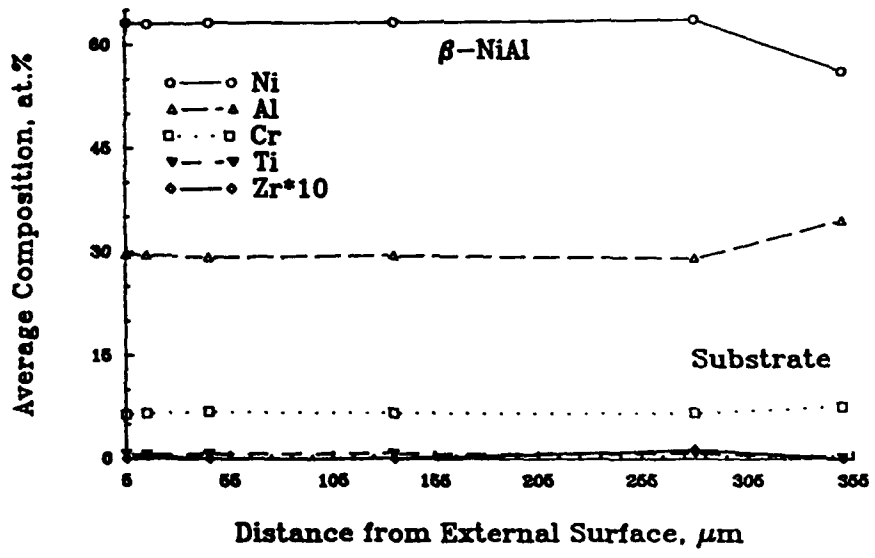

Figure 9: Cross-sectional backscattering electron micrograph and composition profile of an IN 713LC alloy coated at 1150°C for 24 hours in a 4 wt.% $ZrCl_4$-activated pack containing 15 wt.% of Cr-7.5 wt.% Al masteralloy and cyclically oxidized for 500 one-hour cycles at 1100°C in static air. "Above pack" arrangement.

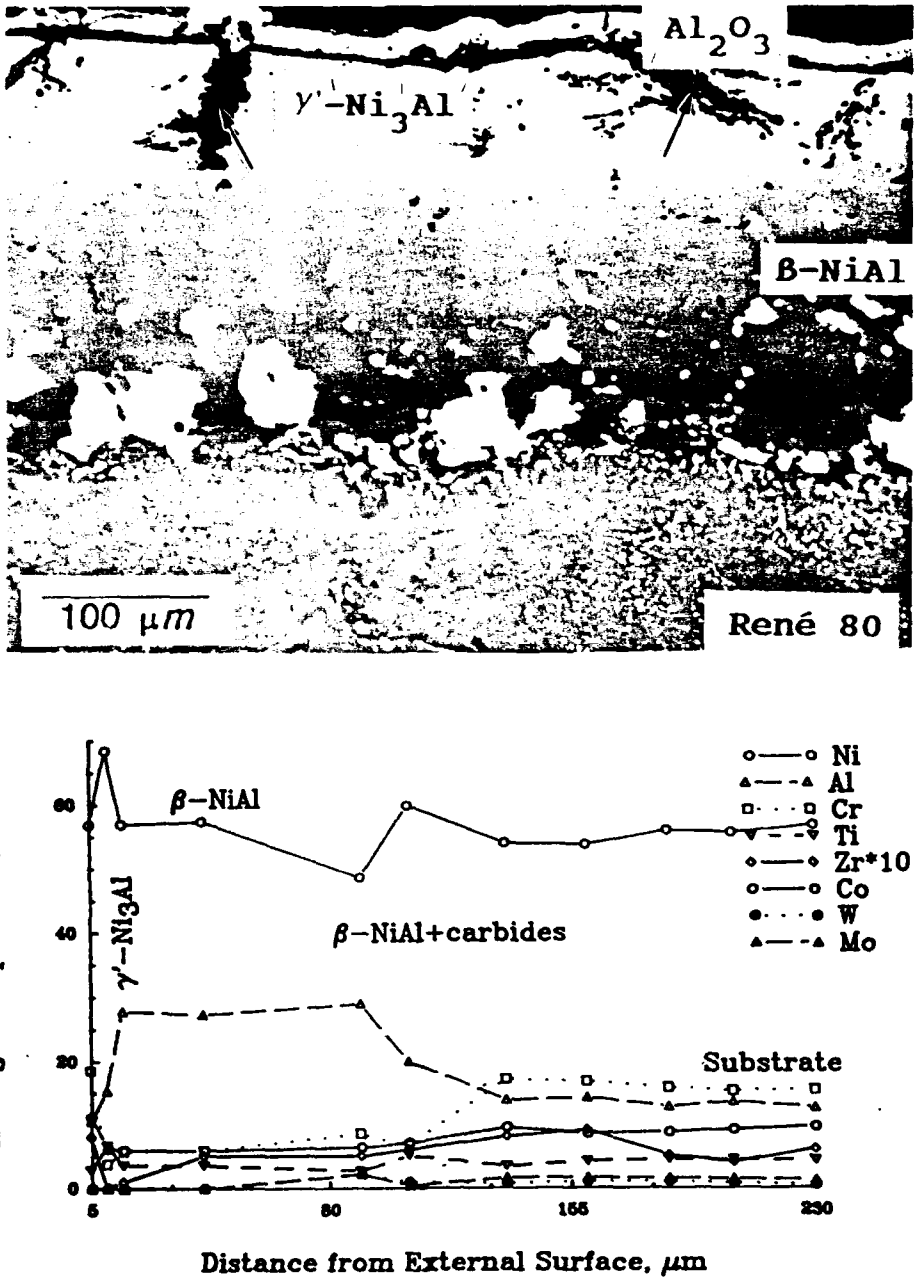

Figure 10: Cross-sectional backscattering electron micrograph and composition profile of a René 80 alloy coated at 1150°C for 24 hours in a 4 wt.% $ZrCl_4$-activated pack containing 15 wt.% of Cr-7.5 wt.% Al masteralloy and cylcically oxidized for 500 one-hour cycles at 1100°C in static air. "Above pack" arrangement.

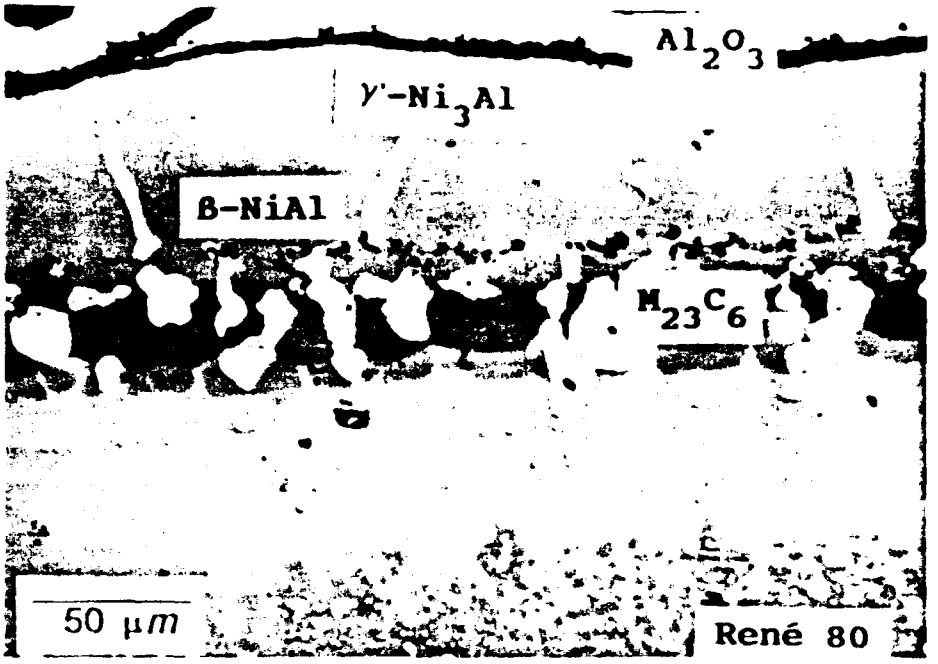

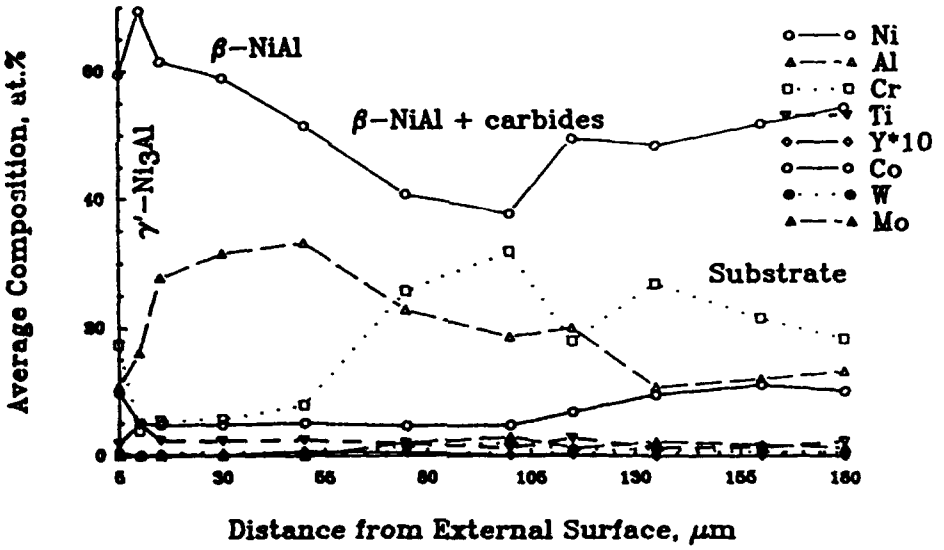

Figure 11: Cross-sectional backscattering electron micrograph and composition profile of a René 80 alloy coated at 1150°C for 24 hours in a 2 wt.% NH_4Cl-activated pack containing 2 wt.% Y_2O_3 and 15 wt.% of Cr-7.5 wt.% Al masteralloy and cyclically oxidized for 500 one-hour cycles at 1100°C in static air. "Above pack" arrangement.

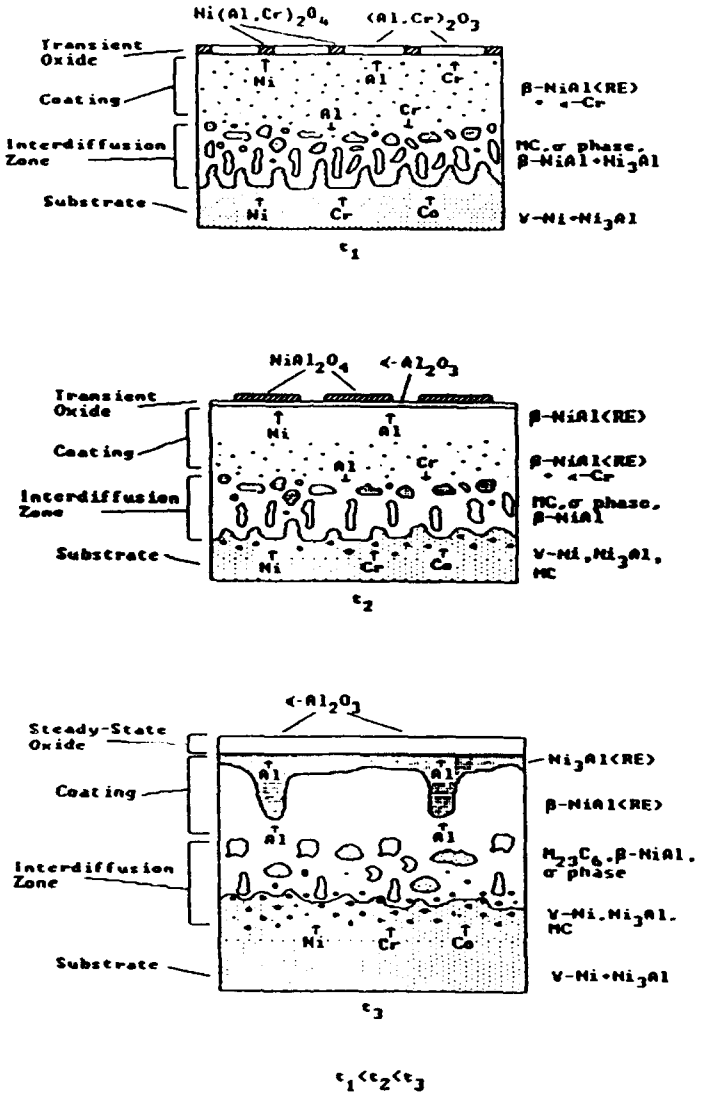

Figure 12: Schematic illustration of the degradation mechanism of the modified aluminide diffusion coatings.

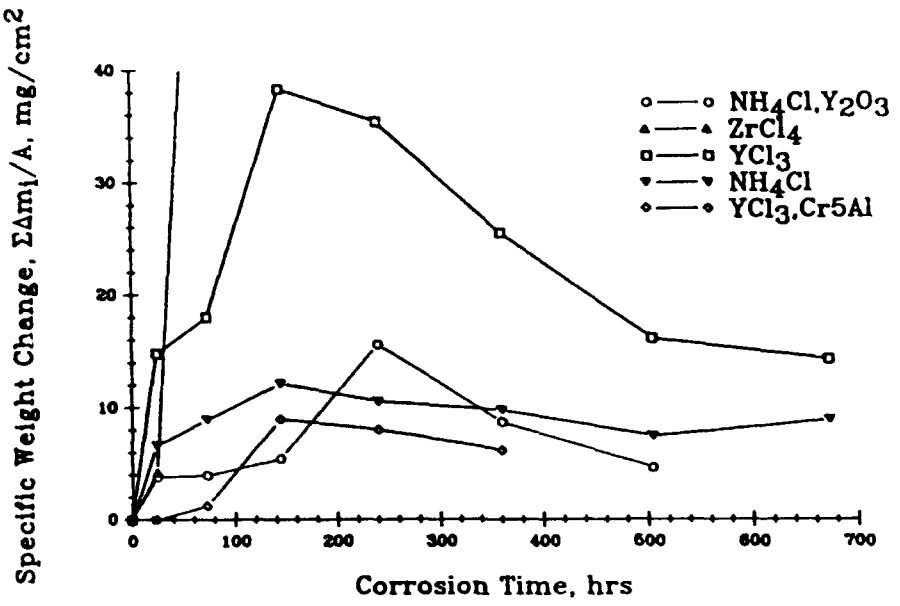

Average Surface Composition (EPMA)

Activator	Ni	Al	Cr	Co	Ti	RE (at.%)
NH_4Cl	45.82	42.22	5.61	5.29	.02	.00
$NH_4Cl.Y_2O_3$*	46.16	43.41	4.87	5.44	.04	.07
YCl_3	48.88	42.69	5.54	5.79	.05	.05
$ZrCl_4$	46.17	44.98	3.28	5.03	.02	.12

*Cr7.5Al wt.% Masteralloy, all else Cr6Al wt.%.

Figure 13: Hot corrosion kinetics and average surface compositions for Mar-M247 alloys coated at 1150°C for 24 hours in a pack containing various activator salts/RE sources with 25 wt.% of Cr-6 wt.% Al masteralloy and isothermally corroded at 900°C in a Pt-catalyzed, 0.1% SO_2/O_2 gas mixture with 5.0 mg/cm^2 Na_2SO_4. "Above pack" arrangement.

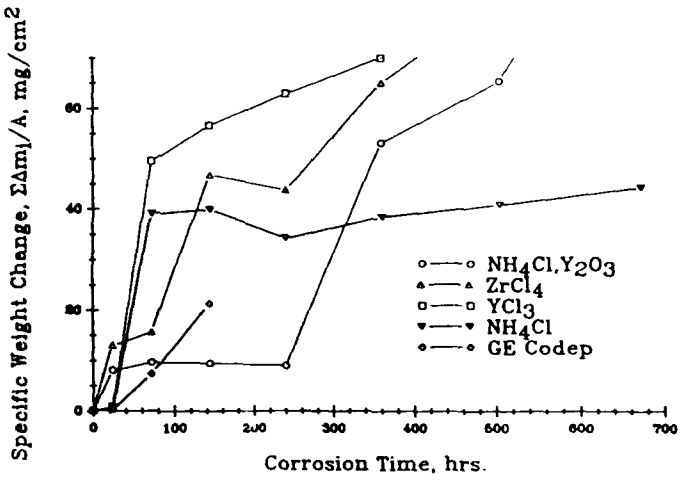

Average Surface Composition (EPMA)

Activator	Ni	Al	Cr	Co	Ti	RE (at.%)
NH_4Cl	46.72	43.88	4.92	4.42	.08	.00
NH_4Cl,Y_2O_3*	47.22	44.36	4.19	4.17	.07	.02
YCl_3	46.45	42.84	4.39	5.15	.17	.04
$ZrCl_4$	47.83	44.59	3.36	2.19	.05	.10

*Cr7.5Al wt.% Masteralloy, all else Cr6Al wt.%.

Figure 14: Hot corrosion kinetics and average surf e
compositions for René 80 alloys coated at 1150°C for 24 hc s
in a pack containing various activator salts/RE sou
with 25 wt.% of Cr-6 wt.% Al masteralloy and isotherm y
corroded at 900°C in a Pt-catalyzed, 0.1% SO_2/O_2 gas mixt
with 5.0 mg/cm² Na_2SO_4. "Above pack" arrangement.

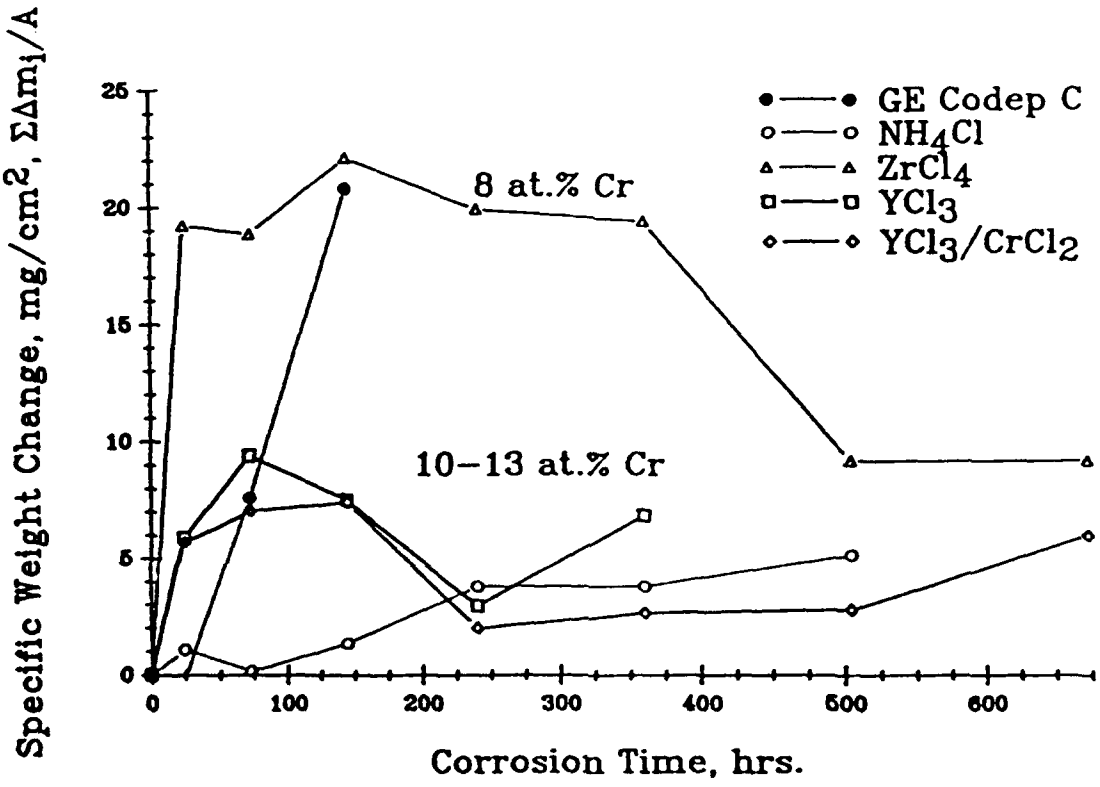

Figure 15: Hot corrosion kinetics for René 80 alloys coated at 1150°C for 24 hours in a pack containing various activator salts/RE sources with 25 wt.% of Cr-7.5 wt.% Al masteralloy and isothermally corroded at 900°C in a Pt-catalyzed, 0.1% SO_2/O_2 gas mixture with 5.0 mg/cm² Na_2SO_4. "Above pack" arrangement.

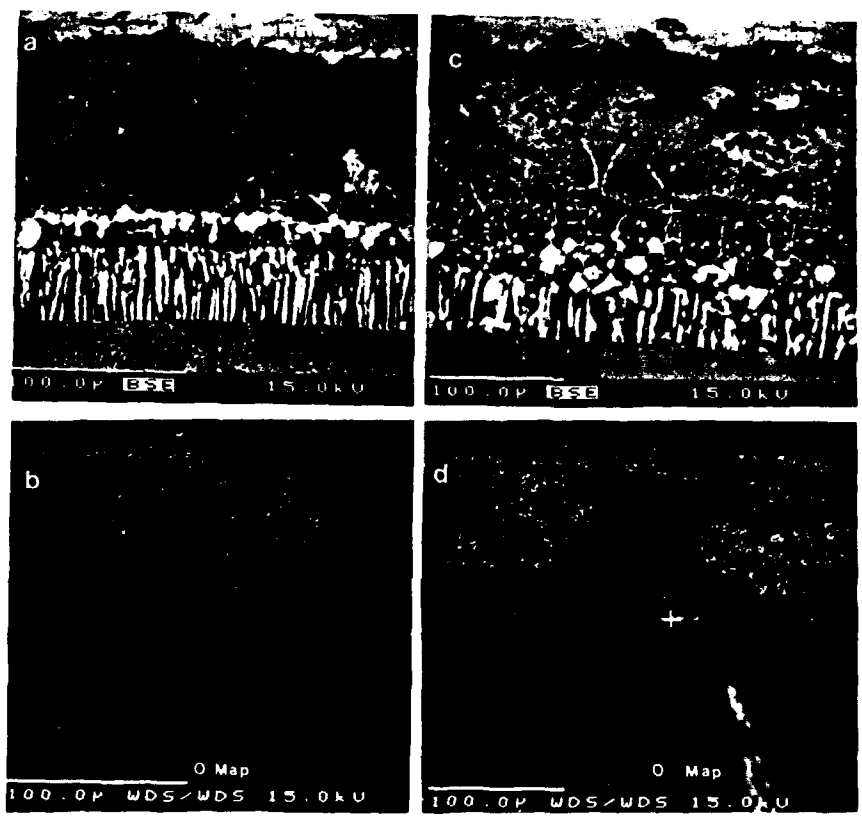

Figure 16: (a,c) Cross-sectional backscattering electron micrograph and (b,d) corresponding oxygen x-ray map for a René 80 substrate coated at 1150°C for 24 hours in a 2 wt.% (a) YCl3or (c) $ZrCl_4$-activated pack containing 25 wt.% of Cr-7.5 wt.% Al masteralloy and isothermally corroded at 900°C for 144 hours in a Pt-catalyzed, 0.1% SO_2/O_2 gas mixture with 5.0 mg/cm^2 Na_2SO_4. "Powder contacting" arrangement.

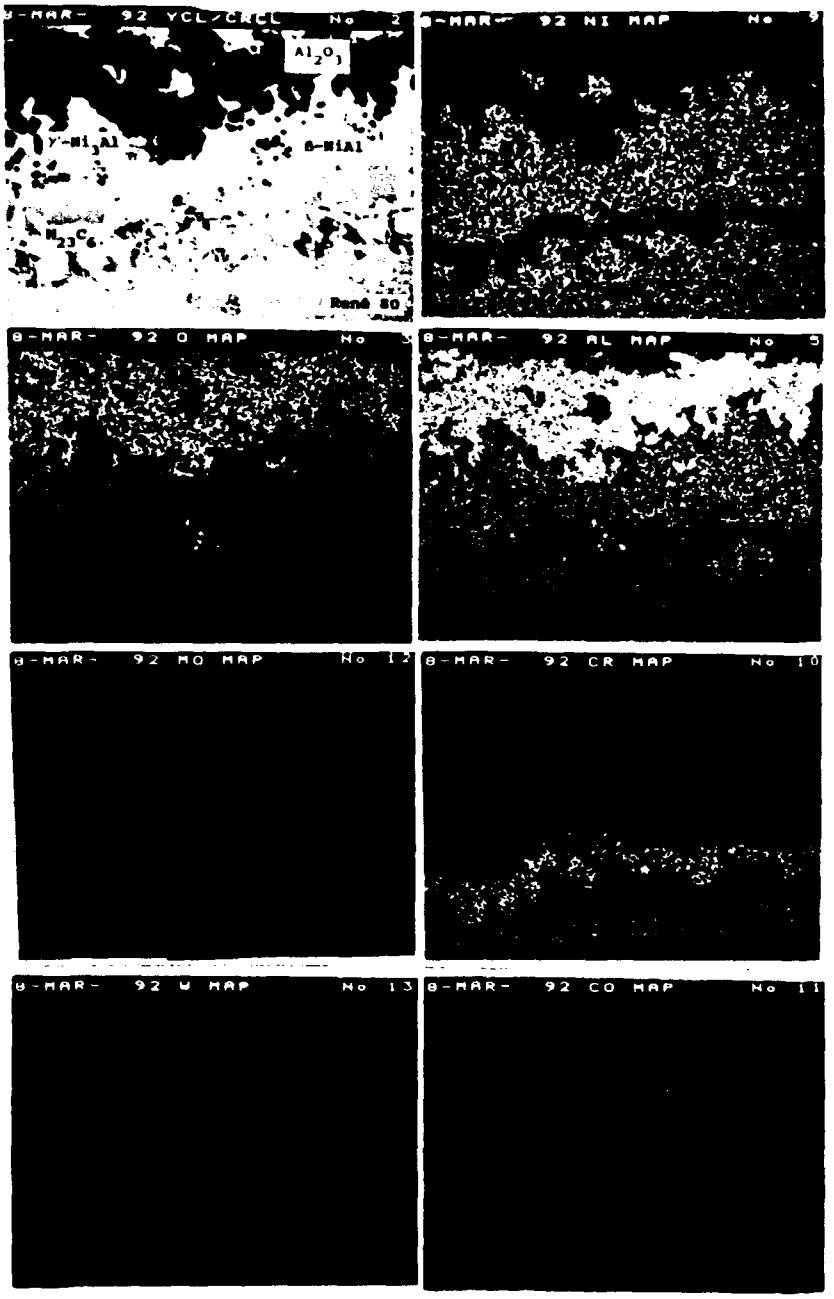

Figure 17: Cross-sectional backscattering electron micrograph and corresponding x-ray maps of Ni, Al, Cr, O, Co, W, and Mo for a René 80 substrate coated at 1150°C for 24 hours in a 2 wt.% (2:1) $YCl_3/CrCl_2$-activated pack containing 25 wt.% of Cr-7.5 wt.% Al masteralloy and isothermally corroded at 900°C for 672 hours in a Pt-catalyzed, 0.1% SO_2/O_2 gas mixture with 5.0 mg/cm^2 Na_2SO_4. "Powder contacting" arrangement.

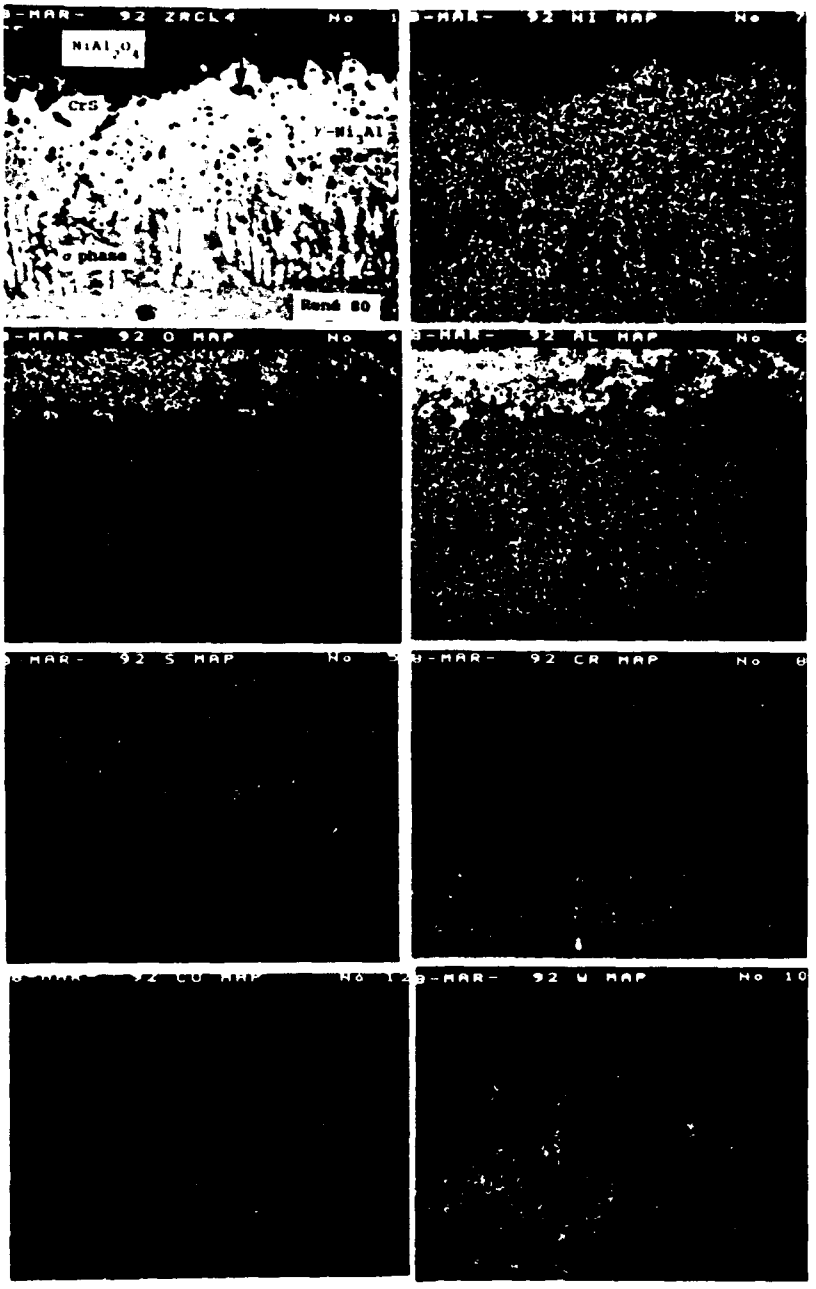

Figure 18: Cross-sectional backscattering electron micrograph and corresponding x-ray maps of Ni, Al, Cr, O, S, Co, and W for a René 80 substrate coated at 1150°C for 24 hours in a 2 wt.% $ZrCl_4$-activated pack containing 25 wt.% of Cr-7.5 wt.% Al masteralloy and isothermally corroded at 900°C in a Pt-catalyzed, 0.1% SO_2/O_2 gas mixture with 5.0 mg/cm^2 Na_2SO_4. "Powder contacting" arrangement.

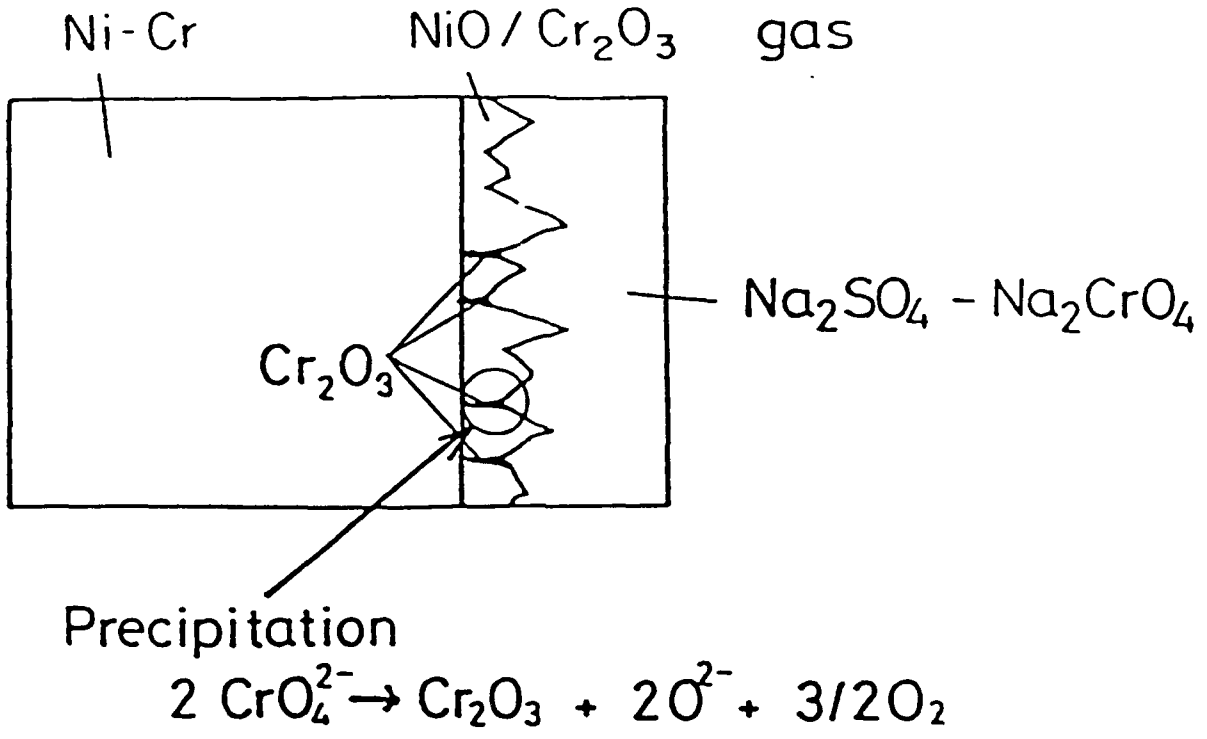

Figure 19: Schematic representation of possible beneficial effect of chromium on hot corrosion of Ni-Cr alloy.[49]